

THE LOW MASS IMF OF YOUNG OPEN CLUSTERS

by

Douglas Michael Williams

A Dissertation Submitted to the Faculty of the

DEPARTMENT OF ASTRONOMY

In Partial Fulfillment of the Requirements
For the Degree of

DOCTOR OF PHILOSOPHY

In the Graduate College

THE UNIVERSITY OF ARIZONA

1 9 9 5

INFORMATION TO USERS

This manuscript has been reproduced from the microfilm master. UMI films the text directly from the original or copy submitted. Thus, some thesis and dissertation copies are in typewriter face, while others may be from any type of computer printer.

The quality of this reproduction is dependent upon the quality of the copy submitted. Broken or indistinct print, colored or poor quality illustrations and photographs, print bleedthrough, substandard margins, and improper alignment can adversely affect reproduction.

In the unlikely event that the author did not send UMI a complete manuscript and there are missing pages, these will be noted. Also, if unauthorized copyright material had to be removed, a note will indicate the deletion.

Oversize materials (e.g., maps, drawings, charts) are reproduced by sectioning the original, beginning at the upper left-hand corner and continuing from left to right in equal sections with small overlaps. Each original is also photographed in one exposure and is included in reduced form at the back of the book.

Photographs included in the original manuscript have been reproduced xerographically in this copy. Higher quality 6" x 9" black and white photographic prints are available for any photographs or illustrations appearing in this copy for an additional charge. Contact UMI directly to order.

UMI

A Bell & Howell Information Company
300 North Zeeb Road, Ann Arbor MI 48106-1346 USA
313/761-4700 800/521-0600

THE LOW MASS IMF OF YOUNG OPEN CLUSTERS

by

Douglas Michael Williams

A Dissertation Submitted to the Faculty of the

DEPARTMENT OF ASTRONOMY

In Partial Fulfillment of the Requirements
For the Degree of

DOCTOR OF PHILOSOPHY

In the Graduate College

THE UNIVERSITY OF ARIZONA

1 9 9 5

UMI Number: 9622985

UMI Microform 9622985
Copyright 1996, by UMI Company. All rights reserved.

**This microform edition is protected against unauthorized
copying under Title 17, United States Code.**

UMI
300 North Zeeb Road
Ann Arbor, MI 48103

THE UNIVERSITY OF ARIZONA
GRADUATE COLLEGE

As members of the Final Examination Committee, we certify that we have
read the dissertation prepared by Douglas Michael Williams
entitled THE LOW MASS IMF IN YOUNG OPEN CLUSTERS

and recommend that it be accepted as fulfilling the dissertation
requirement for the Degree of Doctor of Philosophy

George Rieke

Dr. George Rieke

10/20/95

Date

James W. Liebert

Dr. James Liebert

10/20/95

Date

Erick T. Young

Dr. Erick Young

10/20/95

Date

A. Burrows

Dr. Adam Burrows

Oct 20, 1995

Date

Date

Final approval and acceptance of this dissertation is contingent upon
the candidate's submission of the final copy of the dissertation to the
Graduate College.

I hereby certify that I have read this dissertation prepared under my
direction and recommend that it be accepted as fulfilling the dissertation
requirement.

George Rieke

Dissertation Director

Dr. George Rieke

10/26/95

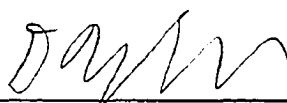
Date

STATEMENT BY AUTHOR

This dissertation has been submitted in partial fulfillment of requirements for an advanced degree at The University of Arizona and is deposited in the University Library to be made available to borrowers under rules of the Library.

Brief quotations from this dissertation are allowable without special permission, provided that accurate acknowledgment of source is made. Requests for permission for extended quotation from or reproduction of this manuscript in whole or in part may be granted by the head of the major department or the Dean of the Graduate College when in his or her judgment the proposed use of the material is in the interests of scholarship. In all other instances, however, permission must be obtained from the author.

SIGNED: _____



ACKNOWLEDGMENTS

I would like to thank Milagros Ruiz for assistance in reducing our Pleiades GESPEC spectra; and Lisa Shier and Chad Engelbracht for assistance in reducing our FSPEC comparison spectra. W. Tad Morgan did much of the initial work on the Pleiades chapter.

Several faculty members deserve special mention. Adam Burrows and Jim Liebert were always willing to discuss and dissect my work, and offered many useful comments. Fernando Comerón laid most of the groundwork for Chapter 5. John Stauffer provided many insightful and valuable suggestions, in addition to much of the optical data. Finally, there's my advisor, George Rieke, to whom I owe the most, from financial support for most of my time at Steward, to developing two research programs, both perfectly suited to the needs at hand, to just being an all-around nice guy. George also provided an uncountable valuable, detailed comments on many (all?) aspects of this work in a very timely fashion.

A number of people provided distractions from this work, and although they may have made my stay in graduate school a bit longer, they also made it much more enjoyable. The largest distraction was provided by Tang Soo Do Master Darryl Khalid, for allowing me to teach his rewarding martial art, and pushing me to achieve my second degree black belt. My officemate David Sprayberry was a fellow cynic, and helped keep me sane during classes, as did Kim McCleod and Peter Tamblyn. Kim also supplied a set of L^AT_EX macros that made producing this dissertation as painless as could possibly be expected. I would also like to thank Rachel Perkins for getting Thunder and Stoli, and leaving without them. Nadine Dinshaw has been tireless in her efforts to get me to finish this dissertation. Pat Hall and Jim Yingst deserve many thanks for showing me the light of *Babylon 5* and hosting their weekly B5 gatherings. Anne Turner also deserves special mention for the extra help she has recently given.

DEDICATION

This dissertation is dedicated to my mother and grandmother who always encouraged me to keep learning and doing my very best.

Table of Contents

LIST OF FIGURES	9
LIST OF TABLES	11
ABSTRACT	12
1 INTRODUCTION	14
1.1 Background	14
1.2 Overview	16
2 TECHNIQUES	18
2.1 Introduction	18
2.2 Photometric Observations	19
2.2.1 Infrared $K(2.2\mu m)$ Observations	19
2.2.2 Optical V and I Observations	20
2.3 Photometric Reductions	21
2.3.1 Celestial Coordinates	22
2.4 Spectroscopic Observations	23
2.4.1 J -band Spectra of Pleiades Sources	23
2.4.1.1 GESPEC	24
2.4.1.2 GESPEC data acquisition and reduction	24
2.4.2 K -band Spectra of ρ Ophiuchus Sources	25
2.4.2.1 FSPEC	25

2.4.2.2	FSPEC Spectral Reductions	26
3	PRAESEPE	27
3.1	Introduction	27
3.2	Analysis	28
3.2.1	Extraction of Praesepe Members	28
3.3	Comparison to Other Work	35
3.3.1	Dynamical Evolution of the Mass Function	36
3.3.2	Limits to the Dynamical Evolution	41
3.4	Conclusions	42
4	THE PLEIADES	45
4.1	Introduction	45
4.2	Analysis	46
4.2.1	Extraction of Pleiades Members	46
4.2.2	Tests of the Extraction Technique	53
4.2.3	Comparison with Other Work	67
4.3	Conclusions	71
5	ρ OPHIUCHIUS	72
5.1	Introduction	72
5.2	Mass Determination in the Stellar Range	73
5.3	Spectra of Low Mass Ophiuchus Sources	76
5.3.1	Approach	76
5.3.2	New Observations and data reduction	77
5.3.3	Spectral Properties of Low Mass Sources	81
5.3.4	Discussion	83
5.4	The Initial Mass Function	87
5.5	Conclusions	91

6	NGC 7160	93
6.1	Introduction	93
6.2	Analysis	95
6.2.1	Extraction of Members	95
6.2.2	The Luminosity and Mass Functions of NGC 7160	98
6.3	Conclusions	106
7	RESULTS	107
7.1	Comparison of Open Clusters	107
7.2	Comparison to the Field	110
8	CONCLUSIONS	114
	REFERENCES	116

List of Figures

3.1	Color-Magnitude (m_V , $V-K$) Plot for Praesepe.	29
3.2	Color-Color ($V-I$, $I-K$) Plot for Praesepe.	31
3.3	Color-Magnitude (m_I , $I-K$) Plot for Praesepe.	32
3.4	Color-Magnitude (m_V , $V-I$) Plot for Praesepe.	33
3.5	Luminosity Function of Praesepe.	37
3.6	Mass Function of Praesepe.	38
3.7	Mass Function Fits for Praesepe.	43
4.1	Color-Magnitude m_V , $V-K$ for the Pleiades.	48
4.2	Color-Color $V-I$, $I-K$ for the Pleiades.	50
4.3	K -band finder charts for objects not previously identified.	52
4.4	Comparison of Temperature Scales.	55
4.5	Comparison of Age and Temperature Effects.	56
4.6	Color-Magnitude m_V , $V-K$ for the Pleiades and SHPRM sources. . .	58
4.7	Color-Color $V-I$, $I-K$ for the Pleiades.	59
4.8	Comparison of 70 and 120 Myr isochrones for the Pleiades.	60
4.9	Spectra of VB10 and PPl 1.	62
4.10	Spectra of VB10 and PPl 2 and PPl 6.	63
4.11	Color-Magnitude m_I , $I-K$ for the Pleiades.	69
5.1	Comparison of mass estimates of CRBR and SKS.	75
5.2	Spectra of ρ Ophiuchus objects.	78

	10
5.3 Comparison of star counts.	88
5.4 The initial mass function for ρ Ophiuchus.	90
6.1 Color-Magnitude Diagram m_V , $V-K$ for NGC 7160.	96
6.2 Color-Color Diagram $V-I$, $I-K$ for NGC 7160.	99
6.3 Luminosity Function of NGC 7160.	102
6.4 Low Mass Functions of NGC 7160 Assuming Different Ages.	103
6.5 Mass Functions of NGC 7160.	105
7.1 Comparison of Open Cluster IMFs to the Field Star MF.	109

List of Tables

2.1	Summary of Observations	19
3.1	Candidate Praesepe Low Mass Stars	38
4.1	Probable Pleiades Members	66
4.2	Pleiades Star Counts ^a	66
5.1	Equivalent widths of some lines and blends	80
5.2	Model Masses of Ophiuchus sources	90
6.1	Probable NGC 7160 M-Dwarfs	100
6.2	The Mass Function of NGC 7160	103

ABSTRACT

We present the results of the investigation of the Initial Mass Function at the end of the Main Sequence in young open clusters. We find that over a large range in age and environment the IMFs are similar to each other, and to recent determinations of the field star IMF.

We have obtained V , I , and K band photometry of fields in the three relatively unembedded open clusters. The photometry reaches down to various masses in each cluster: $0.08\mathcal{M}_{\odot}$ for Praesepe, $0.04\mathcal{M}_{\odot}$ for the Pleiades, and $0.15\mathcal{M}_{\odot}$ for NGC 7160.

We compare the methods for estimating the masses of young, embedded stars developed by Comerón et al. (1993) and by Strom et al. (1995) and show them to be in good agreement. Spectra in the $2\ \mu\text{m}$ region of six low mass objects from Comerón et al. (1993) are also in agreement with the mass estimates using these methods. The spectrum of a brown dwarf candidate is used to place an upper limit on its mass of 60% of the minimum required for hydrogen burning.

The IMFs from these four clusters plus NGC 2024 (Comerón et al. (1995)) are shown to be in agreement with each other. The composite MF can be fitted with a power law between 0.04 and $0.5\mathcal{M}_{\odot}$ with a slope of -0.75 ± 0.3 . There is no evidence for a cutoff at the bottom of the main sequence ($0.08\mathcal{M}_{\odot}$); brown dwarfs appear to be abundant in open clusters. However, the slope of the MF is well above the value of $\lesssim -2$ required for very low mass stars and brown dwarfs to contribute a significant portion of the mass of open clusters.

The composite cluster MF also is in agreement with recent determinations of the field star IMF for stellar masses. The field star data do not extend into the

brown dwarf range; however, if we extrapolate in accordance with the cluster MF, we conclude that brown dwarfs probably do not contribute significantly to the dark matter.

Chapter 1

INTRODUCTION

1.1 Background

The initial mass function (IMF) contains a record of the fragmentation of concentrations of gas, plasma, and dust into low mass stars and sub-stellar objects. The form of the IMF can distinguish different processes that may regulate this fragmentation and it can be used to study the roles of these processes in differing environments. For example, accretion models might predict gaps in the IMF as the result of runaway accretion processes, while pure fragmentation would result in a smooth IMF. Of particular interest is the minimum stellar (or sub-stellar) mass, which in the opacity-limited fragmentation model (Hoyle (1953)) is predicted to be near $0.01\mathcal{M}_{\odot}$ (Hayashi & Nakano (1965)). This limit is expected to be raised to the neighborhood of $0.1 - 0.3\mathcal{M}_{\odot}$ by a variety of effects such as rotation, magnetic fields, coagulation, and accretion (Silk (1987) and references therein). These arguments and others regarding the importance of the low mass IMF as a constraint on theories of star formation are discussed by Lada (1990).

For observational reasons much of the work on the IMF has concentrated on high mass stars, particularly in HII regions of external galaxies, and on intermediate stars in our own Galaxy (see Scalo (1986)). The IMF for low mass stars affects many areas of astrophysics. Low mass stars ($m < 0.5\mathcal{M}_{\odot}$) dominate the known stellar mass in the Milky Way, and may therefore be the location of the baryonic dark matter. Low mass stars also affect the dynamical evolution of open and globular clusters. Knowledge of the low mass IMF, and its possible variations as a function of environment, may also constrain the physics of star formation.

However, the field star IMF, by itself, may not necessarily provide a very strong constraint on star formation theory. This is because the field star IMF is a globally averaged IMF, averaged over both the lifetime of the Galaxy, and over a specific volume of space (i.e. the solar neighborhood). Although many researchers assume that the field star IMF is universal in both space and time, this has never been satisfactorily demonstrated. Open clusters are the smallest spatial size scale over which a meaningful determination of a mass function can be made.

We have therefore undertaken a study of the IMF at the end of the Main Sequence and beyond in young open (Galactic) clusters. Observationally, nearby clusters offer a number of important advantages over investigations of the field or searches for low mass companions to known stars. The most obvious example is that the area of sky that needs to be imaged is restricted to the size of the cluster. This is particularly important if the methodology makes use of a small field of view CCD or IR array. Young clusters have the added advantage that any candidate very low mass/substellar members can be expected to be brighter due to significant ongoing gravitational contraction and the lack of time over which these objects could have radiated this energy away. The fact that all members share a common

distance, metallicity, and age can also aid the search for low mass members of the clusters.

Studying clusters, however, is a tradeoff; there are some disadvantages. The most obvious problems in a study of the lowest mass members of a cluster are contamination from field stars, and the completeness corrections that must be made. The relatively small numbers of stars means there are usually poor statistics involved in the determination of the IMF. Clusters are also in general more distant than field stars. Another disadvantage that makes very young cluster members harder to observe is the presence of obscuring dust.

1.2 Overview

We have used two general methods to investigate the IMF at the end of the Main Sequence. Chapter 2 discusses the observational techniques and data reduction methodologies used throughout this work. Included in Chapter 2 are descriptions of the various instrumentation and telescopes at which the data were taken, the areal coverage of the various surveys, and descriptions of the various data reduction techniques for the optical CCD and infrared array photometric observations, and the infrared spectral observations.

The choice of investigative methods was dictated by the amount of obscuring dust present in the cluster. Chapter 3 gives the full details of our long baseline (V to K) photometric technique as applied to the oldest cluster studied in this work, Praesepe. The method is shown to be very efficient, yet still remarkably complete when compared to previous proper motion studies, which require many years between epochs, and only yield lower quality photographic magnitudes. Praesepe was chosen as our first cluster because at the age of Praesepe, all cluster members

should be close to being on the Main Sequence, thus eliminating the need to choose an isochrone.

Chapter 4 extends the long baseline photometric method to a younger cluster, the Pleiades, where the possibility exists of locating a young brown dwarf since it would be a factor of 25 times brighter at the age of the Pleiades than at the age of Praesepe (Burrows et al. (1993)). Chapter 4 also investigates a number of sources claimed to be Pleiades very low mass members by Stauffer et al. (1989).

The photometric technique breaks down when investigating a heavily embedded cluster, and a different approach is required. Chapter 5 describes our efforts to strengthen and support the methods first described in Comerón et al. (1993), which integrates theoretical models of low mass objects and multiband infrared photometry of embedded sources to provide internally consistent estimates of the mass and extinction of each member of an embedded cluster. This method is also compared with the approach recently described in Strom et al. (1995).

Chapter 6 describes observations of the often overlooked open cluster NGC 7160. The importance of this cluster lies in the fact that its age and amount of reddening make it a perfect link between the younger, embedded clusters and the older, dust free clusters.

Finally, the mass functions of all of these young open clusters are intercompared, and compared with the field star IMF in Chapter 7. Within the expected errors, we find that the IMFs from 0.04 to $2\mathcal{M}_{\odot}$ are consistent from one cluster to another and with the IMF deduced for field stars near the sun. The importance of very low mass stars/brown dwarfs to the problem of the Galactic missing mass problem is discussed.

Chapter 2

TECHNIQUES

2.1 Introduction

The observations reported in the dissertation fall into two broad categories: photometric and spectroscopic. Most of the photometric data were taken with similar instrumentation and underwent similar reductions. Table 2.1 summarizes the data acquired for the different clusters in this dissertation and the instrumentation and telescopes utilized. Because both the Pleiades and Praesepe are so close, the area imaged in these clusters represents about 4% of the total cluster area. NGC 7160, however, was approximately three quarters covered by our observations.

The sections in this chapter describe in detail the instrumentation, the observational methods, and the data reduction techniques used in this dissertation, starting with descriptions of the photometric observations, and followed by descriptions of the spectroscopic observations.

2.2 Photometric Observations

2.2.1 Infrared $K(2.2\mu m)$ Observations

Infrared K images were obtained on the Steward Observatory 2.3m telescope. These data used a camera with either a NICMOS3 256×256 HgCdTe array with the pixel size set to $0''.6$, and a field of view of ~ 6.5 arcmin² (Praesepe and NGC 7160), or a NICMOS2 128×128 HgCdTe with the pixel size set to $1''.2$, and a field of view of ~ 6.5 arcmin² (the Pleiades). Each infrared field was covered with a grid of either 3×3 or 4×4 infrared frames. The telescope was moved $\sim 6''$ (~ 10 -20 pixels) between exposures within an infrared field. Thus, the telescope systematically pointed over a $12''$ or $18''$ box for each infrared field. For calibration, short exposure, defocused images of Elias et al. (1982) standard stars were taken throughout the nights at a variety of airmasses.

All data reduction steps for the infrared fields were performed under IRAF. Offset level and dark current corrections were made simultaneously to each frame by subtraction of a frame which was exposed for the appropriate time to a blank, cooled filter. A separate flat field image was produced from each set of subframes

Table 2.1. Summary of Observations

Cluster	IR	Optical	Total Area (\square') / Number of Objects
Praesepe	256 ² /Steward 2.3m	4-Shooter/Palomar	290
Pleiades	128 ² /Steward 2.3m	4-Shooter/Palomar ^a	400
NGC 7160	256 ² /Steward 2.3m	CCD/Steward 2.3m	50
ρ Oph	FSPEC/MMT & Steward 2.3m	...	9

^aSupplemented by 2 fields with CCD/Steward 2.3m

by first normalizing each subfield by its mean (ignoring bad pixels) and then averaging the resulting subfields together after throwing out the highest value at each pixel (this filters out cosmic rays and because the telescope was moved between exposures also removes stars). Each subfield was flatfielded, and an offset was added to or subtracted from each subfield to obtain a consistent mean. These images were then shifted by integer pixels to align them on the detected stars, and averaged. Bad pixels were assigned a flag value and ignored in the final average.

2.2.2 Optical V and I Observations

The optical data used were obtained at either the Steward 2.3m telescope, or the Palomar 5m. The Palomar data were supplied by John Stauffer. The Steward optical data were taken with the LORAL 2048 \times 2048 CCD, with the pixels binned 2×2 , resulting in 1024 \times 1024 images. In the binned image, each pixel is $0''.3$. The overscan, bias, and flat field signatures were removed using standard IRAF techniques (the dark current was found to be negligible $< 10e^-/\text{pix}/\text{hour}$). Standard stars from both Odewahn et al. (1992) and Landolt (1992) were used for calibration.

The Palomar data were obtained with the Hale 200 in. (5.08m) telescope. Most of the optical images were obtained using a Tektronix 2048 \times 2048 CCD at the prime focus of the 5m, which provided a view of approximately $11' \times 11'$, using a Johnson V , and a Kron-Cousins I filter. Just under half of the images were obtained using the 4-Shooter camera, which employs four 800 \times 800 TI CCDs at the Cassegrain focus of the 5m, with a field of view of about $8.9' \times 8.9'$ and V and I filters from the WF/PC filter set. Both short (60s) and long (5 to 15min) exposures were obtained in each filter to increase the dynamic range of the data. The seeing

varied generally between $1''$ and $2''$ for most of the frames at both telescopes.

The raw CCD frames were bias subtracted, corrected for bad pixels, and flattened using routines within IRAF. Photometry and image profile information needed to discriminate between stars and galaxies were derived using routines within DAOPHOT. The images were calibrated using V and I frames of the same fields obtained with the KPNO 2.1 m and #1 0.9 m telescopes and the “Harris” $BVRI$ filter set. The $V-I$ colors for the small telescope frames, and hence for the 2048^2 images were placed on the Kron system via observations of Pleiades K and M dwarfs with published VRI (Kron) photometry (cf. Stauffer (1984)). The internal precision of the photometry ranges from ~ 0.01 mag for m_V or $m_I \simeq 18$ to ~ 0.1 mag at 22 magnitude. Based on comparison with previous photometry, we believe the systematic errors in our conversion to V and $(V-I)_K$ should be < 0.1 mag.

2.3 Photometric Reductions

Infrared sources were identified with *DAOfind*, and extracted with the aperture photometry routines in IRAF, after adjusting procedures and parameters carefully to maximize the signal to noise ratio for the Pleiades and Praesepe. Due to the crowded fields in the images of NGC 7160, the Point Spread Function (PSF) fitting routines of *DAOphot* were used to correctly determine the magnitudes for objects in these frames. In all cases the infrared frames easily reach $m_K \sim 18$ with a 1 sigma error of ~ 0.6 mag. However, the photometric sources of interest in this dissertation are no dimmer than $m_K \sim 15$ for which the 1 sigma photometric error is $\lesssim 0.05$ mag. We estimate our total RMS K error to be 10% when all factors are considered.

Due to the rather heavy crowding evident in the images of NGC 7160, all of

the data was extracted from the processed frames using the *DAOPhot* package from within IRAF. An object list was first created using *DAOfind*, and simple aperture photometry was computed for each source to serve as a first guess to the more complicated fitting routines. A set of more or less uncrowded stars were chosen for input into the point spread function (PSF) fitting routine. After the first guess PSF was generated, it was used to subtract off the nearest neighbors of the PSF stars, and a new PSF was fit from this neighbor-subtracted image. This second generation PSF was always able to cleanly subtract off the original PSF stars, and was subsequently used to generate instrumental magnitudes for all of the objects identified in the first step using *allstar*. Finally, an aperture correction was determined from an image with all of the stars *except* the PSF stars subtracted. The limits for each of the fields are: $m_K \sim 17.5, m_V \sim 21; m_I \sim 19$.

2.3.1 Celestial Coordinates

Coordinates for the infrared sources were derived in a two-step process. First, plate (x, y) coordinates of ~ 70 SAO stars surrounding the imaged fields were measured using the Grant Measuring Engine and POSS plates located at NOAO. The plate coordinates for a minimum of 3 stars identifiable in each infrared field were also measured. A transformation from plate coordinates (x, y) to celestial coordinates (ra, dec) was computed for the SAO stars. This transformation was then used to generate celestial coordinates for the 3 stars per infrared image. The total RMS error from this fit was $1''.3$. A separate transformation from array coordinates to celestial coordinates was computed for each infrared field based upon the previously calculated celestial coordinates of the 3 measured stars in each field. This transformation was then applied to each infrared source in the field.

RMS errors (when calculable) were typically $\lesssim 1''$. Coordinates for the V and I sources were computed using the known rotation and plate scale of the 4-shooter or prime focus camera plus positions of one or more brighter Praesepe member and/or HST GSC star that fell within the camera field of view. The infrared and CCD positions were overlaid and all sources detected at K and either V or I were extracted and used in the analysis.

2.4 Spectroscopic Observations

Spectra in the $2\mu m$ region of the ρ Ophiuchus sources were obtained with the Steward Observatory 2.3m Bok Telescope and the Multiple Mirror Telescope. M-dwarf comparison stars were observed with the 1.5m telescope. In all cases, we used the spectrometer known as FSPEC, described below, with its 75 l/mm grating, providing a spectral resolution $\lambda/\Delta\lambda = 800$. The observations of the ρ Ophiuchus sources were carried out on 1993 May 9-11, 1994 May 23, 1994 July 19, and 1995 April 10, and all the field stars except vB 10 were observed on 1993 September 7-8. Observations of vB 10 were made on 1993 October 29.

We have also obtained near infrared spectra (J -band) of brown dwarf candidates 1 and 2 of Stauffer et al. (1989) on the Multiple Mirror Telescope on 11 December, 1989, and of candidate 6 on 3 October 1993. We used the Steward Observatory germanium diode spectrometer (GESPEC) with a 150 l/mm grating and a $3''$ entrance aperture, giving a Nyquist-sampled resolution of $\lambda/\Delta\lambda = 200$.

2.4.1 J -band Spectra of Pleiades Sources

2.4.1.1 GESPEC

GESPEC is an infrared, cryogenically-cooled, grating spectrometer that uses two 32 element linear arrays of germanium diodes as detectors, read out by JFET integrating amplifiers. The combination provides read-noises of $\sim 100e^-$, quantum efficiencies greater than 50% between $0.9\mu m$ and $1.5\mu m$ and dark currents below $10e^-/s$. The incoming light is projected onto the two detector arrays through round apertures that have diameters of $2''$ and are separated by $22''$. The individual pixels fill this aperture, so the noise is not degraded by a necessity to combine pixels into a single resolution element. Two gratings provide resolutions of ~ 400 and ~ 1500 ; even at high resolution, the instrument operates near the photon background limit over much of its spectral range.

2.4.1.2 GESPEC data acquisition and reduction

Data were obtained by centering the sources in one of the instrument apertures. After an exposure of typically 60s, the telescope was wobbled to center the object in the other aperture, and a second exposure was obtained. The sequence was repeated. This strategy provides virtually a 100% exposure time efficiency, while monitoring the sky continuously, to minimize the effects of rapid variations in the airglow lines on the final sky-subtracted spectra. The observation sequence was continued until adequate signal to noise ratios had been obtained.

The data reduction is straightforward. Up to the final stage of the data processing, the data from each array are reduced independently. After eliminating deviant readouts, we subtract the sky using the average of adjacent wobbling cycles. This procedure leaves us with a number (typically 3 to 15) of sky-subtracted spectra which are then scaled to the average of their median pixel values and co-added. Co-adding these spectra gives us a good opportunity to estimate the

noise in the combined spectrum by calculating the formal variance of the readouts at each pixel. Subsequently the same procedure is repeated for a bright “flat-field” star near the program object. Ideally, this star should have a featureless spectrum in the spectral range of interest; we chose solar-type stars close to the Pleiades on the sky. This stellar spectrum is used both to flat-field the object spectrum by correcting for pixel-to-pixel variations in the detector sensitivity and to remove atmospheric absorptions. Finally, the flat-fielded spectra from the two detector arrays are combined into a single spectrum.

2.4.2 *K*-band Spectra of ρ Ophiuchus Sources

2.4.2.1 FSPEC

FSPEC is an infrared, cryogenically-cooled, grating spectrometer that has been designed for use at many of Steward Observatory’s telescope facilities, including the future MMT upgrade and Large Binocular Telescope. It currently uses of a NICMOS3 array of 256×256 $40\mu m$ HgCdTe detectors, but can easily accept larger arrays, or arrays with different spectral responses (the optical design is achromatic in the range $1.4 < \lambda(\mu m) < 5$). The detector array has read noise of $\sim 25e^-$ rms and a dark current of about $1e^-/sec$. The design is relatively compact to allow cooling with liquid nitrogen, yet it offers a moderately long slit and high spectral resolution. Stray light is reduced by the presence of a Lyot stop at a cold pupil, an important consideration for IR spectrometers running at cryogenic temperatures. Currently, the instrument has 2 gratings that are enclosed in a drum that can hold 2 pairs of back-to-back gratings, or 1 pair of gratings and a silicon immersed grating. A 75 l/mm grating blazed at $4.75\mu m$ covers the *K*, *H*, and *J* windows

in 2nd, 3rd, and 4th orders respectively at a resolution of $\lambda/\Delta\lambda \sim 800$ (Nyquist sampled); the orders are nearly centered on the atmospheric windows and the spectrometer covers virtually all of each window in a single setting (although the silicon optics will reduce the coverage at J). The second grating has 600 l/mm and is blazed at $2.5\mu m$; it provides a resolution of ~ 3000 . The grating drum is driven by a worm gear and is preloaded with a torsional spring against the worm, which is in turn spring loaded against its thrust bearing. Total backlash in the drive is ~ 1 pixel as measured by comparison lamp lines at the array.

2.4.2.2 FSPEC Spectral Reductions

The spectra were reduced using IRAF tasks and specially designed IRAF scripts. Sky emission lines were removed from our spectra by subtracting from each frame the average of the adjacent ones in time. Atmospheric absorption features were eliminated by ratioing the spectra to those of bright B to G-type stars, observed close to our sources in both position and time and reduced by an identical procedure. At our resolution and signal to noise, the only noticeable intrinsic feature of these comparison stars in the $2\mu m$ region is the strong Brackett γ absorption at $\lambda = 2.166\mu m$, which produces a false Br γ emission in the spectra presented in this paper. The resulting spectra were wavelength calibrated using OH sky emission lines (Oliva & Origlia (1992)). The spectra of the Ophiuchus sources are shown in Figure 5.2. All spectra have been smoothed to a resolution of $\lambda/\Delta\lambda \sim 175$ to increase the ratio of signal-to-noise. The noise increases for wavelengths longer than $\sim 2.25\mu m$ because of emission from thermal background.

Chapter 3

PRAESEPE

3.1 Introduction

The first cluster analyzed using our photometric technique is Praesepe (M44, NGC 2632). Praesepe is an ideal candidate on which to test our method for many reasons. It is relatively close (159pc) and virtually free of reddening, so the cluster members should be bright and restricted to a small portion of the sky. Additionally, there should be no confusion due to variable reddening of different sources. Praesepe is located high above the Galactic plane at $b^{\text{II}} = 32^{\circ}5$, thus limiting the number of background sources which could mistakenly be identified as cluster members. Finally, Praesepe is a older open cluster. At 700 Myr (Mermilliod (1981b)) it is the oldest cluster which will be examined in this dissertation. The advanced age eliminates the need to rely on theoretical isochrones of young low mass objects, since all of these objects should be on, or very near, the Main Sequence. In addition to the physical properties of the cluster itself, there are also two photographic proper motion studies in the literature, Jones & Stauffer (1991)

and Hambly et al. (1995), which serve as excellent comparisons to our technique.

3.2 Analysis

3.2.1 Extraction of Praesepe Members

Figure 3.1 shows the m_V , $V-K$ color-magnitude diagram for all sources within the 290 arcmin^2 sample area. We also plot a young disk main sequence, estimated from local stars, shifted to the distance of Praesepe (159 pc) as a solid line, based on Table 6 from Leggett (1992). For reference, GL406 and VB8 (Berriman & Reid (1987)), shifted to the distance of Praesepe, are included as well. Various isochrones are plotted over the same magnitude and color range in the analysis of similar data for the Pleiades in Figure 4.8.

The upper detection limit in Figure 3.1 is due to CCD saturation for sources brighter than $m_V \sim 17$. The remainder of this chapter will be based on sources with $m_V > 17$, which at the distance of Praesepe corresponds to stars with $M < 0.4M_\odot$. The diagonal lower limit is a combination of the m_V and m_K detection limits of 22 and 18 respectively. For a given spectral type, changes in distance move points vertically in Figure 3.1. Therefore, the great majority of stars, which fall below the Praesepe main sequence for their colors, are dwarfs that lie behind the cluster. There may be a contamination of these counts by red giants at much greater distances than the dwarfs; however, because Praesepe is at relatively high Galactic latitude ($32^\circ 5$), this contamination should be very small.

Based upon our estimates of the photometric errors, on the diameter of Praesepe, and on the uncertainty of the distance to Praesepe, we estimate that any object within 0.45 magnitudes of the solid line in Figure 3.1 could be a member

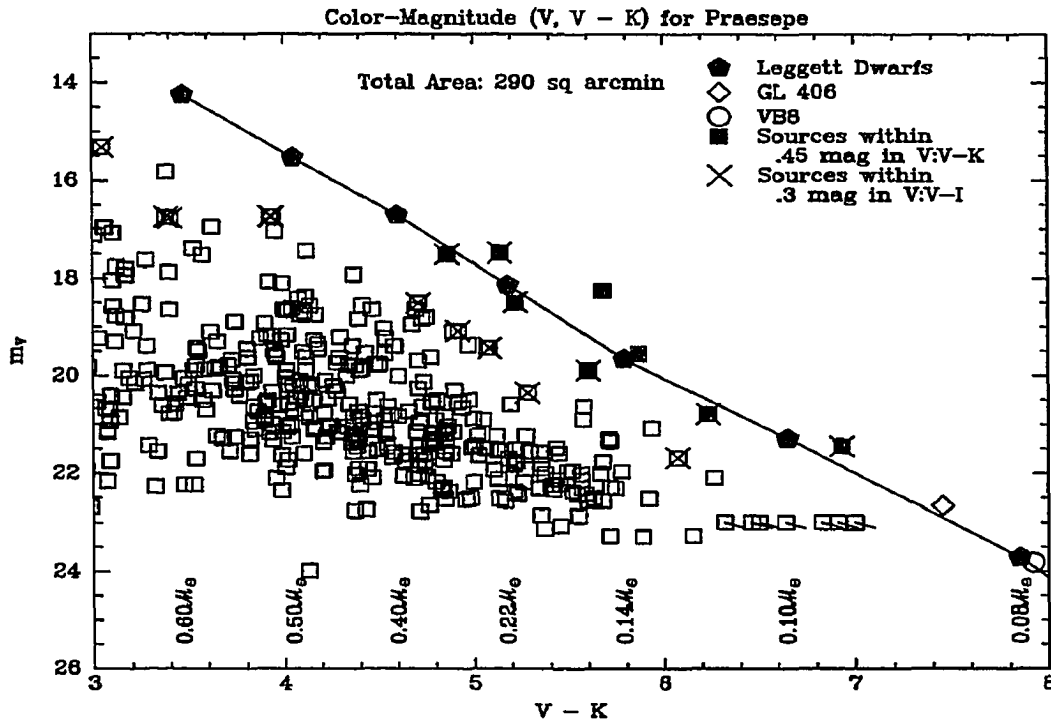


Fig. 3.1.— Color-Magnitude (m_V , $V-K$) Plot for Praesepe.

Solid line shows a young disk sequence from Leggett (1992). Filled squares are within 0.45 mag of the m_V , $V-K$ Main Sequence. Squares with a cross are within 0.3 mag of the m_V , $V-I$ Main Sequence. The only upper limits included in this plot (near $m_V \sim 23$, $V-K \sim 6.5$) are those that fall within 0.45 mag of the m_I , $I-K$ Main Sequence.

of the cluster. Objects that meet this criterion are shown as filled squares in the $m_V, V-K$ diagram of Figure 3.1, and in the $V-I, I-K$ color-color diagram of Figure 3.2. Squares (open or filled) with a cross through them are sources which lie within 0.3 magnitudes of the $m_V, V-I$ main sequence (see Figure 3.4). In Figure 3.2 the stars selected from $m_V, V-K$ diagram all fall close to the expected isochrone except for one which is more than 0.5 mag removed. We draw attention to the excellent separation of background stars from the Praesepe main sequence in the $m_V, V-K$ diagram.

Although our V detections do not extend below $\sim 0.1\mathcal{M}_\odot$, in $m_I, I-K$ our survey should be complete for Praesepe members with $0.08 < m(\mathcal{M}_\odot) < 0.4$. Figure 3.3 is an $m_I, I-K$ color-magnitude diagram of all of our detections. The previously identified 8 sources are drawn as filled squares. All sources within 0.45 magnitudes of the $m_I, I-K$ Praesepe main sequence with $m_I < 19$ were either previously identified as Praesepe members or have m_V magnitudes which preclude them from Praesepe membership. We therefore conclude that we have not missed any sources more massive than $M = 0.08\mathcal{M}_\odot$. The previously identified source at $m_I \sim 16.5$ $I-K \sim 2.15$ appears to have an anomalous m_I color and is eliminated from further consideration.

Figure 3.4 is an optical color magnitude diagram ($m_V, V-I$). Symbols are the same as in Figure 3.1. There appears to be a clean separation of background stars from cluster members in the plot. However, even with a tighter selection criterion (0.3 mag compared to 0.45 mag) roughly half of the cluster members that would be identified using this plot alone are objects which are clearly identified as background stars in Figure 3.1.

It is tempting to base low mass star investigations on colors redder than V

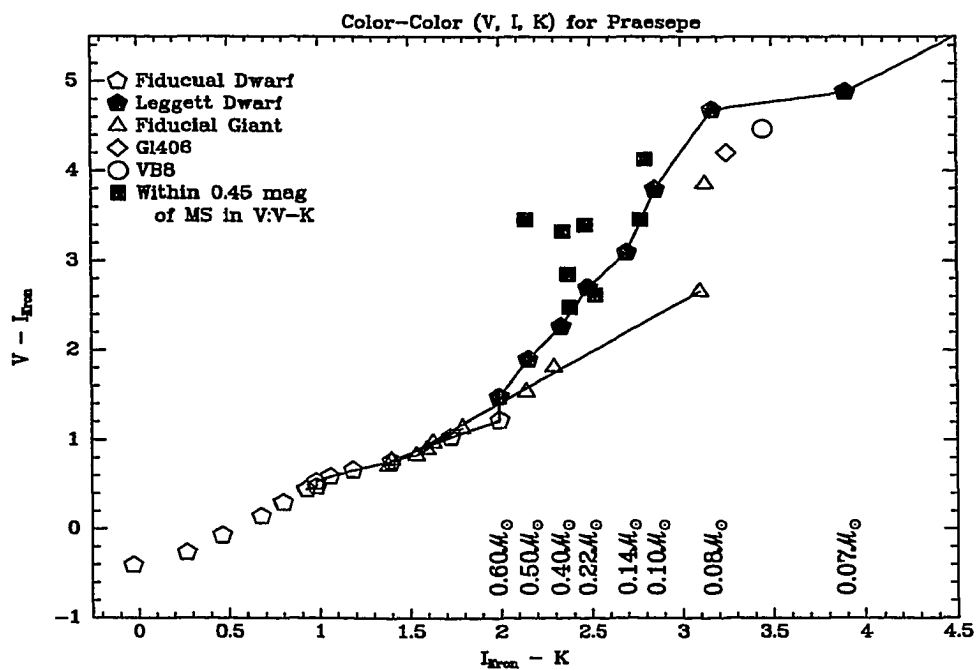


Fig. 3.2.— Color-Color ($V-I, I-K$) Plot for Praesepe.
Only those points within 0.45 magnitudes of the $m_V, V-K$ Praesepe Main Sequence are included.

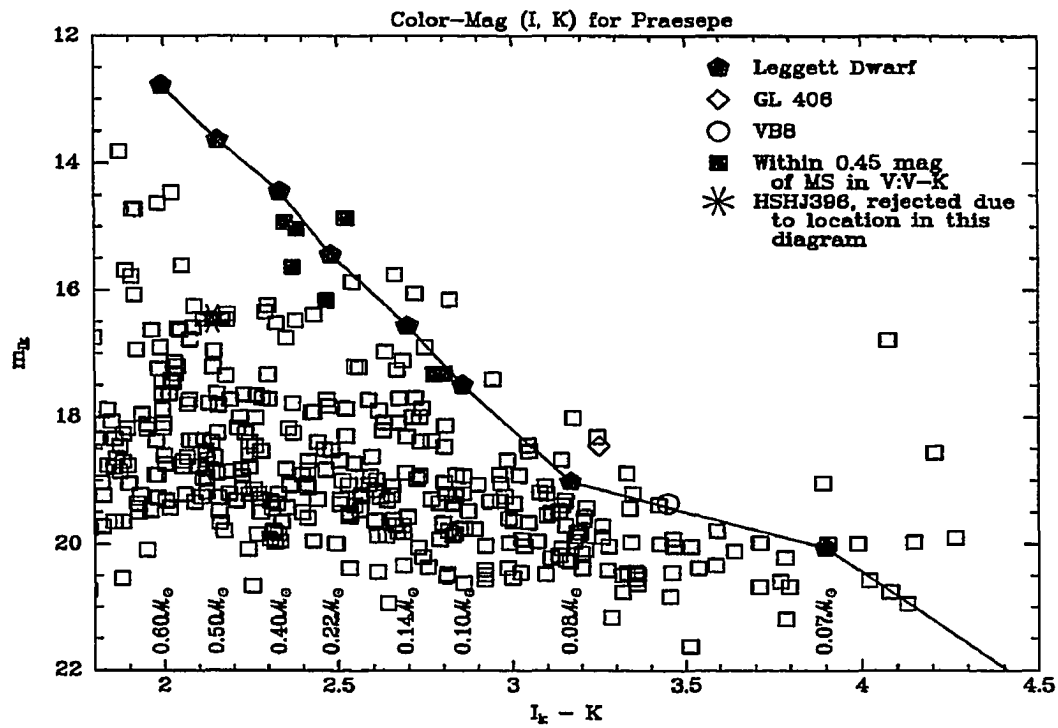


Fig. 3.3.— Color-Magnitude (m_I , $I-K$) Plot for Praesepe. Solid line indicated the ZAMS of Leggett (1992). Solid points are within 0.45 mag of Main Sequence in m_V , $V-K$. All detections within 0.45 mag of the m_I , $I-K$ Main Sequence with $m_I < 19$ were either picked up or ruled out in the m_V , $V-K$ diagram.

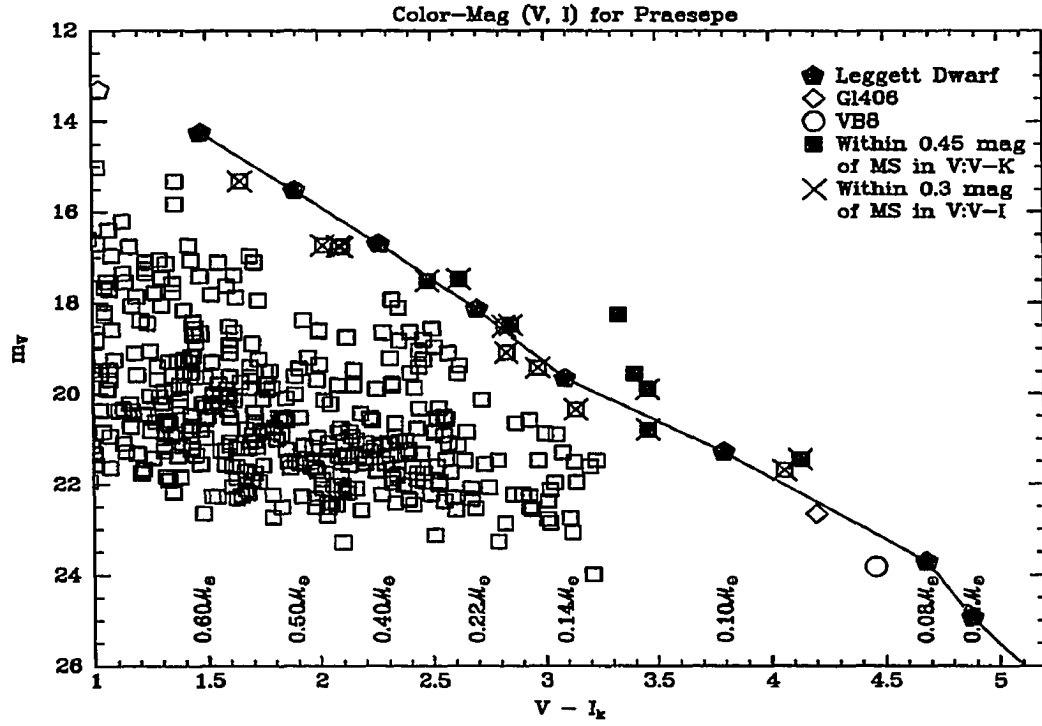


Fig. 3.4.— Color-Magnitude (m_V , $V-I$) Plot for Praesepe. Filled squares are within 0.45 mag of the m_V , $V-K$ Main Sequence. Squares with a cross are within 0.3 mag of the m_V , $V-I$ Main Sequence.

because cool objects should be more easily detectable in that manner. However, we find that separation of cluster members from the background population is compromised unless the full V to K baseline is utilized. This point is illustrated by comparing Figures 3.1 and 3.3; in the m_I , $I-K$ diagram the background stars are not well separated from the cluster main sequence. Alternately, because of the mature large format optical detector technology, many studies have been based on V and I photometry. Our results show that these colors produce samples that are still modestly contaminated by background stars. However, intermediate colors are useful for consistency and completeness tests.

The contamination level from background and foreground objects in this sample can be estimated from reference fields located at -24° galactic latitude imaged at V , I , and K for comparison with the Pleiades and analyzed using techniques identical to those used for Praesepe (galactic latitude $+32^\circ$). We find zero stars in the reference fields that pass all the tests that would have led us to associate them with Praesepe. The reference area contained 150 arcmin^2 . A second class of contamination is from true low mass stars not associated with Praesepe which happen to be located within the sampled volume. Using the luminosity function of Henry & McCarthy (1992) for stars within 8pc, and a scale height of 350pc (Reid & Majewski (1993)), we expect to find 1 non-Praesepe low mass interloper with $11 < M_V < 16$ in the sampled volume. Therefore, we conclude that 6 of the 7 stars we have identified in Praesepe are probable members of the cluster with masses between $0.4\mathcal{M}_\odot$ and $0.08\mathcal{M}_\odot$. These sources are listed in Table 3.1. Future improvements to this data set include obtaining reference fields which are closer to Praesepe, and imaging a larger fraction of the cluster.

3.3 Comparison to Other Work

Hambly et al. (1995) (HSHJ) imaged 19 square degrees in Praesepe and used proper motions within this field to identify cluster members. All of our imaged fields fall within their covered area, and our positions agree to $\sim 2''$. Three of our sources (WRS1, WRS3, and WRS5) appear in HSHJ (see Table 3.1 for HSHJ ID numbers). Four of our sources did not show up in HSHJ. Three of these missing sources (WRS4, WRS6, and WRS7) are faint and may be below their completeness limit. The remaining source, WRS2, is bright enough to have shown up in HSHJ, but there is nothing at the appropriate coordinates. In the other direction, there were seven sources in HSHJ which fell within our imaged area. Three of these were identified above. Another three (HSHJ245, HSHJ247, and HSHJ265) were too bright and would not have been included in our survey. The final HSHJ source, HSHJ396, was the source rejected because of its anomalous color in Figure 3.3. Within the limits imposed by area and sensitivity, our surveys agree well and produce similar samples, despite the different selection techniques.

The luminosity function for the relatively bright stars in Praesepe has been determined by Jones & Stauffer (1991), who used a combination of photometry and proper motions to identify members of the cluster. Figure 3.5 shows their LF as a bargraph, scaled to an area of 1 square degree. The decrease at the faint end of their LF is an artifact of the completeness limit, and Jones & Stauffer (1991) claim that their LF is still rising at the limit of their survey. The 6 sources identified in this chapter have been scaled to 1 square degree and are grouped together in one bin from $M_V = 11$ to $M_V = 16$. This point is plotted as a diamond in Figure 3.5. The vertical error bars are based on Poisson counting statistics in each bin; the horizontal error bars represent the binning size of our sources. For comparison, the luminosity functions for the Hyades (Reid (1993)) and the Pleiades (Hambly et al. (1991)), scaled to match at $M_V = 7$, are also shown. The latter data have been

transformed from M_I as described in Reid (1993).

The LF of Figure 3.5 has been converted to the Mass Function (MF) of Figure 3.6. The absolute V magnitudes from Jones & Stauffer (1991) were converted to masses using Henry & McCarthy (1993). Our sources were transformed from Figure 3.5 using the same method and are plotted as the diamond in Figure 3.6. The vertical error bars are based on Poisson counting statistics in each bin; the horizontal error bars represent the binning size of our sources. The dashed line is a power law fit to all the data excluding the last bin of Jones & Stauffer (1991). The least squares best fit is $N(m) = 19.54 \times m^{-1.34 \pm 0.25}$. There is no turnover towards low masses apparent in these data.

3.3.1 Dynamical Evolution of the Mass Function

The process of evaporation of stars from a cluster was originally discussed by Ambartsumian (1938), Ambartsumian (1985) and Spitzer (1940). Within the cluster, encounters between stars will tend to produce a Maxwellian velocity distribution. From the virial theorem, under equilibrium the mean kinetic energy of a cluster star is one half the potential energy of the cluster per star, and one fourth the mean potential energy of the cluster stars (Spitzer (1940)). Therefore, any star with the mean potential energy but a velocity more than twice the mean will escape. As a result, stars in the high energy tail of the Maxwellian distribution will continuously evaporate away from the cluster at the rate of $\sim 0.7\%$ per cluster relaxation time, T_r , which is a measure of the time required for deviations from a Maxwellian distribution to be significantly decreased. Binney & Tremaine (1987) show that the relaxation time can be written as:

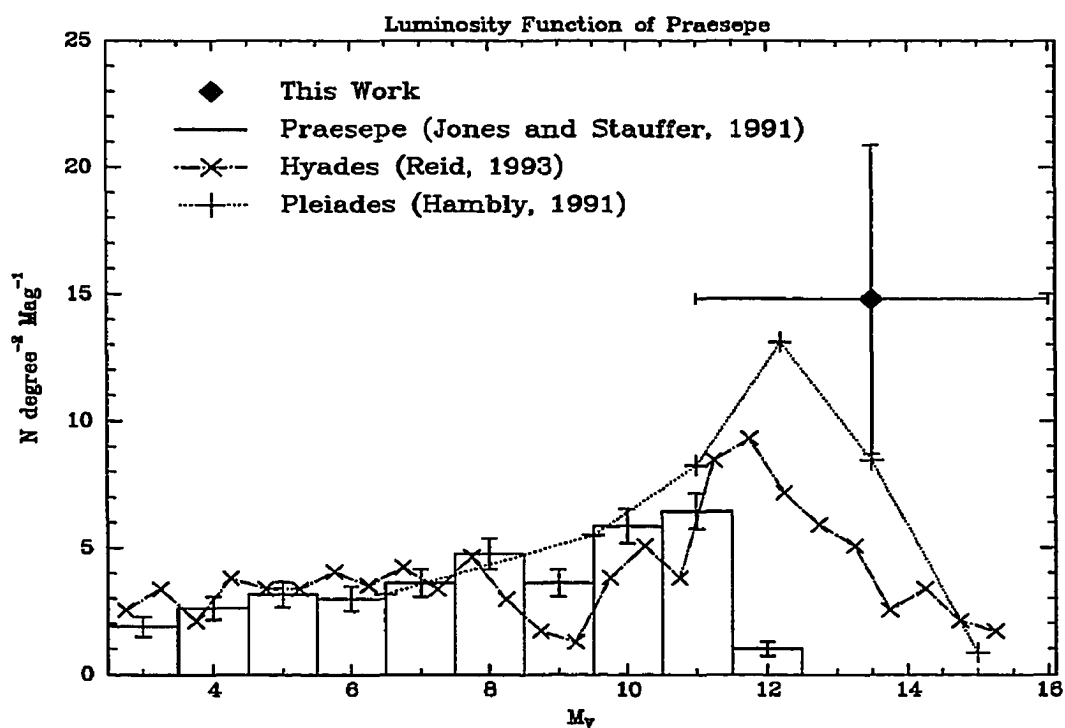


Fig. 3.5.— Luminosity Function of Praesepe.

Values below $M_V = 13$ are taken from Jones & Stauffer (1991). Their data point at $M_V = 12$ is incomplete, an artifact of the completeness limit; however, the authors claim that their LF is still rising at the limit of their survey.

Table 3.1. Candidate Praesepe Low Mass Stars

Number	RA ^a	DEC ^a	m_K ^b	M_V ^b	$V-K$ ^b	$V-I$ ^b	$I-K$ ^b	m ^c	HSHJ ^d
								$m(M_\odot)$	ID
WRS1	08:34:13.94	19:27:27.6	13.27	12.48	5.22	2.85	2.37	0.23	151
WRS2	08:34:35.26	20:04:41.5	12.65	11.50	4.86	2.48	2.38	0.33	...
WRS3	08:35:45.60	19:26:01.9	12.34	11.47	5.14	2.62	2.52	0.39	212
WRS4	08:36:20.63	19:40:53.6	14.56	14.78	6.23	3.46	2.77	0.13	...
WRS5	08:36:38.80	20:08:52.0	12.58	12.25	5.68	3.33	2.35	0.35	267
WRS6	08:38:42.44	19:36:09.3	14.52	15.44	6.93	4.13	2.80	0.13	...
WRS7	08:39:12.66	19:43:27.5	13.69	13.55	5.87	3.40	2.47	0.18	...

^aAll coordinates are for the 1950.0 equinox

^b10% error

^cusing the $M_K - m$ relationship of Henry & McCarthy (1993)

^dHambly et al. (1995)

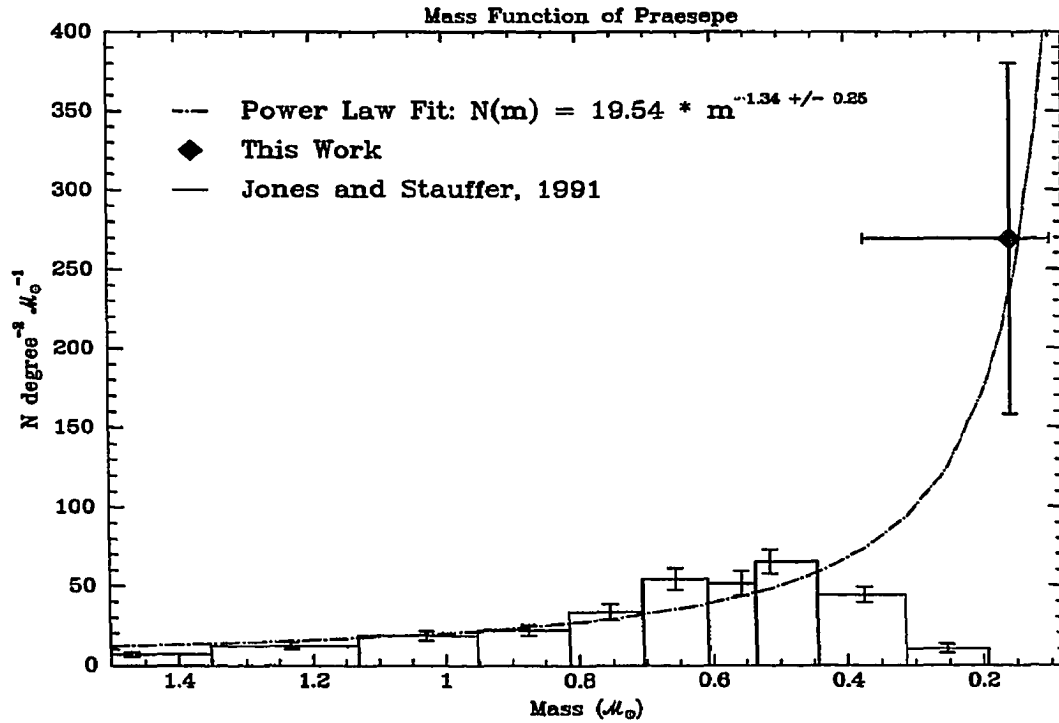


Fig. 3.6.— Mass Function of Praesepe.

Figure 5 was converted to a mass function using Henry & McCarthy (1993). The least squares best fitting power law has a slope $\alpha = -1.34 \pm 0.25$.

$$T_r = \frac{0.1N}{\ln N} t_{cross} \quad (3.1)$$

Here, N is the total number of stars in the cluster, and t_{cross} is the crossing time of a star across the cluster. Binney & Tremaine (1987) also show that an upper limit to the lifetime of any bound stellar system due to evaporation is $T_{evap} = 136T_r$. For Praesepe, this rough upper limit is of the order of 10^{10}yr , using appropriate values ($N \sim 800$; $t_{cross} \sim 5 \times 10^6\text{yr}$).

Due to equipartition, the low mass members of the cluster will have the highest velocities and hence will evaporate the most quickly and the heavier stars will slow down and sink towards the center. An estimate of the half-mass relaxation time (T_{rh}) that characterizes this process of mass segregation has been put into a convenient form by Spitzer (1987) based on an 'idealized' cluster:

$$T_{rh} = \frac{2.05 \times 10^6 [r_h(\text{pc})]^{3/2} N^{1/2}}{[\langle m \rangle (\mathcal{M}_\odot)]^{1/2} \ln N/2} \text{yr}. \quad (3.2)$$

Here, r_h is the radius containing half the mass of the cluster, N is the total number of stars all of which have mass $\langle m \rangle$. T_{rh} is uncertain because of its dependency on the mass function for the cluster members through both N and $\langle m \rangle$, and because of the assumption of a single stellar mass. However, the range of plausible values ($r_h \sim 6\text{pc}$, $N \sim 800$, $\langle m \rangle \sim 0.5\mathcal{M}_\odot$) for Praesepe places $T_{rh} = 10^8$ years within a factor of two. If the age of Praesepe is 7×10^8 yr (Mermilliod 1981), the cluster has gone through about 2.5 to 10 half mass relaxation times. One might expect a significant fraction of the low mass members of the cluster to have escaped or moved to the outer parts of the cluster over this many half-mass relaxation times, but more detailed calculations show that the process is relatively slow and spread over a range of masses.

As discussed by Spitzer (1940), equipartition will be achieved by the massive members of the cluster in a relaxation time or less. However, for low mass stars, acceleration to full equipartition velocities is a result of many distant encounters and requires a time substantially in excess of the half-mass relaxation time (see eqn (48) in Spitzer (1940) and the discussion following it). Therefore, the evaporation of even very low mass members of the cluster will occur over a number of half-mass relaxation times, with a gradual flattening of the mass function as low mass members are lost preferentially. Johnstone (1993) describes numerical simulations of this process in globular clusters (see also Lee et al. (1991)). These simulations are more applicable to this discussion because a range of stellar masses was included in the simulations, as well as simplified effects of stellar evolution. Taking the example of NGC 6572 from Johnstone (1993) (which is the most similar to the deduced current-day mass function for Praesepe), a power law initial mass function ($N(m) \propto m^\alpha$) will retain approximately a power law character but will flatten with age; an initial index of -2.2 will increase to ~ -2 after two half-mass relaxation times and to ~ -1.7 after eight.

Simulations for open clusters have been computed by Terlevich (1987) who included a power-law mass spectrum and the effects of stellar evolution. The basic physics should be similar; but, because of its lower mass and weaker gravitational field, an open cluster should be more strongly affected by tidal forces from the galaxy than are globular clusters. In addition, the dominant effect leading to stellar ejection is probably single close encounters, particularly of members with widely differing masses. Tides will reduce the potential energy barrier for escape. However, since most escapes occur from interactions in the cluster core and the relative change in escape velocity from the core is small, it can be expected that there will be no qualitative change due to this cause from the behavior calculated

for globular clusters. A second effect of tides is to increase the angular momentum dispersion of the more distant, low mass members of the cluster, preventing them from returning to the central regions and leading to increased mass segregation and depletion of the cluster core of low mass stars (Terlevich (1987)). By reducing the number of encounters of low mass stars with high mass ones in the core, this mechanism may slow down the dynamical evolution of the cluster mass function. Terlevich's (1987) calculations show only a modest flattening of the mass function due to loss of low mass cluster members over the relevant timescales; the behavior is qualitatively similar to that found for NGC 6572 by Lee et al. (1991). Further theoretical studies of open cluster dynamics would be desirable to define this behavior better.

3.3.2 Limits to the Dynamical Evolution

Given the observational uncertainties in the parameters that control the relaxation time, plus the theoretical uncertainties in the effects of the Galactic tidal forces, it is of interest to see if a significant level of dynamical evolution has occurred in the mass function of Praesepe. Because there are no adequate determinations of the initial mass function for open clusters, we must assume that the IMF of field stars is characteristic also of open clusters.

However, there is not only substantial controversy about the slope of the field star IMF in the range $0.08 < m(\mathcal{M}_{\odot}) < 0.5$, there is disagreement about whether a power law is even a useful model. Tinney (1993) found significant structure in the IMF of low mass stars identified in the POSSII and UKSRC surveys. The most obvious structure is a pronounced turnover at $\sim 0.25\mathcal{M}_{\odot}$, followed by an upturn for $0.08 < m(\mathcal{M}_{\odot}) < 0.1$. He concluded that the resulting distribution was poorly

modeled by a single power law. However, at the resolution of our study, a power law fit with a slope of ~ -1 would be an adequate representation of Tinney's data. Henry & McCarthy (1992) were able to fit a power law to the MF of low luminosity companions of nearby M dwarfs. The slope of their mass function was -0.80 , and they concluded that the MF is undoubtedly rising to the end of the main sequence. Basu & Rana (1992) find some evidence for structure but again a power law with slope ~ -1.25 is an adequate approximation at the resolution of our work. An approximate fit to the various proposed forms of the local IMF (Scalo (1986), Basu & Rana (1992)) is a broken power law with a slope of -1.25 for stars with $m < 0.6\mathcal{M}_\odot$ and a slope of -2.7 for stars with $m > 0.6\mathcal{M}_\odot$. We have tested whether the data for Praesepe are compatible with this fit. The results are shown in Figure 3.7. While the reduced χ^2 for the broken power law fit is larger than the reduced χ^2 for a power law, the broken power law is still consistent with our data.

We find that the MF for Praesepe is well fit by a single power law from $0.08 < m(\mathcal{M}_\odot) < 1.4$ whose slope is -1.34 . This slope is larger than that found for field stars by Henry & McCarthy (1992), but is consistent with that value within the relatively poor statistics of our study. Both values are less than the classic value of -2.35 from Salpeter (1955). We conclude that evaporation of low mass stars has not had any dramatic effect on the MF of Praesepe. The poor statistics of our data do not allow a test of subtle effects from evaporation, but they do let us conclude that nothing drastic has occurred beyond the theoretical predictions.

3.4 Conclusions

We have used optical and infrared photometry to identify 6 stars that we believe have very low mass and are members of the Praesepe cluster. The faintest

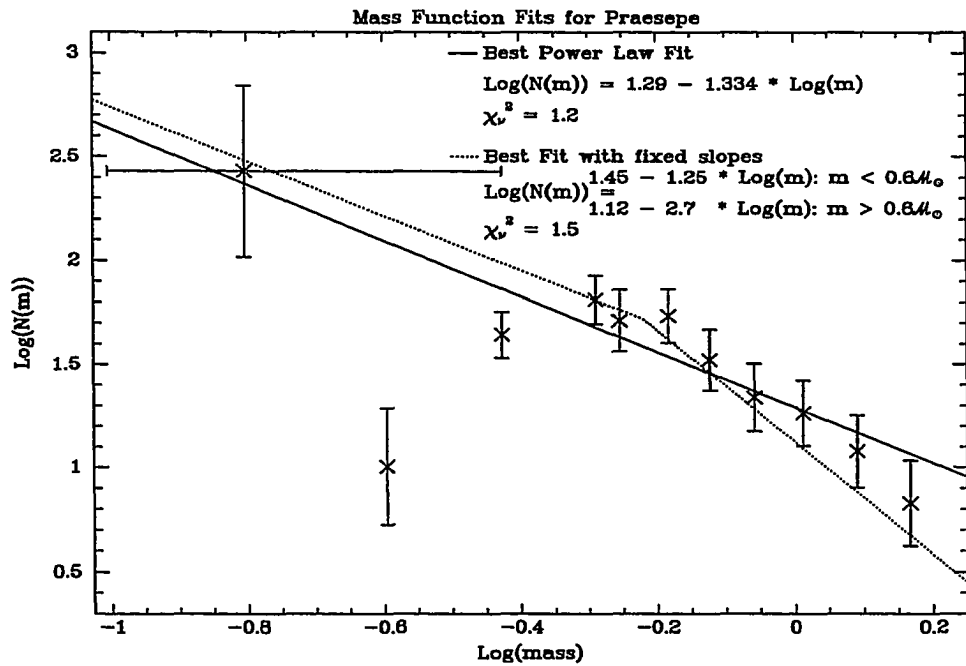


Fig. 3.7.— Mass Function Fits for Praesepe.

Solid line shows a power law fit, dashed line shows a broken power law fit which is an approximation to the local IMF of Scalo (1986) and Basu & Rana (1992).

members have masses near $0.10\mathcal{M}_{\odot}$. The Mass Function for Praesepe continues to rise at these masses and shows no sign of a turnover towards lower masses; it agrees well with the field star mass function. We conclude that evaporation of low mass stars has not occurred by a substantial amount in Praesepe.

Chapter 4

THE PLEIADES

4.1 Introduction

Despite years of effort, the search for brown dwarfs has been mostly a failure (see Stevenson (1991) and references therein). This lack of success is mostly in searches for brown dwarfs as binary companions to higher mass stars. We have chosen a different approach. Our goal is to locate single brown dwarfs as members of a young, nearby, relatively rich, unembedded cluster. This chapter reports a deep optical/infrared search for such objects in the Pleiades.

The most difficult part of a cluster survey for low mass (hence dim) members is determining membership probabilities. Classical methods for determining membership probabilities are based on proper motion studies and spectroscopic followup. However, for the very low luminosity sources this method is impractical because existing first epoch plates do not reach faint enough magnitudes. Chapter 3 discussed a photometric technique using a very large wavelength baseline (V ($0.55\mu m$) to K ($2.22\mu m$)), that is efficient, complete, and reliable. We have used

this same approach in the work reported here.

Stauffer et al. (1989) (SHPRM) imaged $\sim 900 \text{ arcmin}^2$ of the Pleiades at V and I , with followup K photometry of a very few members. They identified 12 Pleiades brown dwarf candidates. To extend this survey to lower masses, we have added K photometry of 300 arcmin^2 of this region, plus 100 arcmin^2 of new V , I , and K data. In addition, we report new K photometry of two additional sources from SHPRM.

4.2 Analysis

4.2.1 Extraction of Pleiades Members

Figure 4.1 shows the m_V , $V-K$ color-magnitude diagram for our data. We also plot a young disk main sequence at the distance of the Pleiades (126pc), based on Table 6 of Leggett (1992), as a dashed line. The isochrone for stars and substellar objects at the age (taken to be 70 Myr) and distance of the Pleiades is indicated by the dotted line. This line is based on theoretical calculations provided by W. B. Hubbard (private communication) which in turn are based on Model X of Burrows et al. (1993). The theoretical effective temperatures were converted to photometric colors by applying the work of Kirkpatrick et al. (1993) to relate T_e to M dwarf spectral type. Colors for the appropriate M dwarfs in the Cousins system were taken from Leggett (1992); we assumed that the colors of pre-main-sequence objects would be identical to those of M dwarfs of identical effective temperature. This procedure provides an observationally based set of colors and absolute magnitudes even for objects with masses well below the bottom of the main sequence, since at the age of the Pleiades these objects have not yet cooled below the temperatures

of evolved M dwarfs. We have indicated the masses of objects along the Pleiades isochrone.

A number of general features of Figure 4.1 need comment. Because the CCD saturated above $m_V = 17.5$, we base the following discussion on sources with $m_V > 17.5$. For the Pleiades, $m_V = 17.5$ corresponds to a star of $M = 0.25M_\odot$, so our discussion will include no stars more massive than this value. The boundary to the distribution of detected sources extending from $m_V = 19.5$, $V-K=2$ to $m_V = 24$, $V-K=6.5$ arises from the K detection limit of $m_K \sim 17.5$. We believe the survey is complete for $m_K \lesssim 17$. The V limit of the survey is $m_V = 22.5$ to 23. However, where a K detection was achieved, we examined the CCD frames for a faint source below the limit for independent detection. We believe a typical limit for source detection at K is $m_V = 23.5$. Sources not detected at V but detected at K or at I and K are shown as upper limits corresponding to $m_V = 23.5$ with tails extending in the direction they would move as m_V is made larger than 23.5. For a given spectral type, changes in distance move points vertically in Figure 4.1. Therefore, the great majority of stars, which fall below the Pleiades isochrone for their colors, are dwarfs that lie behind the cluster. There may be a contamination of these counts by red giants at much greater distances than the dwarfs; however, because the Pleiades are at relatively high Galactic latitude (24°), this contamination should be very small. Stars far above the isochrone are likely to be foreground dwarfs. Based on the counts of stars within 8pc by Henry & McCarthy (1992) with $11 < V < 18$, we estimate that there should be about 1 low mass dwarf between us and the cluster; 4 stars appear well above the Pleiades isochrone, in rough agreement with this expectation.

We draw attention to the excellent separation of the background stars from the

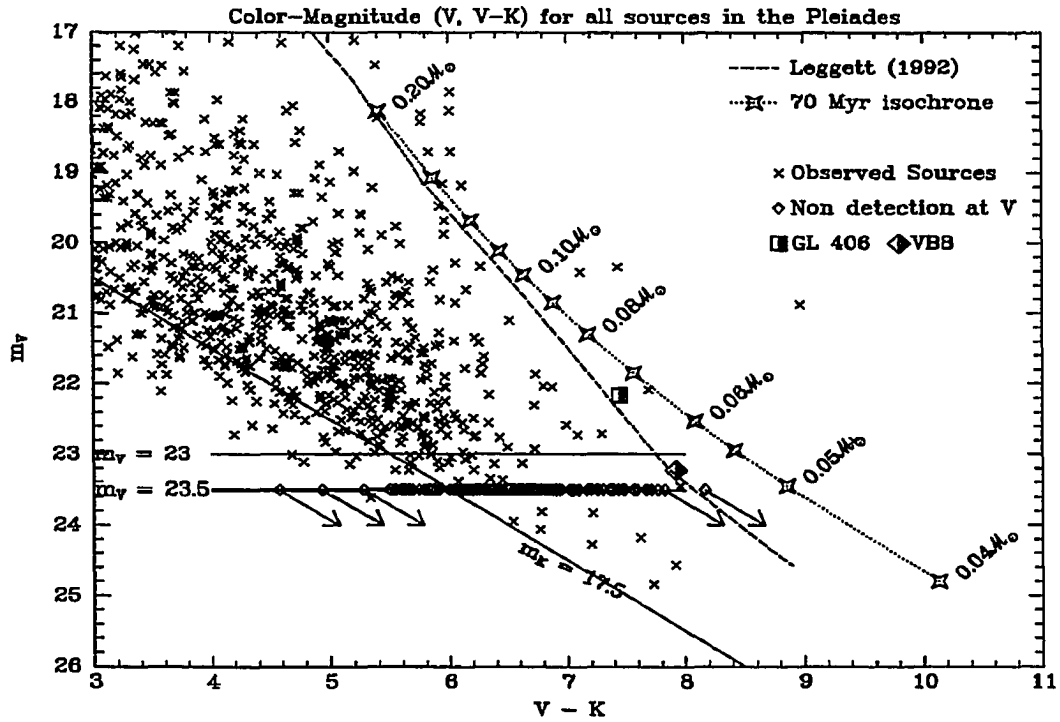


Fig. 4.1.— Color-Magnitude m_V , $V-K$ for the Pleiades. All sources are plotted. Dashed line shows a young disk sequence from Leggett (1992). Dotted line is the adopted 70 Myr isochrone from Burrows et al. (1993). Upper limits are shown with tails.

Pleiades isochrone in the m_V , $V-K$ diagram. It is tempting to base low mass star investigations on colors redder than V because cool objects should be more easily detectable in that manner. However, we find that separation of cluster members from the background population is compromised unless the full V to K baseline is utilized. This point is discussed in more detail in Chapter 3.

Based on our estimates of photometric errors, on the diameter of the Pleiades, and on the uncertainty of the distance to this cluster, we estimate that any object within 0.35 magnitudes of the isochrone in Figure 4.1 could be a single-star member of the cluster. Unresolved double stars of equal magnitude could lie as far as 1.15 magnitudes above the isochrone. Objects that meet the $+1.15, -0.35$ magnitude criterion are plotted on a $V-I$, $I-K$ color-color diagram in Figure 4.2. In addition to objects with full V , I , and K detections, we also include an object without V information, shown as the appropriate limit. This is the second reddest limit shown in Figure 4.1, which is just outside the selection band, but the sense of the limit quickly makes it a candidate.

In Figure 4.2, the solid line is the locus of dwarfs, from Leggett (1992) (given the way we estimate the colors of Pleiades members, they should fall on this line). The dashed line shows the locus of red giants. With the exception of two objects, the potential Pleiades members all fall on the dwarf locus within the photometric errors, which is consistent with their being true cluster members. The two exceptions ($I-K \sim 3.0$, $V-I \sim 2.75$, $m_V \sim 18.3$, $V-K \sim 5.75$) are assumed to be background giants and will be dropped from further discussion. Two additional sources fall below the m_V , $V-I$ isochrone (not shown) and are also assumed to be background sources. The remaining candidate Pleiades members are listed in Table 4.1. K -band finder charts for objects not previously identified in Stauffer

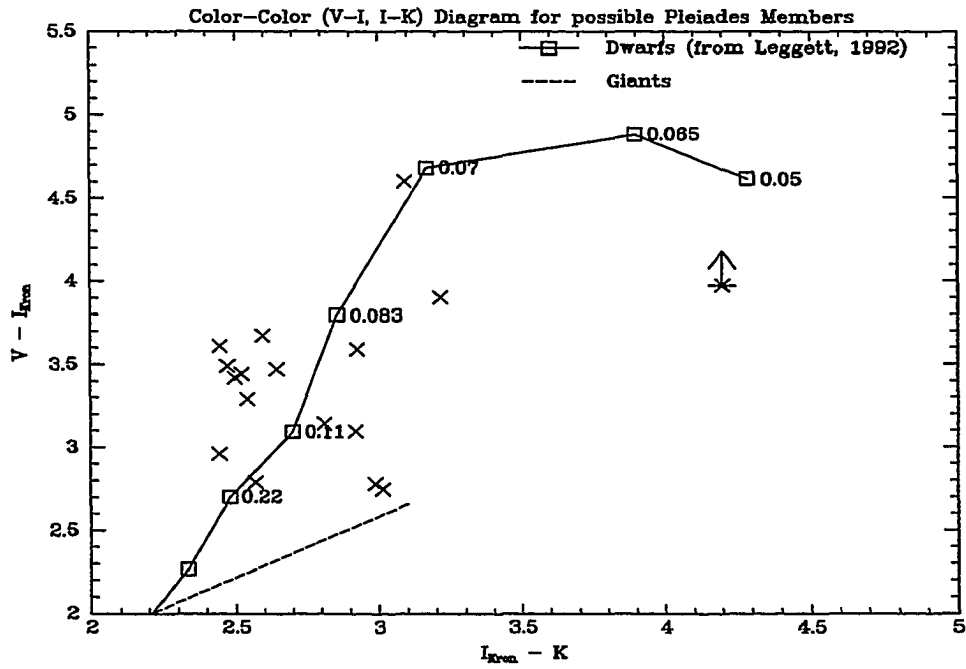


Fig. 4.2.— Color-Color $V-I$, $I-K$ for the Pleiades. Only sources within $+1.15, -0.35$ magnitudes of the 70 Myr isochrone from Figure 4.1 are plotted. Solid line shows a young disk sequence from Leggett (1992).

et al. (1989) or Hambly et al. (1993) (see below) are given in Figure 4.3.

Our K images should be complete for brown dwarfs with masses $\gtrsim 0.02\mathcal{M}_{\odot}$, including objects with V upper limits with masses $\gtrsim 0.035\mathcal{M}_{\odot}$. Unfortunately, we have no way of sorting these very low mass objects out from the contaminating background stars. However, our survey should be complete and relatively uncontaminated for Pleiades members with $0.04\mathcal{M}_{\odot} < M < 0.25\mathcal{M}_{\odot}$. Using the $+1.15, -0.35$ magnitude tolerance, we find 11 potential members more massive than $0.08\mathcal{M}_{\odot}$, *i.e.*, stars, and 2 potential members (including the V limit) between 0.04 and $0.08\mathcal{M}_{\odot}$, *i.e.*, brown dwarfs.

We can estimate the contamination level in this sample from a reference field at the same Galactic latitude but removed from the Pleiades by 5° which contains approximately half the size of our Pleiades survey ($\sim 175 \text{ arcmin}^2$) and which we imaged in V , I , and K and have analyzed using techniques identical to those used for the Pleiades. The density of sources well below the Leggett sequence is consistent with the ratio of areas covered. There were 68 sources in the Pleiades images in the box defined by $20 < m_V < 21; 4 < V - K < 5$. In the same ranges of magnitude and color, there were 31 objects in the reference field images. We find zero stars in the reference field that pass all the tests that would have led us to associate them with the Pleiades. A second class of contamination is from true low mass stars not associated with the Pleiades which happen to be located within the volume sampled by our tolerance to define Pleiades members. Using the luminosity function of Henry & McCarthy (1992) for stars within 8pc, we expect to find 4 non-Pleiades low mass stars with $11 < M_V < 16$ interloping in the volume for the $+1.15, -0.35$ magnitude tolerance, where we find 11 potential stellar members, so the background-corrected estimate is 7 ± 3.9 . The possibility that the brown dwarf

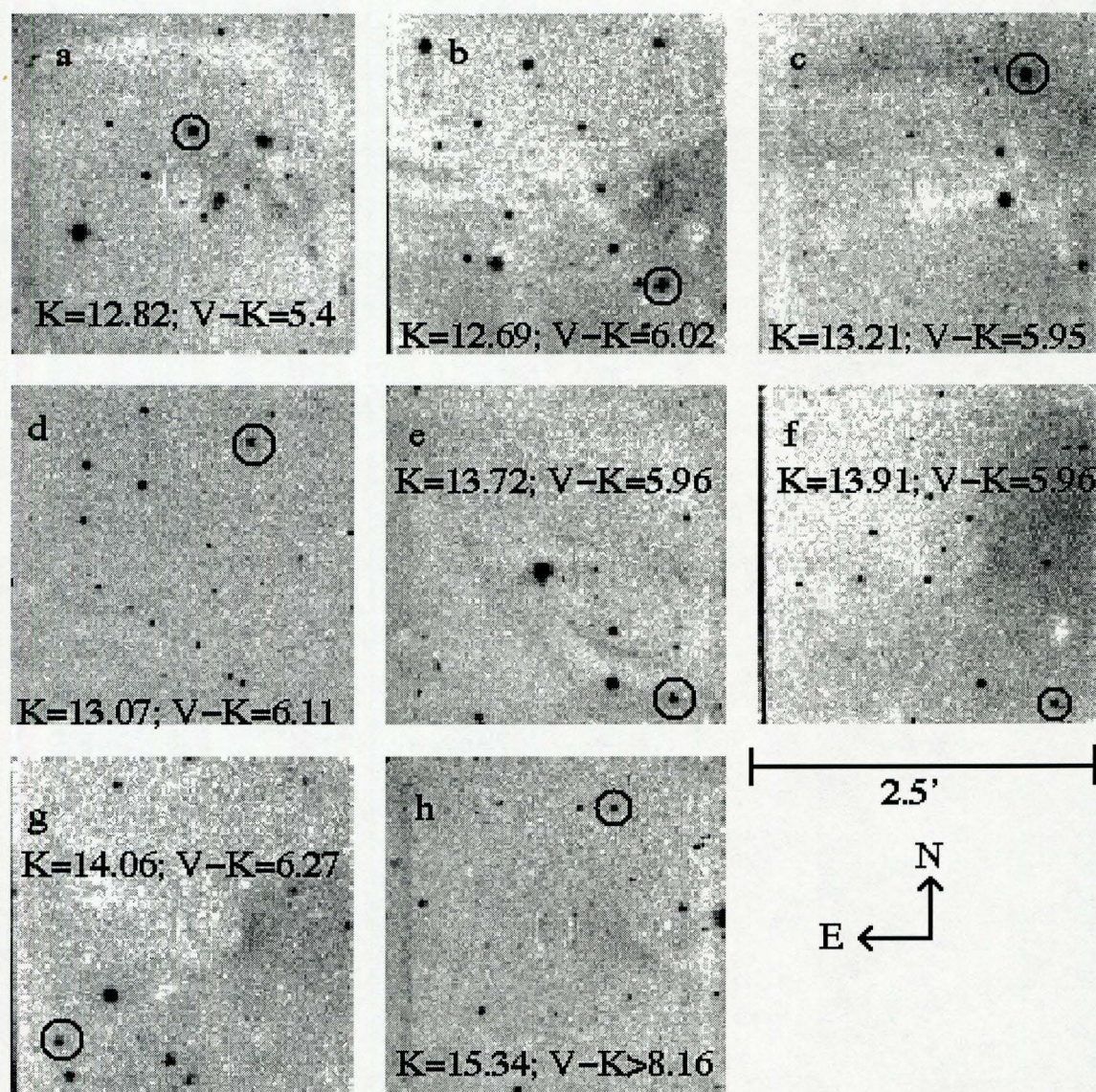


Fig. 4.3.— K -band finder charts for objects not previously identified.

K -band finder charts for objects not previously identified. Each image is $2.5'$ on a side, with North up and East to the left; a = Object 1; b = Object 2; c = Object 4; d = Object 5; e = Object 7; f = Object 8; g = Object 10; h = Object 13.

candidates are contaminating sources is discussed below and found to be unlikely.

4.2.2 Tests of the Extraction Technique

Particularly for the brown dwarf candidates, our technique depends on the theoretical model calculation and the procedure we have used to convert it into isochrones. For these particular fields, we note there are essentially **no** additional viable brown dwarf candidates on the m_V , $V - K$ diagram, even should the isochrone be in error by a significant amount. However, a test of the procedure is still of interest and will be important in terms of future applications of our method on other young, open clusters such as NGC 7160 (see Chapter 6), IC 4665, IC 348, Collinder 121, and NGC 1502.

The temperature scale for very red stars remains an outstanding challenge as described by Burrows & Liebert (1993). We have investigated the temperature scales of Kirkpatrick et al. (1993), Berriman et al. (1992), and Bessel (1991). In Figure 4.4, we plot the first step of our conversion from theoretical parameters to observable quantities: the conversion from T_{eff} to spectral type. The line through the open squares of Kirkpatrick et al. (1993) represents the adopted relationship. It can be seen in Figure 4.4 that there is a large range in the T_{eff} s assigned to a particular spectral type, a difference of approximately 400K. We have chosen the temperature scale of Kirkpatrick et al. (1993) because the other temperature scales all produce inconsistencies for the lowest temperature objects. For example, Burrows et al. (1993) predict that a $0.04M_{\odot}$ object at 70Myr should have a temperature of $T_{eff} \sim 2500K$ (which is close to the same value predicted by D'Antona & Mazzitelli (1994)). The scales of both Berriman et al. (1992) and Bessel (1991) would imply a spectral type of M7. The $V - K$ for this object would

be ~ 7.5 (Leggett (1992)), making this object no redder than Gl 406 and vB 10 – *i.e.*, it would fall to the blue of the zero age main sequence.

Figure 4.5 shows the changes in the 70 and 120 Myr isochrones if we adopt a temperature scale 100K cooler than Kirkpatrick et al. (1993), *i.e.*, a given spectral type will be assigned a temperature 100K less than the adopted relationship in Figure 4.4. The effects of the cooler temperature scale can be seen by comparing the heavy lines (cooler scale) with the thin lines (the adopted scale). The effect of both aging the cluster and cooling the temperature scale is to dim the isochrone for a given color, and pull it away from sources which we believe to be cluster members from other studies.

Although we have assigned the locus for substellar objects from our own conversion of theoretical models to observed colors, strong support is provided by the location in m_V , $V-K$ and $V-I$, $I-K$ of PPl 15 (Stauffer et al. (1994a)), which falls almost exactly where we would predict in Figures 4.6 and 4.7. Basri, Marcy, & Graham (1995) have detected lithium absorption in this object, which supports its identification as a brown dwarf just below the bottom of the main sequence (Stauffer et al. (1994a)). Basri et al. (1995) suggest from the apparent depletion of lithium in PPl 15 that the age of the Pleiades may exceed 70 Myr; a self-consistent interpretation of their results implies an age of 110-125 Myr for the Pleiades. We have investigated this suggestion by creating a 120 Myr isochrone as described above, and reanalyzing our data. The two isochrones are shown in Figure 4.8. The adjustments caused by the age difference are twofold. First, there is a slight change in exactly which objects we would assign Pleiades membership, but no net change in the number of objects assigned membership. The source which is identified below as PPl 7 falls too far above the 120 Myr isochrone to be

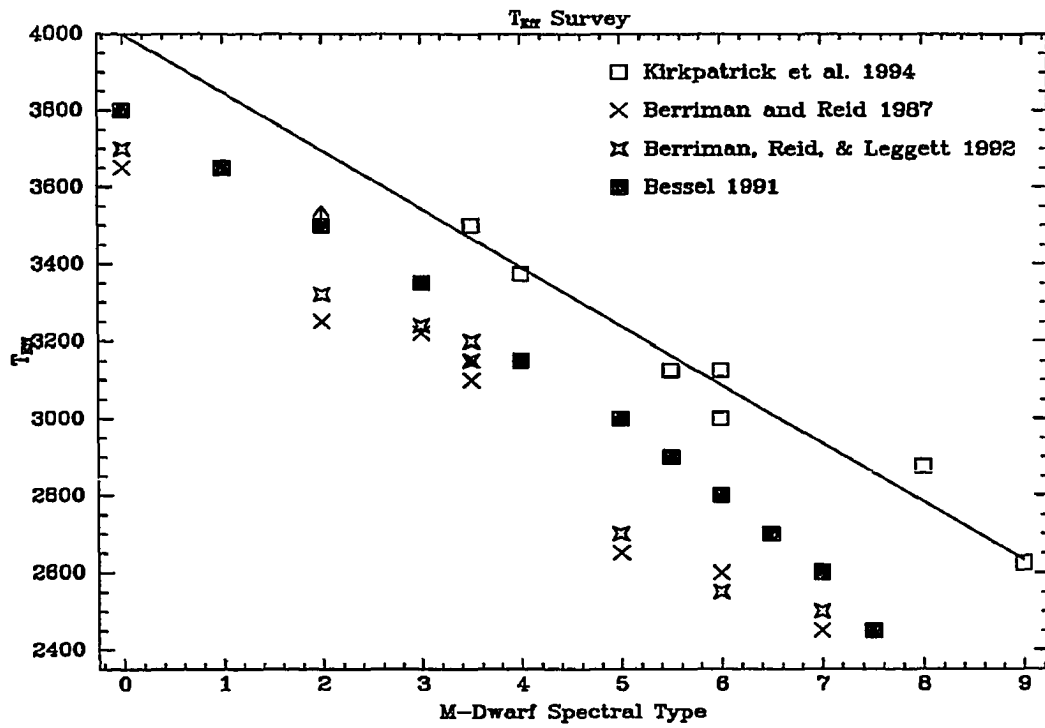


Fig. 4.4.— Comparison of Temperature Scales.
The temperature scales of Kirkpatrick et al. (1993), Berriman et al. (1992), and Bessel (1991) are compared.

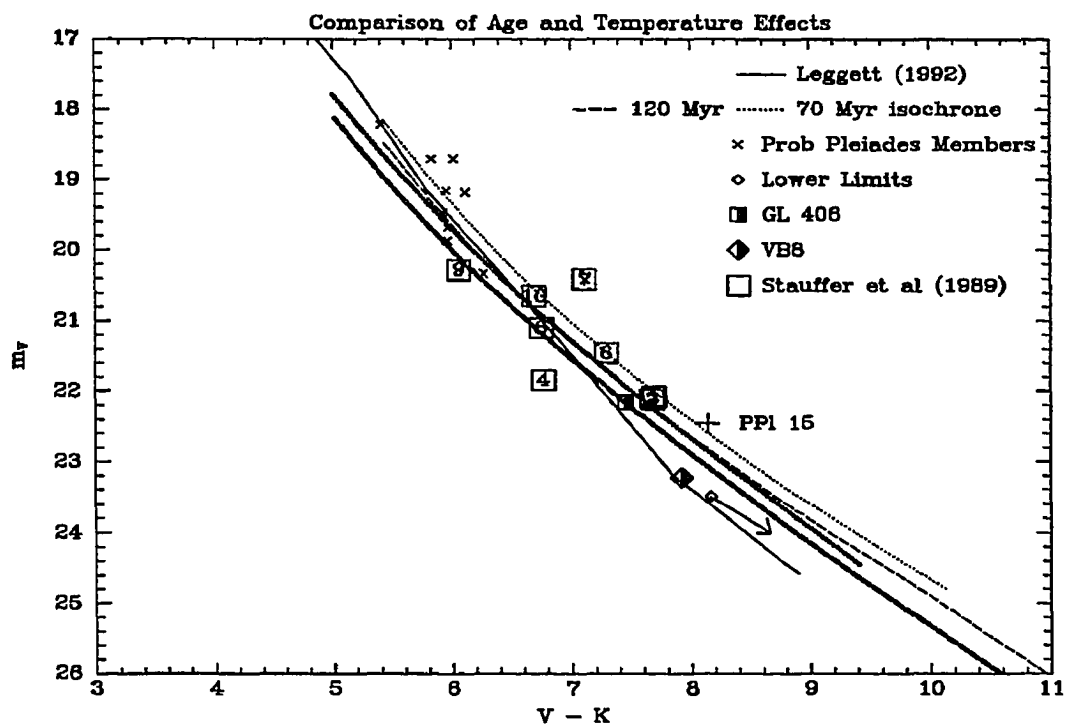


Fig. 4.5.— Comparison of Age and Temperature Effects.

70 and 120 Myr isochrones are converted to colors and magnitudes with two temperature scales. Thin lines represent the temperature scale of Kirkpatrick et al. (1993), and thick lines represent a temperature scale 100K cooler. The independent observations of PPI 15 rule out the combination of a cooler temperature scale and an age of 120 Myr.

considered even a pair of Pleiades objects. However, a different source is acquired with the 120 Myr isochrone which is assumed to be a background object when the 70 Myr isochrone is used. This source is located at $m_V \sim 21$; $V-K \sim 6.6$ in Figure 4.1. Second, the masses assigned to object below $\sim 0.09\mathcal{M}_\odot$ are increased as the age of the cluster is increased. In particular, the brown dwarf status of PPl 1 and 2 would be brought into question. In any case, the adjustments would be small and would not significantly affect any of our conclusions about the shape of the IMF. Additionally, the observations of PPl 15, while not inconsistent with either the older age for the Pleiades, or a cooler temperature scale, are inconsistent with the combination of an older age and a cooler temperature scale – see Figure 4.5.

Another encouraging result can be seen from the density of possible Pleiades members along the isochrone. Because of the cooling of brown dwarfs, the theoretical isochrones in m_V , $V-K$ and $V-I$, $I-K$ are “stretched” below $0.08\mathcal{M}_\odot$. That is, a given factor of change in mass below $0.08\mathcal{M}_\odot$ corresponds to a larger interval in, say, $V-K$ than it does above $0.08\mathcal{M}_\odot$. In agreement with this prediction, the density of candidate members along the isochrones appears to drop abruptly near $0.08\mathcal{M}_\odot$. Figure 4.2 shows this effect very clearly.

In Figures 4.6 and 4.7, we show on the m_V , $V-K$, and $V-I$, $I-K$ diagrams 8 of the 9 Pleiades objects with $m_V > 20.4$ from the study of SHPRM and PPl 15 from Stauffer et al. (1994a); the objects are labeled as listed in those papers and will be referred to with a ‘PPl’ prefix (see Stauffer et al. (1994a)). PPl 3 was omitted because it is blended with another object and its colors may be inaccurate; however, if its V magnitude is increased to correct for the blending, it does not move towards the Pleiades isochrone and we conclude it may not be a cluster member. PPl 1 is the candidate with full photometric measurements found in our

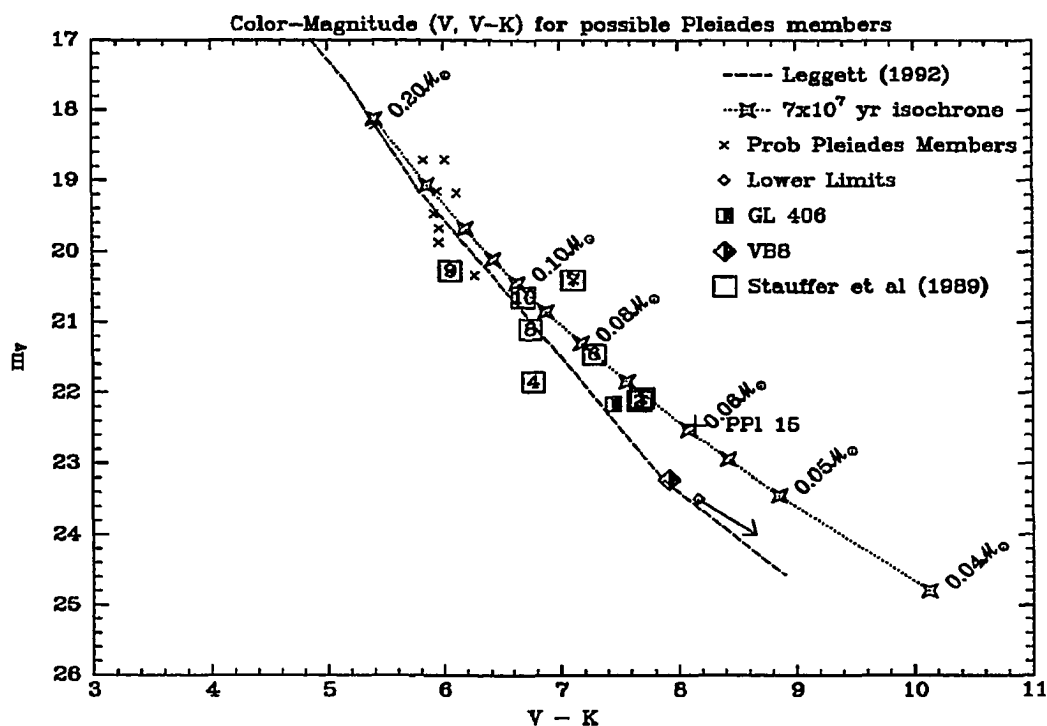


Fig. 4.6.— Color-Magnitude m_V , $V-K$ for the Pleiades and SHPRM sources. Color-Magnitude m_V , $V-K$ for the Pleiades. Sources within $+1.15, -0.35$ magnitudes of the 70 Myr isochrone are plotted. Also shown are 7 sources originally identified in SHPRM, labeled as identified in that paper. Sources 1 and 2 overlap.

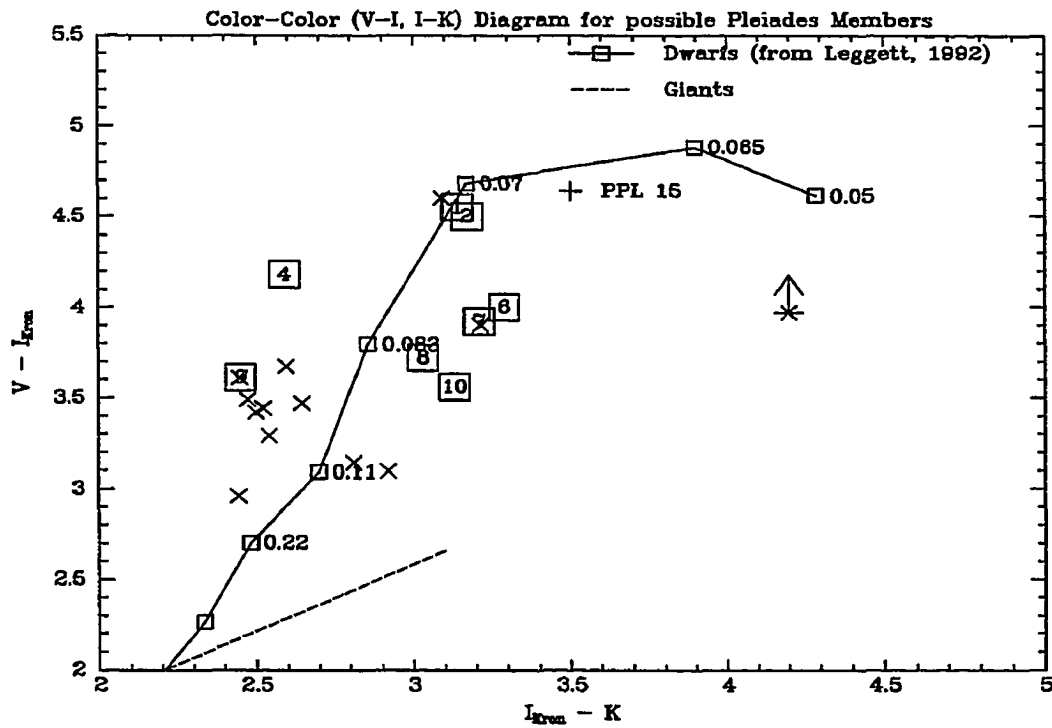


Fig. 4.7.— Color-Color $V-I$, $I-K$ for the Pleiades.
 Color-Color $V-I$, $I-K$ for the Pleiades. Sources within $+1.15$, -0.35 magnitudes of the Pleiades isochrone are plotted. Also shown are 7 sources originally identified in SHPRM, labeled as identified in that paper.

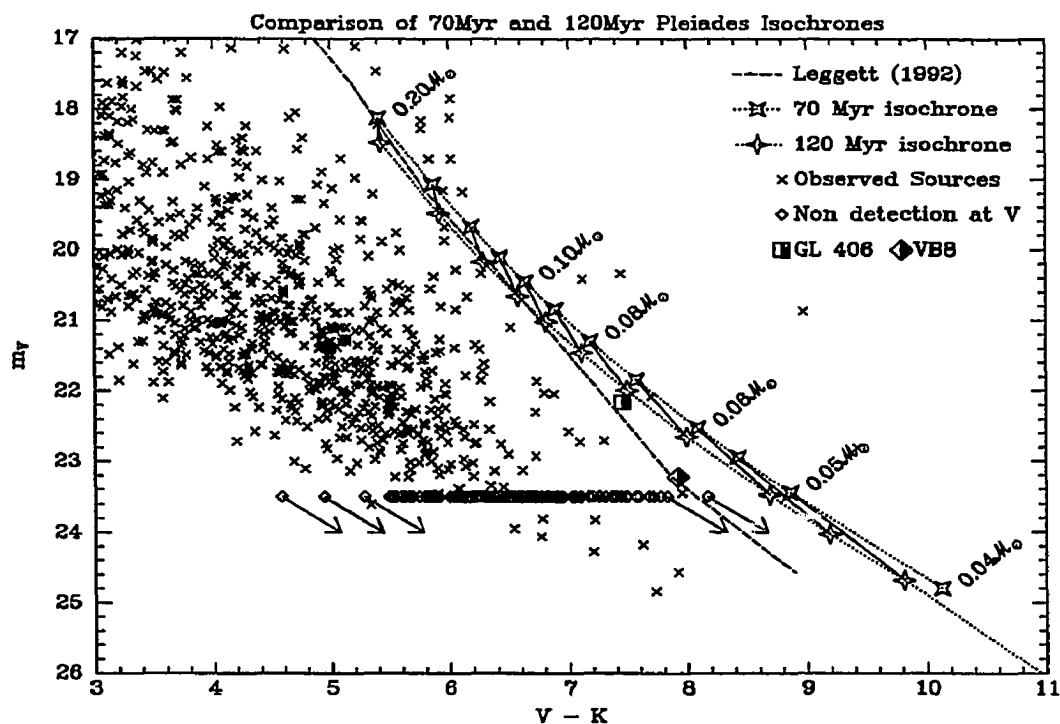


Fig. 4.8.— Comparison of 70 and 120 Myr isochrones for the Pleiades. Comparison of 70 and 120 Myr isochrones for the Pleiades. Isochrones for 70 and 120 Myr are compared for the Pleiades data. An age of 120 Myr has been proposed by Basri et al. (1995) based on the lithium depletion of PPl 15. The results are not significantly effected by the choice of isochrone.

survey (Object 12). PPl 7 was also observed as part of this survey (Object 11). We have also determined the K magnitude of PPl 4 in a followup observation. The sources plotted fall very close to the isochrone, lending support both to the methods we have used to derive the isochrone and to the identification of the faintest 3 of these 6 objects as candidate brown dwarfs.

Additionally, PPl 7 and PPl 10 were determined to be Pleiades members in the proper motion study of Hambly et al. (1993), (HHJ14 and HHJ10, respectively). Marcy et al. (1994) supported the membership claim of PPl 7 by observing $H\alpha$ in emission; however, they feel that PPl 7 is not a brown dwarf due to the lack of a lithium $\lambda 6708\text{\AA}$ absorption as predicted by Rebolo et al. (1992) and Magazzu et al. (1993), in very good agreement with our results. The radial velocity of PPl 7 was also shown by Basri & Marcy (1995) and Stauffer et al. (1994b) to be consistent with the radial velocity of the Pleiades. The membership claim of PPl 10 was furthered by Stauffer et al. (1995) based on both $H\alpha$ and radial velocity arguments.

One alternate hypothesis is that these objects are background sources. From their position on the $V-I$, $I-K$ diagram, we can exclude that they are either red giants or distant normal galaxies. In Figures 4.9 and 4.10 we show near infrared spectra of PPl 1, PPl 2, and PPl 6 in comparison with the spectrum of vB10. The presence of the steam feature at $1.33\mu m$ requires PPl 1 and PPl 2 to be cool stars and is fully consistent with our identification of them as members of the Pleiades. PPl 6, however, does not show this steam feature. Although its bluer $V-K$ would lead us to expect a weaker feature than for the other two sources, the lack of any detection calls its status as a member of the Pleiades into question.

A second alternate explanation for the position of the two remaining candidates (PPl 1, PPl 2) is that they are independent M dwarfs close to the

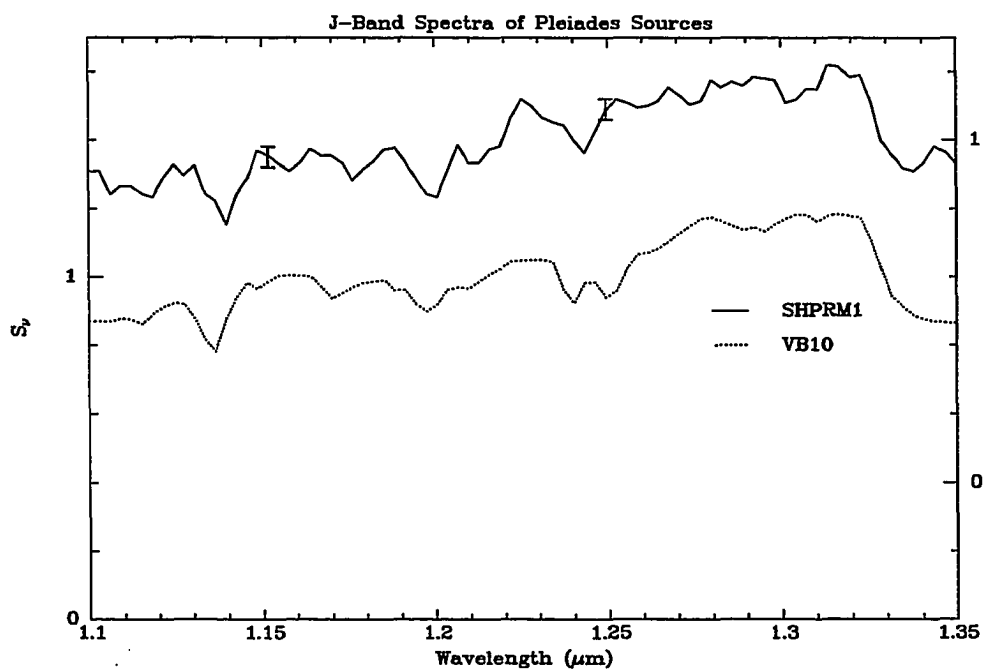


Fig. 4.9.— Spectra of VB10 and PPl 1.

Spectra of VB10 (bottom) and PPl 1 (top). The spectra are normalized to one; the scale for VB10 is shown on the left side of the frame and that for PPl 1 on the right (they have been offset for clarity). Note the steam feature at $1.33\mu\text{m}$.

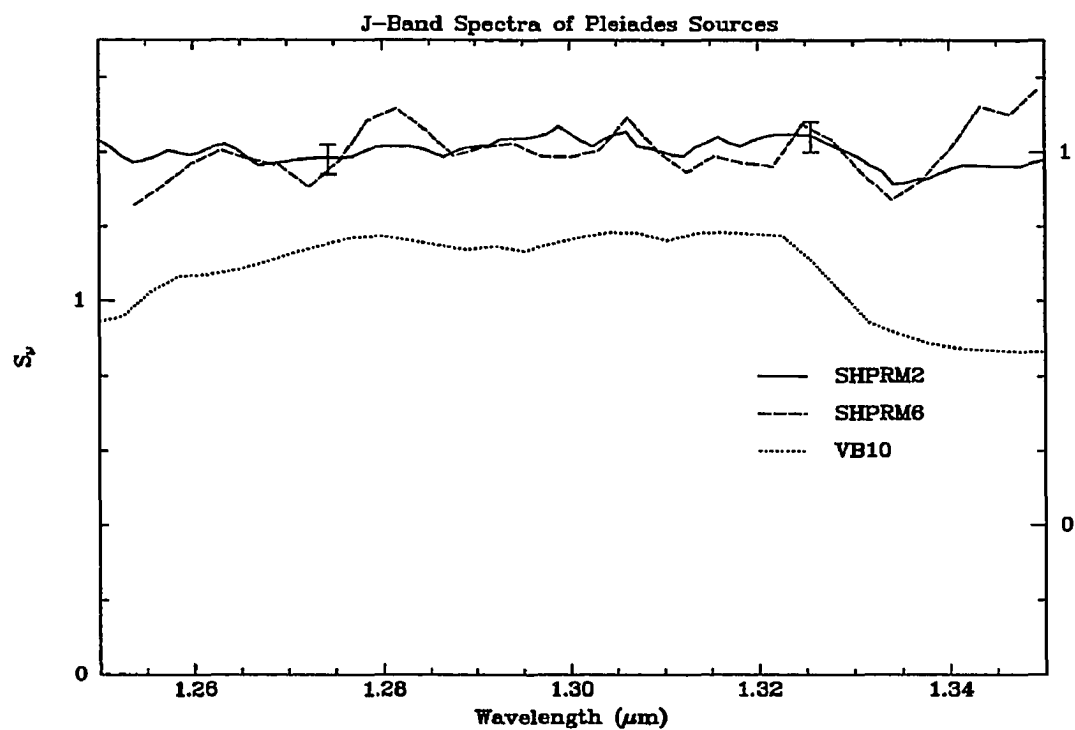


Fig. 4.10.— Spectra of VB10 and PPl 2 and PPl 6.
Spectra of VB10 (bottom) and PPl 2 (top, solid line) and PPl 6 (top, dashed line).
Details as in Figure 4.9.

Pleiades. Adopting this hypothesis, a distance of ~ 90 pc for both objects can be estimated from the distance in m_V between their apparent positions in Figure 4.6 and the main sequence. We compute a generous upper limit to the probability that these objects are foreground by computing the volumes of pyramids extending from the earth to these distances and with bases equal to the total area surveyed by SHPRM, *i.e.*, 871 arcmin^2 . We then multiply each of these volumes by the density of stars or pairs of stars of M6 or later type ($M_V > 15$) observed within 8 pc of the earth by Henry & McCarthy (1992). (The photometric colors of PPl 1 and PPl 2 correspond to $\sim M7$ (Leggett (1992))). We find that the probability that both of these objects are nearby dwarfs is < 0.08 , although it is conceivable that either of them is a nearby object. A similar argument applies to the new brown dwarf candidate we have found but which is undetected in V .

We agree that the CCD survey of SHPRM did correctly identify two probable brown dwarfs in the Pleiades in an angular area of 871 arcmin^2 , their objects 1 and 2. Our K survey of 400 arcmin^2 , although it extends to lower brown dwarf mass, has identified at most one additional brown dwarf candidate with mass $\gtrsim 0.04 M_\odot$. The extended CCD survey of Stauffer et al. (1994a) identified one more object, PPl 15, that appears to be a confirmed transition object (Basri et al. (1995)) and has properties remarkably similar to PPl 1 and PPl 2. Based on their V magnitudes and $V - I$ colors, PPl 13 and PPl 14 may also be very low mass Pleiades members.

From these data, we can place constraints on the initial mass function (IMF) in the Pleiades. For simplicity, we assume that the IMF goes as $N(M)dM \propto M^{-1}dM$, including and extending into the brown dwarf regime with this same dependence (Comerón et al. (1993)). This is also in good agreement with the MF of the

old M-dwarf population near the Sun, whose slope is between -0.70 and -1.85 (Kroupa et al. (1993)). We normalize this functional dependence to the counts between 0.45 and $0.6\mathcal{M}_{\odot}$ from Stauffer et al. (1991) (after converting their LF to a MF using Henry & McCarthy (1993)), and scaling by the ratio of the 400 arcmin^2 of our survey to the $4^{\circ} \times 4^{\circ}$ area of Stauffer et al. (1991). We predict 3.4 stars in our survey between 0.08 and $0.25\mathcal{M}_{\odot}$ and 2.1 brown dwarfs between 0.04 and $0.08\mathcal{M}_{\odot}$, where our detection rates are respectively 7 stars and 2 brown dwarfs (including the limit). If we combine our counts over the entire 0.04 to $0.25\mathcal{M}_{\odot}$ range and include in the statistics the subtracted contaminating stars, we find a total of 9 ± 4.1 Pleiades members where the M^{-1} IMF would predict 5.5 – *i.e.*, the agreement is within one standard deviation (see Table 4.2). If we consider only candidate brown dwarfs and combine the surveys of SHPRM, Stauffer et al. (1994a), and our new data, we find at least 4 brown dwarf candidates where 7 are predicted. The observed rates are not significantly different from the $1/M$ IMF dependence; a larger area must be surveyed to establish any deviations. Given the small number of brown dwarf candidates, our study is probably also consistent with an IMF that flattens toward very low masses. However, our detection rates do contradict much steeper dependencies. For example, if the IMF goes as M^{-2} , then we would have predicted 13.3 stellar members and 19.5 brown dwarf members within our survey completeness limits. See Table 4.2.

These conclusions are unaffected by the fact that some of these Pleiades members are likely unresolved binaries. The type of binary that would lie farthest above the single star isochrone – 0.8 mag – would be a system of two identical stars. If we limit cluster members to objects which fall within $\pm 0.35 \text{ mag}$ of the isochrone in the $m_V, V-K$ diagram, we would exclude three objects from our list. However, the volume included by this smaller tolerance is 4.4 times smaller than

Table 4.1. Probable Pleiades Members

Number	RA ^a	DEC ^a	m_V	m_I	m_K	Previous ID ^b
1	03:45:34.2	23:43:31.8	18.22	15.26	12.82	
2	03:44:11.8	23:16:42.0	18.71	15.61	12.69	
3	03:45:31.2	23:48:59.2	18.71	15.42	12.88	HHJ132
4	03:42:27.0	23:47:37.4	19.16	16.02	13.21	
5	03:42:40.7	23:47:44.2	19.18	15.71	13.07	
6	03:45:43.5	24:18:13.7	19.47	16.05	13.55	HHJ44
7	03:46:02.9	23:29:10.1	19.68	16.19	13.72	
8	03:40:56.9	23:37:35.5	19.87	16.43	13.91	
9	03:41:01.5	23:38:35.1	20.28	16.67	14.22	PPl 9
10	03:42:16.3	23:12:08.9	20.33	16.66	14.06	
11	03:42:14.4	23:44:26.4	20.41	16.51	13.30	PPl 7; HHJ14
12	03:42:43.0	23:44:50.3	22.08	17.48	14.39	PPl 1
13	03:42:16.9	23:45:13.6	...	19.53	15.34	

^aAll coordinates are for the 1950.0 equinox and accurate to $\sim 3''$

^bPPl = Stauffer et al 1995; HHJ = Hambly et al 1993

Table 4.2. Pleiades Star Counts^a

Method	# Stars $0.08M_{\odot} - 0.25M_{\odot}$	# Brown Dwarfs $0.04M_{\odot} - 0.08M_{\odot}$	# Very Low Mass $0.04M_{\odot} - 0.11M_{\odot}$
This paper	7	2	9 ± 4.1
Simons & Becklin 1992	44 ± 20
$n = -1$	3.4	2.1	5.5
$n = -2$	13.3	19.5	24.8

^aAll counts normalized to Stauffer et al. (1991) at $0.45M_{\odot} < M < 0.6M_{\odot}$ and scaled to 400 arcmin^2

that for the tolerance that includes possible double sources, decreasing the number of expected interlopers from 4 to 1. The combined effect produces no change in the number of stellar members. Thus, our conclusions are unchanged.

4.2.3 Comparison with Other Work

Hambly et al. (1993) (HHJ) located probable Pleiades members using a proper motion survey of a $5^\circ \times 5^\circ$ area around the cluster center. Two HHJ objects, HHJ344 and HHJ440, completely saturated the arrays, thus we cannot tell if we would have declared them members. Two of our eight objects with $m_V < 20$ appear on their list (Object 3 = HHJ132; Object 6 = HHJ44), and the coordinates agree well within the errors. The only two objects removed from our list because they were too bright (but otherwise fit our membership criteria) correspond to HHJ255 and HHJ315. Based on HHJ's claim of 70% completeness in this range and assuming a high completeness ratio for our survey, we would expect to see ~ 7 out of these 10 objects appear in both surveys, where in fact 4 do. HHJ203 was one of the objects that appeared along the red giant locus in the $V-I$, $I-K$ diagram and was dismissed as a possible member. In the range $20 < m_V < 21$ where HHJ has an estimated 30% completeness ratio, we find 2 possible members not in their survey, and one common source (object 11 = HHJ14 = PPl 7). There are no other HHJ sources within our sample area. As with our similar study of Praesepe in Chapter 3, we conclude that our photometric technique is in good agreement with cluster memberships assigned from proper motions.

Two other recent similar studies claim to find large numbers of brown dwarfs in the Pleiades, leading to an IMF that rises more steeply than M^{-1} . Simons & Becklin (1992) surveyed 200 arcmin² and a control area of 75 arcmin² in I

and K . They used a procedure similar to ours but on the $I, I-K$ diagram to define the Pleiades isochrone and determine possible Pleiades members. After correcting for the objects extracted in the same manner from a control field, they concluded that there were 22 ± 10 objects with $\sim 0.04M_{\odot} < M < \sim 0.11M_{\odot}$, or 44 ± 20 in 400 arcmin^2 . In 400 arcmin^2 we find at most 9 ± 3.3 objects with $0.04M_{\odot} < M < 0.11M_{\odot}$. First, we note that the two estimates are formally consistent (within 2σ). Second, the limited color baseline used by Simons & Becklin (1992) did not provide nearly as clear a differentiation of Pleiades members from the background as in our study, so we suspect that any differences between the studies may arise from contamination of their sample by background stars. If we apply a 0.35 mag selection to our data in the $I, I-K$ diagram shown in Figure 4.11, and correct for counts in the same band in the reference field, we obtain 27 ± 5.4 members in the same mass range. The agreement between this value, and the counts from Simons & Becklin (1992) supports our claim of background contamination in the study of Simons & Becklin (1992). Figure 4.11 also strengthens our claim of reaching $0.04M_{\odot}$, since all objects with $m_V \lesssim 20$ have m_V magnitudes or limits which preclude them from Pleiades membership.

Although the number counts from the two studies are consistent, the slopes of the derived mass functions are not. An MF with a slope of -1 normalized as described above predicts 3.0 objects in this mass range in this area, while an MF with a slope of -2 predicts 24.8 objects. See Table 4.2.

Steele et al. (1993) have also used the $I, I-K$ diagram to extract Pleiades members, so their sample may also be contaminated by background objects. In addition, age was left as a free parameter in identifying potential brown dwarfs and many of their candidates are suggested to be much younger than the youngest

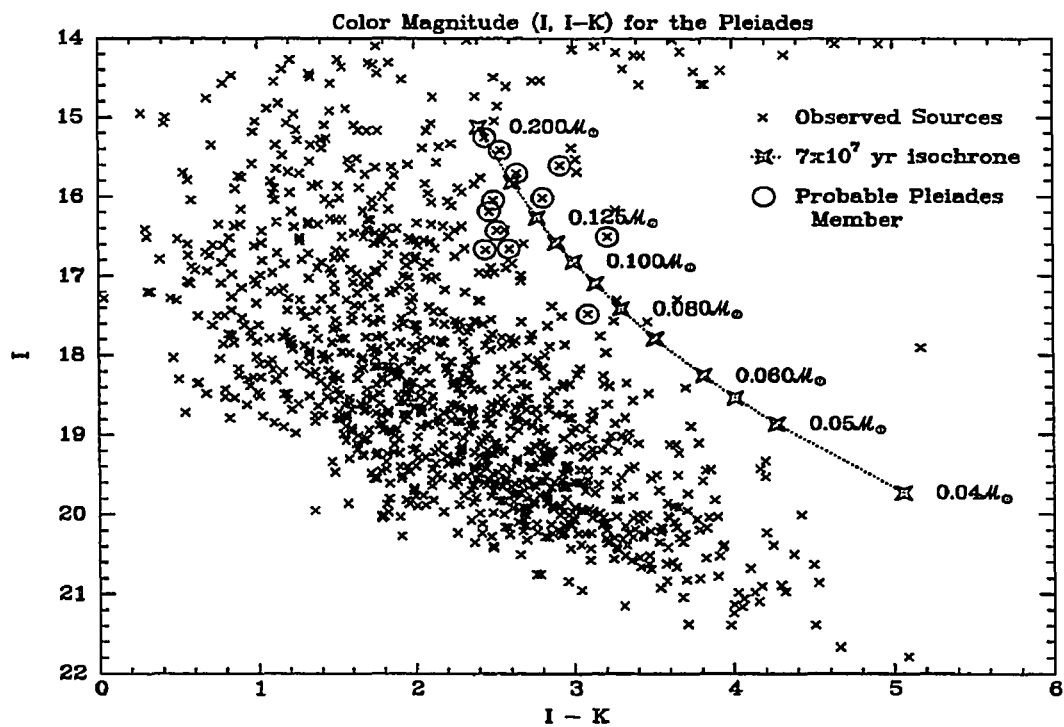


Fig. 4.11.— Color-Magnitude m_I , $I-K$ for the Pleiades. All sources are plotted. Dotted line is the adopted 70 Myr isochrone from Burrows et al. (1993). Upper limits are shown with tails. Probable members selected earlier are circled. Note that this sample is complete to $m = 0.04 M_{\odot}$.

well-studied stars in the cluster. More recently, Steele & Jameson (1995) reanalyzed the original data and now believe the data are best interpreted in terms of a single and a double star sequence, both of the age of the Pleiades. This effectively halves the number of brown dwarf candidates from the original analysis.

Some initial efforts to measure the IMF in embedded clusters have also been reported. One would expect these regions to have identical distributions of stellar masses to those in older unembedded clusters like the Pleiades. A comparison of the two stages in cluster formation can therefore test the assumptions made in analyzing the observations as well as providing a test of the theoretical models of low mass stars and brown dwarfs of varying ages. Comerón et al. (1993) and Chapter 5 find that the low mass IMF in ρ Ophiuchus goes roughly as $M^{-1.1}$ in linear mass units, or as $M^{-0.1}$, nearly flat, in logarithmic units. Strom & Strom (1994) conclude, using a different analysis technique, that the IMF in L1459E is roughly flat in logarithmic units at low masses or alternately could be fitted by an IMF with a bend at $\sim 0.3\mathcal{M}_{\odot}$ and which falls to either side of this mass. Strom et al. (1995) find the ρ Ophiuchus IMF to be flat in logarithmic units. Within the still rather large uncertainties, our results on the Pleiades, and these other studies are all consistent with each other.

Low mass members account for a significant portion of the integrated mass of a stellar population only if the IMF in linear units is at least as steep as $N(M)dM \propto M^{-2}dM$. There is now a significant body of evidence that the IMF in open clusters for single stars and the primary members of doubles is roughly one power of mass less steep than this critical dependence. If the properties of binary systems in these clusters resembles the properties of binaries in the solar neighborhood (Duquennoy & Mayor (1991)), then it can be shown that unresolved

secondary stars in binaries do not contribute significantly to the integrated mass. Therefore, it appears that low mass stars and massive brown dwarfs appear to contribute only a small portion of the integrated mass of an open cluster. If the general IMF behaves similarly, then such objects cannot be an important constituent of dark matter.

4.3 Conclusions

We have used optical and infrared photometry and infrared spectroscopy to identify potential low mass Pleiades members. We agree that the CCD surveys of Stauffer et al. (1994a) and Stauffer et al. (1989) identified at least three possible brown dwarfs in the Pleiades in an area of 1400 arcmin^2 . Our K survey of 400 arcmin^2 , although it extends to lower brown dwarf mass, has identified at most one additional brown dwarf candidate, and suggests that there are 9 stellar members in this area with masses between 0.08 and $0.25 M_{\odot}$. The initial mass function derived from these counts is consistent with a simple power law ($N(M)dM \propto M^n dM$) with an index of $n = -1$ in linear mass units, equivalent to a flat dependence in logarithmic mass units. Our results are inconsistent with steeply falling low-mass IMFs, for example with $n = -2$, as have been found in other studies. If the IMF in open clusters is representative of star formation generally, then massive brown dwarfs and very low mass stars do not account for a very large fraction of the mass in a volume of space, *i.e.*, such objects do not provide significant dark matter.

Chapter 5

ρ OPHIUCHIUS

5.1 Introduction

Improvements in detector technology in the near infrared have made possible extensive surveys of the young stellar populations embedded in interstellar clouds. However, methods to analyze these new data to obtain estimates of the characteristics of the low mass cluster members have lagged behind the observational advances. One approach was proposed by Comerón et al. (1993) (hereafter CRBR) and used to determine the initial mass function in the ρ Ophiuchi embedded cluster. Recently, a second method has been developed by Strom et al. (1995) (hereafter SKS) and used on the same cluster. We show that the results of these two approaches are in close agreement over the considerable range of mass where they should both be expected to yield good estimates.

Only the technique of CRBR is at present capable of estimating the masses of substellar objects. We test this method further with new K -band spectra of six sources considered by them to be candidate low mass objects. The spectra

appear to confirm the essential assumptions made by CRBR. The properties of these sources have been updated with the improved models of stellar interiors of Burrows et al. (1993). All of these results support the source characteristics assigned previously and indicate that at least one of the candidate very low mass objects is possibly a young brown dwarf.

The initial mass functions derived for the ρ Ophiuchus population by SKS and CRBR are in close agreement. We have therefore combined the data from both works to improve the statistical significance with which the IMF is determined. It appears that the IMF is roughly flat (in logarithmic mass units) through the low mass region (i.e., between 0.03 and 1 \mathcal{M}_{\odot}).

5.2 Mass Determination in the Stellar Range

CRBR developed a method that, for the first time, integrated theoretical models of low mass objects and multiband infrared photometry of embedded sources to provide internally consistent estimates of the mass and extinction of each member of an embedded cluster. In their method, a suite of trial stellar spectra was calculated for a range of assumed temperature, reddening, and degree of infrared excess; the appropriate luminosities were determined from the theoretical models. One of these trial spectra was adopted for an embedded source if a fit to multiband photometry reproduced accurately both the colors and the brightness of the source; sources with either poor fits or strong excess emission were rejected. In the accepted cases, a mass was assigned from the theoretical model used for the trial spectrum.

SKS have recently described another technique that is similar in philosophy but differs significantly in execution. They compare the embedded stars with other,

previously studied stars and determine a subset whose JHK spectrum is dominated by photospheric emission. Stars with strong excess emission are rejected at this first stage. The accepted sources are dereddened according to their $J-H$ colors to determine their J luminosities. The masses are determined by comparing the J luminosities with the predictions of theoretical models.

Each of these methods has advantages. The approach of SKS is more closely tied to stellar observations and makes the dependence on theoretical models more explicit by not having to invoke them until the final stage. However, it is not applicable to possible substellar objects, for which there is as yet no observational database. The greater dependence of the method of CRBR on the models could lead to larger errors. However, their approach integrates the fitting of substellar objects into the procedure in a consistent fashion, so it is useful for examining the behavior of the IMF below the bottom of the main sequence.

CRBR carried out extensive tests to show that their method was robust against the expected uncertainties of the theoretical models. However, with the new method developed by SKS, it is now possible to perform a more critical test by comparing the results of the two approaches directly. This comparison is based on independent data sets as well as different modeling approaches, so it gives a true reflection of the net differences including contributions from photometric errors and source variability as well as modeling approaches. Figure 5.1 shows the derived masses for all objects in common between the two studies. In the spirit of the correlation of infrared excess with age used in the fitting of CRBR, we have used the older mass value from SKS for the class III objects and the younger mass value for the single class II object, 2407.7–2726 (whose ID in CRBR was 2407.3–2735).

Although the close agreement in Figure 5.1 is noteworthy, it must be

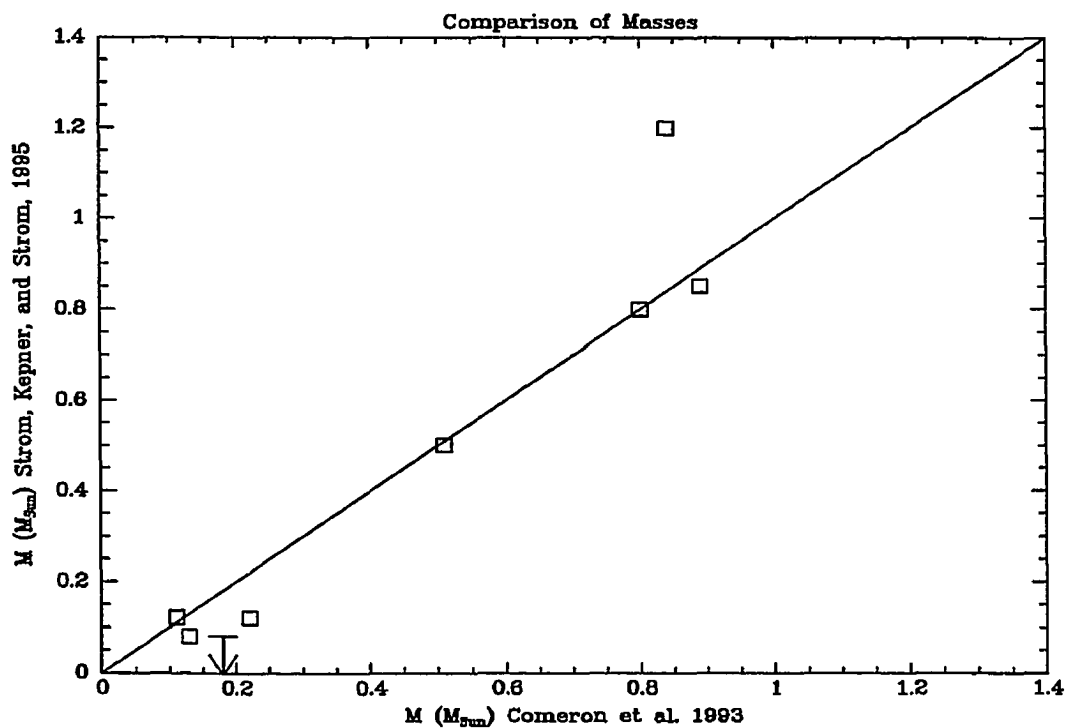


Fig. 5.1.— Comparison of mass estimates of CRBR and SKS.

Comparison of mass estimates of CRBR and SKS for all objects in common between the two studies. We have used the older mass estimates from SKS for the Class III objects, and the younger mass estimate from SKS for the single Class II object

remembered that both of these approaches still require calibration against independent measures of the nature of the embedded sources, such as optical and infrared spectra. In addition, the timescales used by CRBR and SKS for the embedded objects differ by about a factor of two. As a result, one would expect CRBR to derive systematically slightly larger masses than SKS; there is hint of this effect in the comparison, but perhaps not as strongly as expected. Finally, it must be emphasized that the two techniques of photometric modeling are designed to be useful in a statistical sense and to facilitate selection of interesting sources for followup. The derived properties of any single source should be interpreted cautiously.

5.3 Spectra of Low Mass Ophiuchus Sources

5.3.1 Approach

Below the bottom of the main sequence we do not have an independent confirmation of the photometric modeling of CRBR. The agreement with SKS at higher masses and simple continuity arguments would suggest that it should be reasonably trustworthy there also. However, as an independent test, we have obtained spectra of six low mass objects to compare their properties with the predictions of the modeling.

Because the brown dwarf candidates in the ρ Oph cloud are very young, their temperatures should be similar to those of older cool stars. As a result, we can compare their spectra and those of embedded very low mass stars with features expected from observations of nearby, evolved stars. Spectral sequences in the near infrared based on the equivalent widths of lines sensitive to effective temperature

and gravity are comparatively easier to establish than in the visible range for late type stars (Kleinmann & Hall (1986); Kirkpatrick et al. (1993); Davidge & Boeshaar (1993); Jones et al. (1994)).

The main features in the K -band correspond to the NaI blend near $\lambda = 2.207\mu m$ and molecular bandheads due to ^{12}CO at $\lambda = 2.294\mu m$ and longer wavelengths. Weaker features due primarily to the FeI lines at $\lambda = 2.226\mu m$ and $\lambda = 2.239\mu m$, and the CaI blend near $\lambda = 2.263\mu m$ may also be present.

Atmospheric models of Mould (1978) predict that the equivalent width of the NaI blend increases with decreasing temperature between spectral types G and M, but is rather insensitive to surface gravity. However, the observations show no clear dependence on temperature, as already remarked by Mould (1978) and Jones et al. (1994). On the other hand, the strength of the first ^{12}CO bandhead at $\lambda = 2.294\mu m$ is found to be well correlated with temperature, increasing as one proceeds to later spectral types. For the coolest stars, a broad absorption band due to H_2O steam in the stellar atmosphere produces a decrease in flux at the short wavelength end of the band. Other features observable in the $2\mu m$ window are found to be rather insensitive to temperature and surface gravity, according to both models and observations.

5.3.2 New Observations and data reduction

The acquisition and data reduction techniques for the ρ Ophiuchus sources were described in detail in Chapter 2. The spectra of the Ophiuchus sources are shown in Figure 5.2. All spectra have been smoothed to a resolution of $\lambda/\Delta\lambda \sim 175$ to increase the ratio of signal-to-noise. The noise increases for wavelengths longer than $\sim 2.25\mu m$ because of thermal background.

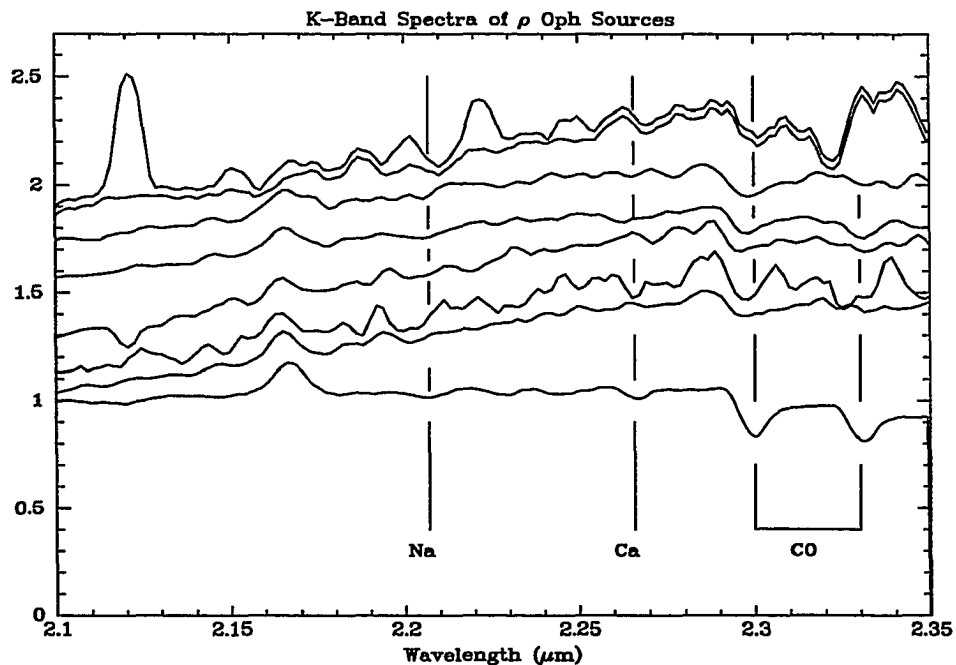


Fig. 5.2.— Spectra of ρ Ophiuchus objects.

The spectrum of Oph 2320.8-1721 is presented at the top of this plot with and without subtraction of the features due to Br γ absorption in the spectrum of the reference star, and to interstellar H_2 gas. The other spectra are, in descending order: Oph 2326.5-1958, Oph 2320.0-1915, Oph 2320.8-1708, Oph 2404.5-2152, Oph 2317.3-1925, and vB10. The lower boundary of the frame corresponds to zero flux for the lowermost spectrum.

The observations of Oph 2320.8–1721 lead us to conclude that it was significantly (by a factor of 1.5 to 2) fainter on 1994 July 19 than for our previous photometry and spectroscopy. The seeing was comparable on all three nights, and an infrared acquisition system was in place for the dimmest observation of Oph 2320.8–1721, which allowed us to accurately place the source on the spectrometer slit in place of centering on another source visible in the optical acquisition system and offsetting the telescope to Oph 2320.8–1721’s position. Although this conclusion is based on the spectrophotometry, it is reinforced by the much greater equivalent width of H_2 when we believe the source was faint. Since the H_2 originates in a surrounding, extended nebulosity which should have been transmitted equally on all occasions by our spectrometer slit on the 2.3m, the simplest explanation for the increase in equivalent width is that the source continuum had become fainter.

Our data on M dwarfs were reduced identically to the spectra of the sources in ρ Ophiuchus. Equivalent widths of the most relevant features for all sources are listed in Table 5.1. The estimated uncertainties in the listed equivalent widths based on the signal-to-noise ratios are around 5% for Gl 725A, Gl 725B, Gl 873 and vB 10, around 10% for Wolf 922, Ross 248 and L789-6. The features in our spectra are in good agreement with the other studies cited in the preceding section. The only exception to the expected trends discussed in the preceding section within our data is Ross 248. However, this star is known to possess a high space velocity characteristic of Population II objects. Its low metallicity is also suggested by the relative weakness of other lines as compared to stars of similar spectral types; the weak ^{12}CO and other lines are therefore expected. We are therefore confident in using the extensive set of comparisons made possible by these studies in classifying the ρ Ophiuchus sources.

Table 5.1. Equivalent widths of some lines and blends

Star	Sp. type	T_{eff}	NaI $\lambda 2.207$	CaI $\lambda 2.263$	^{12}CO $\lambda 2.294$
Gl 725A ^a	M3V	3600	5.2	2.1	4.3
Gl 725B ^a	M3.5V	3500	4.2	2.8	5.0
Gl 873 ^a	M3.5V	3500	5.6	3.7	5.8
Wolf 922 ^b	M4V	3375	5.0	3.5	6.0
Ross 248 ^b	M5V	3200	5.0	3.0	3.0
L789-6 ^b	M5V	3200	7.0	3.0	7.0
vB 10 ^a	M8V	2875	2.6	3.8	25.1
Oph 2320.0–1915 ^c			5(?)	4(?)	16
Oph 2320.8–1708 ^c			4(?)	...	16
Oph 2326.5–1958 ^c			2	2	24
Oph 2317.3–1925 ^c			15
Oph 2404.5–2152 ^c			11(?)	5	19
Oph 2320.8–1721 ^c			12	...	16

^aEquivalent width errors $\sim 5\%$ ^bEquivalent width errors $\sim 10\%$ ^cEquivalent width errors $\sim 40\%$

5.3.3 Spectral Properties of Low Mass Sources

The spectra of the embedded Ophiuchus objects displayed in Figure 5.2 confirm them to be cool, low luminosity objects when compared to the spectra of field stars. The continuum slope of these sources is mostly due to the wavelength dependence of the intervening dust extinction which heavily obscures them. Although the much lower signal-to-noise ratios in these spectra make the equivalent widths entered in Table 5.1 rather uncertain (errors are of order 40%), bands characteristic of the photospheres of cool stars, particularly the first CO overtone, can be recognized in all of them (see Table 5.1).

In addition to the stellar features, emission at $\lambda = 2.121\mu m$ from shocked H_2 (Brand (1993)) can be easily recognized in the spectrum of Oph 2320.8–1708 and Oph 2320.8–1721. This feature is extended along the slit position (i.e., in the north/south direction) for Oph 2320.8–1721 and therefore originates in the surrounding medium. A similar explanation is likely for the feature in Oph 2320.8–1708. Fainter H_2 emission can also be distinguished in the spectrum of Oph 2320.8–1721 at $\lambda = 2.073, 2.154, \text{ and } 2.223\mu m$. These non-photospheric features, plus the already mentioned false Br γ emission, have been artificially removed from the unsmoothed spectrum of Oph 2320.8–1721 by linearly interpolating the adjacent continuum; the cleaned spectrum is displayed in Figure 5.2.

The $2.121\mu m$ emission from shocked H_2 can be seen extending at least five pixels ($\sim 6''$) in one direction from the location of Oph 2320.8–1721. At the distance of ρ Ophiuchus (160pc), this corresponds to a linear extent of at least 800AU. The spectra were not flux calibrated; however, estimates of the flux can be made using the K -band flux measurement of 13.55 from Comerón et al. (1993),

and the measured equivalent widths of the H_2 lines. There were only three H_2 lines that were strong and isolated enough to accurately measure. These were the $(1-0)S(1)$ $2.121\mu m$, the $(1-0)S(0)$ $2.223\mu m$, and the $(2-1)S(1)$ $2.247\mu m$ lines, which had measured equivalent widths of $-0.0060\mu m$, $-0.0014\mu m$, and $-0.0004\mu m$, respectively. The spectra were extracted by summing 5 pixels along the slit centered on the object; the total solid angle is thus 2.7×10^{-9} steradians. The total intensity radiated in these three lines is $I_{(1-0)S(1)} = 3.1 \times 10^{-6}$, $I_{(1-0)S(0)} = 7.2 \times 10^{-7}$, and $I_{(2-1)S(1)} = 2.1 \times 10^{-7} (\frac{erg}{cm^2 s ster})$. If the hydrogen molecules are approximately in thermal equilibrium, the intensity of a molecular line can be written as follows:

$$I_{vJ,v'J'} = (A_{vJ,v'J'} E_{vJ,v'J'} N_{vJ} e^{-\tau}) / 4\pi \quad (5.1)$$

where $I_{vJ,v'J'}$ is the observed intensity of the transition from the upper state with vibrational quantum number v and rotational quantum number J to the lower state with vibrational quantum number v' and rotational quantum number J' , in units of $erg/s/cm^2/sr$; $A_{vJ,v'J'}$ is the transition probability from the upper state to the lower state (s^{-1}), $E_{vJ,v'J'}$ is the transition energy, N_{vJ} is the column density (cm^{-2}) of molecules in the upper state; and τ is the dust optical depth at energy $E_{vJ,v'J'}$. Here, we note that since H_2 rotational transitions emit optically thin quadrupole radiation, dust absorption is more important than self-absorption.

Equation 5.1 can be used to determine the temperature of the shocked H_2 by solving for the ratio of the intensities of the two transitions mentioned above. In this calculation, we have used the transition probabilities of Turner et al. (1977) ($A_{(1-0)S(1)} = A_{13,01} = 2.09 \times 10^{-7} s^{-1}$; $A_{(1-0)S(0)} = A_{12,00} = 2.9 \times 10^{-7} s^{-1}$; $A_{(2-1)S(1)} = A_{23,11} = 3.18 \times 10^{-7} s^{-1}$). The ratio of the two strongest lines ($(1-0)S(0)$, $(1-0)S(1)$) cannot be used reliably for a temperature

determination because their upper levels are separated by less than $500K$. The upper levels of $(1-0)S(1)$ and $(2-1)S(1)$ differ by $5587.7K$, making the ratio of these transitions a better temperature indicator. The temperature implied by the above values and the observed equivalent widths imply a temperature of $\sim 1800K$. CRBR derived an extinction value of $A_v = 17$ for Oph 2320.8–1721, which using the reddening law of Rieke & Lebofsky (1985) corresponds to 1.9 magnitudes of extinction towards this source, or equivalently an optical depth $\tau = 1.75$. The number of H_2 molecules in the state with vibrational quantum number $v = 1$ and rotational quantum number $J = 3$ can be estimated using Equation 5.1 and the observed intensity of the $(1-0)S(1)$ line to be $1.14 \times 10^{15} \text{cm}^{-2}$. Sauval & Tatum (1984) have computed polynomial fits to the temperature dependent partition function for H_2 . For $T = 1800$, the partition function has the value 11.15. The total column density of shocked H_2 in close proximity to Oph 2320.8–1721 is $\sim 2 \times 10^{16} \text{cm}^{-2}$.

5.3.4 Discussion

Our fitting procedure was discussed in detail by CRBR, who used the theoretical evolutionary tracks computed by D’Antona & Mazzitelli (1985). We have updated this work by using the more recent models of Burrows et al. (1993). These models can be expected to produce more accurate results, mainly through an improved treatment of the boundary condition represented by the stellar atmosphere based on the models of Lunine et al. (1989). The revised fits are listed in Table 5.2, which includes fits for a broad variety of possible ages. The best fitting near infrared spectral index n (Adams et al. (1987)), is found to be fairly independent of the chosen isochrone, and the same value has been used for all the

isochrone fittings of each object, selected from a fit to the source assuming it has reached the deuterium burning phase.

Although five of the sources are indicated to be close to the stellar/substellar limit, only Oph 2320.8–1721 is indicated to be in the substellar range by an amount that exceeds the likely uncertainties of the method. The temperatures of all five very low mass sources are fit to be just under 3000K, in good agreement with the depth of the CO bands in their spectra. Oph 2320.0–1915 is fitted with a temperature somewhat above 3000K, and may be more massive than estimated by CRBR. If fits are made which force the source to have no infrared excess ($n = -3.0$), then the masses are increased slightly except for that of Oph 2320.8–1721, which rises to $0.07M_{\odot}$ if it is more than 2 Myr old. However, for this forced fit the residuals are unacceptably large. Thus, the new fits reinforce the conclusions by CRBR that these objects are very low mass stars or are substellar and our spectra are in good agreement with this conclusion. Since the temperature that would be assigned from the spectra are consistent with the modeling, we would have reached similar conclusions about all these sources if we had started with the spectrally determined temperatures and dereddened them accordingly before computing luminosities.

Oph 2320.8–1721 is a dim and rather blue object, with a noticeable infrared excess at longer wavelengths. No fits to its colors are possible for masses in the stellar range, unless either the excess is overridden or it has an age in excess of 30Myr years, which is at least ten times larger than the estimated age of the ρ Ophiuchi cluster population (Wilkings et al. (1989), Greene & Meyer (1995)). However, the infrared excess characteristic of very young objects and the variability of the source argue against that possibility.

The spectrum of Oph 2320.8–1721 provides a number of new insights relevant to the modeling that leads us to identify this object as a candidate brown dwarf. The possibility that the object is a background red giant that is seen through a thin spot in the cloud, or is some other chance interloper, was previously argued against on statistical bases. The spectrum and other data reinforce the probable cloud membership of this source in a number of ways. First, the CO absorption bands are weak for a typical cool red giant. Second, the association of a small cloud of H_2 with the source indicates that it is embedded in the ρ Ophiuchus molecular cloud. Third, the apparent variability of the source is consistent with it being a very young object, but would be unexpected for an interloping M dwarf or background red giant. Finally, the probable weak infrared excess detected by Rieke & Rieke (1990) at $10\mu m$ again indicates the source is likely to be young and embedded in the cloud.

A critical assumption in the modeling of CRBR is that the near infrared colors apply to the photosphere of the object. The CO absorption bands in all of these sources confirm that assumption, at least in the $2\mu m$ region. At shorter wavelengths, some very young T Tau stars have strong blue excess emission from an accretion zone that veils the normal stellar spectral features. This behavior is accompanied by very strong Br γ emission (Giovanardi et al. (1991)). Since the false Br γ we observe in Oph 2320.8–1721 (and in the other sources) is no stronger than expected from the absorption in our calibration star, we conclude that such a strong blue excess is unlikely for this source (and for the others as well).

We can also derive an upper limit to the mass of Oph 2320.8–1721 in a way that is largely independent of our modeling technique. By comparing our spectrum of the source with the sequences determined by us and by Jones et al. (1994), we

adopt GL406 as the warmest permissible M dwarf analog of Oph 2320.8–1721. To maximize the luminosity, we assume that the entire J , H , and K flux densities are from the photosphere of the source; assuming that the intrinsic colors are identical to those of GL406, we find an upper limit to the reddening of $A_V \leq 11$. We use this upper limit to compute a lower limit to the absolute, dereddened magnitude of the source, $M_K \geq 6.33$. We then apply the relation between M_K and luminosity for GL406 (e.g., Kirkpatrick et al. (1993) and references therein) to convert the lower limit on the absolute magnitude to an upper limit on the luminosity, namely $L \leq 0.017 L_\odot$. Because we have measured Oph 2320.8–1721 at J (16.4), H (14.8), K (13.55), L' (12.1), and N (8.7) (CRBR), we can also include in this estimate any possible excess emission, on the conservative assumption that it represents reradiation of a blue excess that is not included in the luminosity based on GL406. The excess at L' under the assumptions adopted for this limiting calculation is not important energetically. We therefore estimate the additional luminosity as νF_ν , measured at N ($10.6\mu m$). We get an additional $0.004 L_\odot$, or a total luminosity of $L \leq 0.021 L_\odot$. Finally, we use this upper limit on the luminosity to derive an upper limit on the mass by taking the age of Oph 2320.8–1721 to be 3 Myr, the full age of the embedded cluster, despite the evidence for the relative youth of the object. From Model X of Burrows et al. (1993), we find $M \leq 0.05 M_\odot$.

Greene & Meyer (1995) have recently reported infrared spectroscopy of a number of embedded sources in the ρ Oph cluster. They conclude that all these sources are no more than about 1 Myr years old. This result is surprisingly discordant with the age of the cluster determined previously by optical spectroscopy (e.g. Wilking et al. (1989)). It may indicate either that the embedded sources are systematically much younger than the ones visible optically, or that further efforts are needed to reconcile differing age estimators. We note that the discrepancies

found by Greene & Meyer (1995) with the masses fitted by CRBR for sources in the low-to-moderate mass range are largely due to the much younger ages they have assigned, as shown by the trend with age in Table 5.2 for Oph 2320.0–1915. However, for the lowest mass objects the masses are virtually independent of age over the possible range, since these objects are all near the deuterium burning main sequence where their properties change only slowly with age.

In conclusion, the spectra of six low mass objects are in good agreement with the predictions of the modeling of the photometry. Further confirmation through spectra of additional sources is still needed, but it appears that the method of CRBR is reasonably effective even for the lowest mass objects detected in the ρ Ophiuchus cloud.

5.4 The Initial Mass Function

As expected from the excellent agreement of the modeling, the initial mass functions derived by CRBR and SKS are also in reasonable agreement as shown by the star counts of Figure 5.3 (the statement about disagreements in the IMFs in SKS is the result of a misunderstanding). In this Figure, the counts of SKS have been normalized by 1.29 to give the same total number of stars in the range $0.1 < M(M_{\odot}) < 5$. SKS had a slightly more conservative criterion than did CRBR for inclusion of objects with infrared excesses. This difference is perhaps justified in both cases because the photometry of SKS extended only to $2.2\mu m$, while that of CRBR extended to $3.4\mu m$ and hence allowed more accurate modeling of any excesses. In any case, there appear to be only three objects in this category, not enough to influence the results significantly one way or the other.

Since the two surveys are in such good agreement, we can combine them

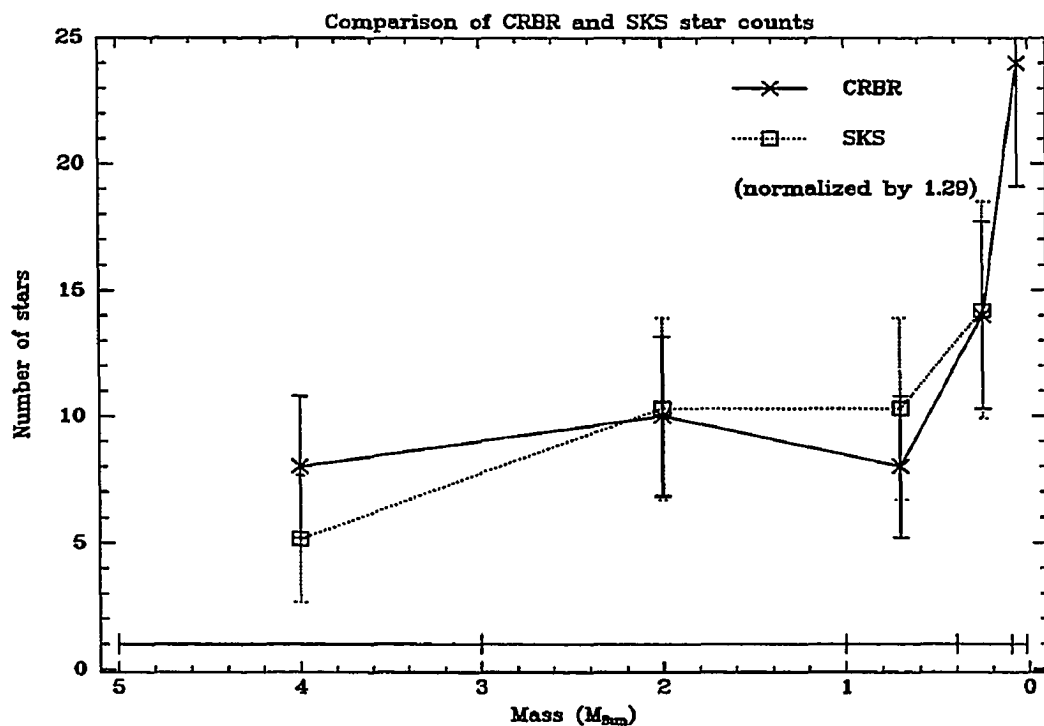


Fig. 5.3.— Comparison of star counts.

The star counts of CRBR and SKS are compared. The bins used are the same as in CRBR and are shown at the bottom of the Figure. The counts of SKS have been normalized by 1.29 to give the same total number of stars in the range $0.1 < M(M_{\odot}) < 5$. Note the agreement of the two surveys.

by averaging the masses derived for sources in common and including all other sources with mass $\geq 0.1\mathcal{M}_{\odot}$ from either study (the study of SKS extended to an additional cloud core compared with that of CRBR). For substellar objects, we have renormalized the results of CRBR by the ratio of the number of objects in the combined IMF to that in the IMF of CRBR alone, and we have included the modest completeness correction derived by CRBR to account for the systematic omission of heavily obscured low mass objects in their survey (the statement by SKS that CRBR did not make such completeness corrections is also a misunderstanding). This improved IMF is shown in Figure 5.4. The error bars in Figure 5.4 are based on counting statistics of the number of objects in each bin and do not include possible systematic errors. Figure 5.4 implies strongly that the IMF in the ρ Oph cluster continues into the substellar range without a rapid termination below the bottom of the main sequence. Within the errors, the IMF can be fitted either by a power law of slope ~ -1.1 (linear mass units) or ~ -0.1 (logarithmic units). However, given the possible systematic errors, a modest flattening of the IMF cannot be ruled out.

Finally, we consider whether the source properties we derive should be preserved after the embedding cloud has dissipated. André & Montmerle (1994) have obtained extensive observations of the circumstellar material in the ρ Ophiuchus system at 1.3mm. They find that the circumstellar material has virtually all been dissipated by the time a source has reached class II, i.e., with a modest infrared excess, so that sources of classes II and III cannot be expected to accrete significant additional masses of interstellar material. Since the photometric methods of both CRBR and SKS are based only on sources of classes II and III, we conclude that the derived IMF should be representative of the mass distribution in a more mature open cluster. It is also noteworthy that André & Montmerle (1994)

Table 5.2. Model Masses of Ophiuchus sources

Object	n	0.5 Myr	1 Myr	2 Myr	3.5 Myr	8 Myr
Oph 2317.3-1925	-2.5	0.07	0.07	0.07	0.11	0.3
Oph 2320.0-1915	-3.0	0.15	0.15	0.4	0.5	0.8
Oph 2320.8-1708	-2.5	0.08	0.08	0.08	0.2	0.3
Oph 2320.8-1721	-0.5	0.02	0.02	0.03	0.03	0.03
Oph 2326.5-1958	-2.5	0.06	0.06	0.07	0.08	0.2
Oph 2404.5-2152	-2.0	0.05	0.06	0.06	0.06	0.15

Note. — These fits are based on the models in CRBR with the improvements discussed in Section 5.2. n is the best fitting near infrared spectral index (Adams et al. (1987)); all masses are in units of M_{\odot} .

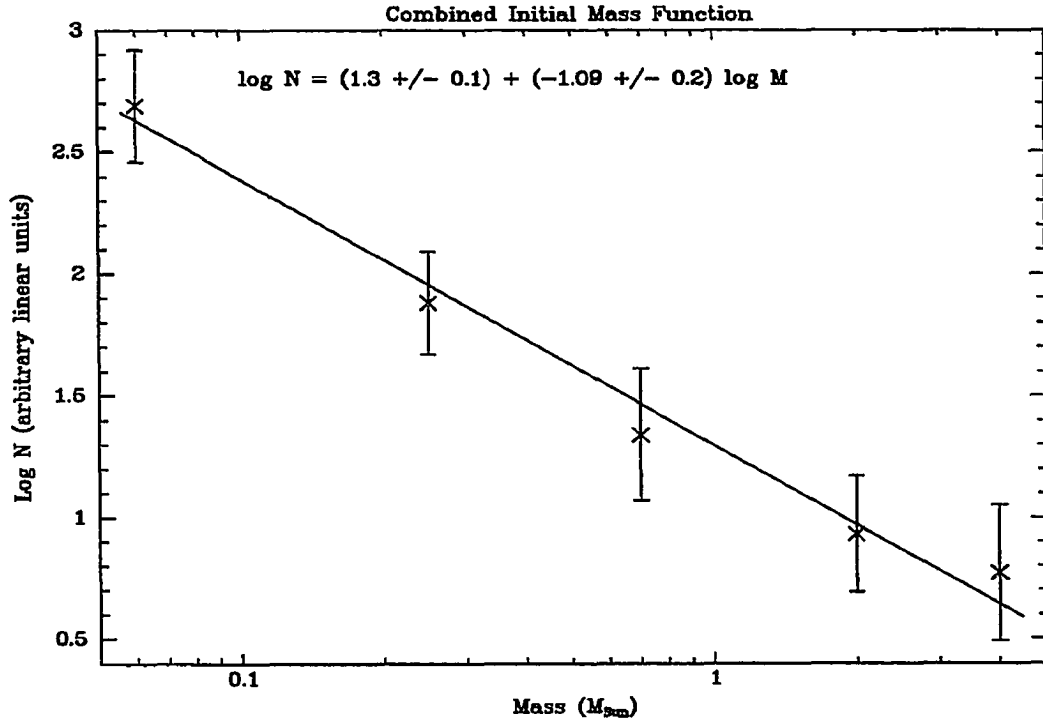


Fig. 5.4.— The initial mass function for ρ Ophiuchus. Derived from the merger of CRBR and SKS source counts. The error bars reflect \sqrt{N} counting errors. The best fitting power law ($N(M)dM \propto M^n dM$) has a slope (n) of -1.09 ± 0.2

observed Oph 2320.8–1721 and obtained only an upper limit, so that the very low mass indicated for this object should not be increased by future accretion.

5.5 Conclusions

We have reconsidered methods to derive masses of embedded young stars from near infrared photometry by examining the results obtained for sources in the cores of the ρ Ophiuchus cloud. We find that the two methods proposed for this derivation (Comerón et al. (1993) and Strom et al. (1995)) are in agreement over the range of 0.1 to $1 \mathcal{M}_{\odot}$, where both are applicable. In the substellar range, however, only the method proposed by Comerón et al. (1993) is applicable. To test its performance on very low mass objects, we have obtained K -band spectra of six sources, including a brown dwarf candidate, and of some field M-dwarfs. Comparison with field stars shows that the spectra of the ρ Ophiuchus sources display characteristics of the photospheres of cool stars. The constraints on the source temperatures determined from the spectra are consistent with a re-analysis of the photometry presented by CRBR using new evolutionary tracks for low mass objects, and confirm that the initial hypotheses underlying the analysis procedure developed by CRBR are valid for these sources. An important result is that the low mass previously assigned to Oph 2320.8–1721 is supported by the spectrum of this source; the new analysis would suggest a mass of about $0.03 \mathcal{M}_{\odot}$, with an upper limit of $0.05 \mathcal{M}_{\odot}$.

The initial mass functions derived for the ρ Ophiuchus embedded cluster by Comerón et al. (1993) and by Strom et al. (1995) are in agreement. If we combine these IMFs to improve the statistical significance, they show the IMF to rise from low stellar masses into the brown dwarf regime as a power law with index ~ -1.1

(linear mass units) or ~ -0.1 (logarithmic units).

Chapter 6

NGC 7160

6.1 Introduction

NGC 7160 is an open cluster 750 pc away (Becker & Fenkart (1971); Conti & van de Heun (1970); Hagen (1970); Lyngå(1987); Mermilliod (1981a); and Hron (1987)), has a very young estimated age of 10 – 20 Myr (see below), and is relatively dust free with $A_V = 0.36$ (Johnson et al. (1961); Simonson III (1968); Mermilliod (1981a); and Hron (1987)). These features are appealing because clusters at this age are important as bridges between the older unembedded clusters such as the Pleiades and Praesepe and the very young, heavily embedded clusters like ρ Ophiuchus and NGC 2024.

Before this dissertation, most of the photometric data on NGC 7160 members was based on the exceptional photographic and photoelectric survey of Hoag et al. (1961). They identified some 30 members of the cluster photographically with magnitudes in the range $6.69 < m_V < 14.48$ and measured them photoelectrically. However, this survey neglects any contamination from background sources, a

fact which many later users of these data ignore. The completion limit for the photoelectric data seems to be $m_V \sim 12$, as 4 stars observed only photographically have been shown to be cluster A stars (the brightest of which has $m_V = 12.58$) (Conti & van de Heun (1970)). In a subsequent analysis of the data Johnson et al. (1961) determined that the cluster had a distance of 830pc and a turnoff $B-V$ color of -0.30 , implying that the earliest spectral type present in the cluster was O9.5.

A drawback of NGC 7160 is that the age is poorly determined. Various estimates place the age as low as 7 Myr (Mermilliod & Maeder (1986); Grigsby & Morrison (1995)) and as high as 20 Myr (Conti & van de Heun (1970); and Janes & Adler (1982)). The earliest estimate for the age comes from Gray (1965) who used the $B-V$ turnoff, $B-V_t = -0.30$ of Johnson et al. (1961) and compared this value with an empirical sequence derived by Sandage (1963) to determine an age of 2.5 Myr. A more recent determination of the age using a similar method was performed by Janes & Adler (1982) who derived $B-V_t = -0.20$ and an age of 18 Myr. Lyngå(1987) assumed the turnoff color of -0.20 to determine an age of 10 Myr. Lindoff (1968) used a method that was based observationally on the second brightest star and the number of stars down to a certain magnitude limit and theoretically on models from Iben (e.g. Iben (1966)); the age determined by this method was an upper limit of 10 Myr. More accurate age determinations using theoretical isochrones are difficult for most open clusters due to the paucity of bright high mass stars present. The approach taken by Mermilliod (1981c), Mermilliod (1981a), and Mermilliod & Maeder (1986) has been to group similarly aged clusters together to improve the statistics of the fits. NGC 7160 was placed in the NGC 2362 age group, which was assigned an age of 7 Myr. We have taken the age to be 10 Myr based on the fact that the earliest spectral type present

(for HD208440) is a B0 (Hron (1987); Mermilliod (1981b); Mermilliod & Maeder (1986)) or a B1 (Hoag & Applequist (1968); Grigsby & Morrison (1995)).

6.2 Analysis

6.2.1 Extraction of Members

Figure 6.1 shows the m_V , $V-K$ diagram for all the objects observed. Also plotted is a young disk sequence from Leggett (1992), and our adopted isochrone (10 Myr at our adopted distance of 750 pc). This isochrone is based on the theoretical calculations of D’Antona & Mazzitelli (1994) for masses down to $0.2\mathcal{M}_\odot$ and Burrows et al. (1993) for masses below $0.2\mathcal{M}_\odot$. The theoretical effective temperatures were converted to photometric colors by applying the work of Kirkpatrick et al. (1993) to relate T_e to M dwarf spectral type. Colors for the appropriate M dwarfs in the Cousins system were taken from Leggett (1992); we assumed that the colors of pre-main-sequence objects would be identical to those of M dwarfs of identical effective temperature. This procedure provides an observationally based set of colors and absolute magnitudes even for objects with masses well below the bottom of the main sequence, since at the age of NGC 7160 these objects have not yet cooled below the temperatures of evolved M dwarfs. We have indicated the masses of objects along the isochrone.

The models of Burrows et al. (1993) were used below $0.2\mathcal{M}_\odot$ for consistency with previous chapters. At the assumed age of NGC 7160 of 10Myr, the differences between the theoretical models of Burrows et al. (1993) and D’Antona & Mazzitelli (1994) for a $0.1\mathcal{M}_\odot$ object are another possible source of error. However, when converted to observable quantities, this difference is well within

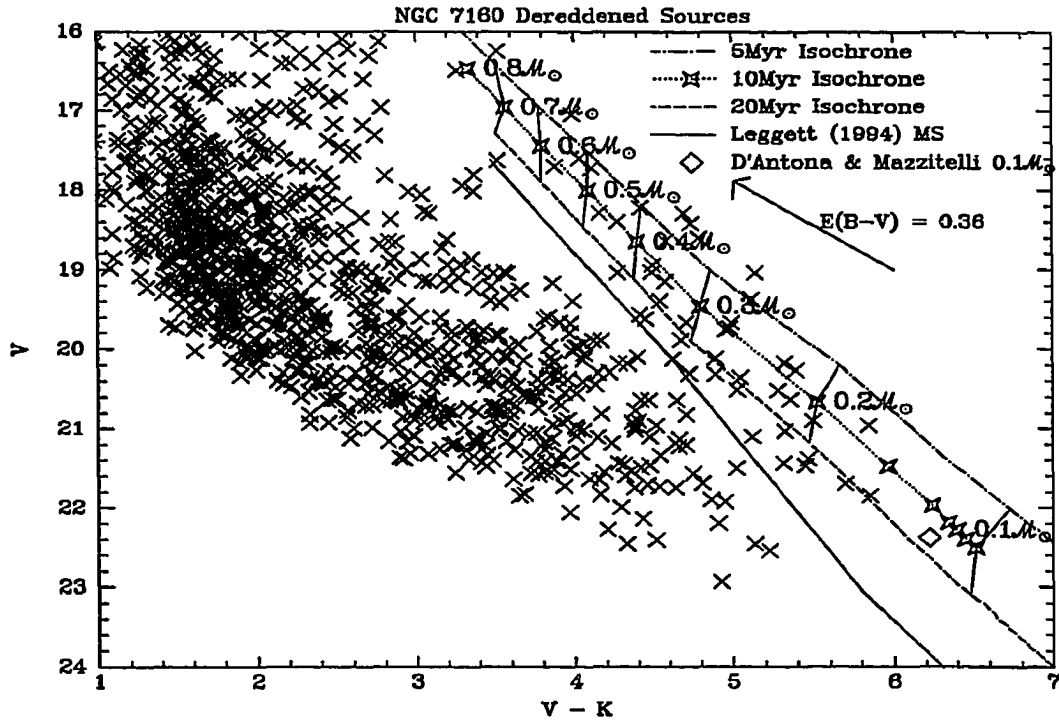


Fig. 6.1.— Color-Magnitude Diagram m_V , $V-K$ for NGC 7160. All sources are plotted. Our adopted 10 Myr isochrone, based on D'Antona & Mazzitelli (1994) and Burrows et al. (1993) is plotted as a dotted line. Isochrones for 5 and 20 Myr are also plotted. A young disk based on Leggett (1992) is plotted as a solid line.

the expected observational errors. D’Antona & Mazzitelli (1994) predict an effective temperature of $T_{eff} = 3162K$ and a luminosity of $L/L_{\odot} = 0.0127$, where Burrows et al. (1993) predict a slightly cooler, but slightly more lumious object at $T_{eff} = 3105; L/L_{\odot} = 0.0143$. This change can be seen in Figure 6.1 after conversion to observable properties as described above. The diamond near $V-K \sim 6.2, m_V \sim 22.4$ represents the D’Antona & Mazzitelli (1994) prediction. This agreement is excellent, but not unexpected. The set of D’Antona & Mazzitelli (1994) models (Alexander opacities and MLT convection) used in this study was chosen to match Model X of Burrows et al. (1993) at $0.2M_{\odot}$. For a $0.1M_{\odot}$ object at the canonical age of the Pleiades (70Myr), the discrepancies are much larger. The D’Antona & Mazzitelli (1994) models predict an object that is $150K$ warmer and 7% brighter than the model of Burrows et al. (1993).

Our method as applied to Praesepe and the Pleiades has been described more fully in Chapters 3 and 4. These two chapters show that the method is both complete and relatively uncontaminated by background stars, at least for reasonably high galactic latitudes. We also show a very good correspondence between our identifications of members and memberships from proper motion searches. This is an important point since there are no previous searches for low mass members of NGC 7160, either photometrically or with proper motion searches.

A number of general features of Figure 6.1 need comment. Because the CCD saturated above $m_V = 16$, we base the following discussion on sources with $m_V > 16$. For NGC 7160, $m_V = 16$ corresponds to a star of $M = 0.8M_{\odot}$, so our discussion will include no stars more massive than this value. The boundary to the distribution of detected sources extending from $m_V = 19, V-K=1$ to $m_V = 23$,

$V-K=5$ arises from the K detection limit of $m_K \sim 17.5$. We believe the survey is complete for $m_K \lesssim 17$. For a given spectral type, changes in distance move points vertically in Figure 6.1. Therefore, the great majority of stars, which fall below the NGC 7160 isochrone for their colors, are dwarfs that lie behind the cluster. There may be a contamination of these counts by red giants at much greater distances than the dwarfs. The galactic latitude of this cluster is very low, $\sim 7^\circ$, so this contamination could be significant, and is the reason that an equal area was imaged at the same galactic latitude for reference fields. Foreground contamination should not be a problem; based on the counts of stars within 8pc by Henry & McCarthy (1992) with $11 < V < 18$, we estimate that there should be about 0.01 low mass dwarfs between us and the cluster in the surveyed volume. Finally, the reddening vector in Figure 6.1 illustrates that errors in reddening will not effect our identifications of cluster members but will influence the assigned masses.

Based upon our estimates of the photometric errors, on the diameter of NGC 7160, and on the uncertainty of the distance to NGC 7160, we estimate that any object within 0.40 magnitudes of the solid line in Figure 6.1 could be a member of the cluster. Objects meeting this criteria are shown in the $V-I$, $I-K$ color-color diagram of Figure 6.2. The adopted isochrone is also shown in this Figure. Perhaps surprisingly, there only seem to be 2 contaminating background giants in our m_V , $V-K$ selected objects. These will be dropped from discussion. All of the remaining sources are listed in Table 6.1.

6.2.2 The Luminosity and Mass Functions of NGC 7160

The sources listed in Table 6.1 determine the low mass IMF in the cluster. The listing is incomplete below $0.2\mathcal{M}_\odot$ because of our detection limit at V and

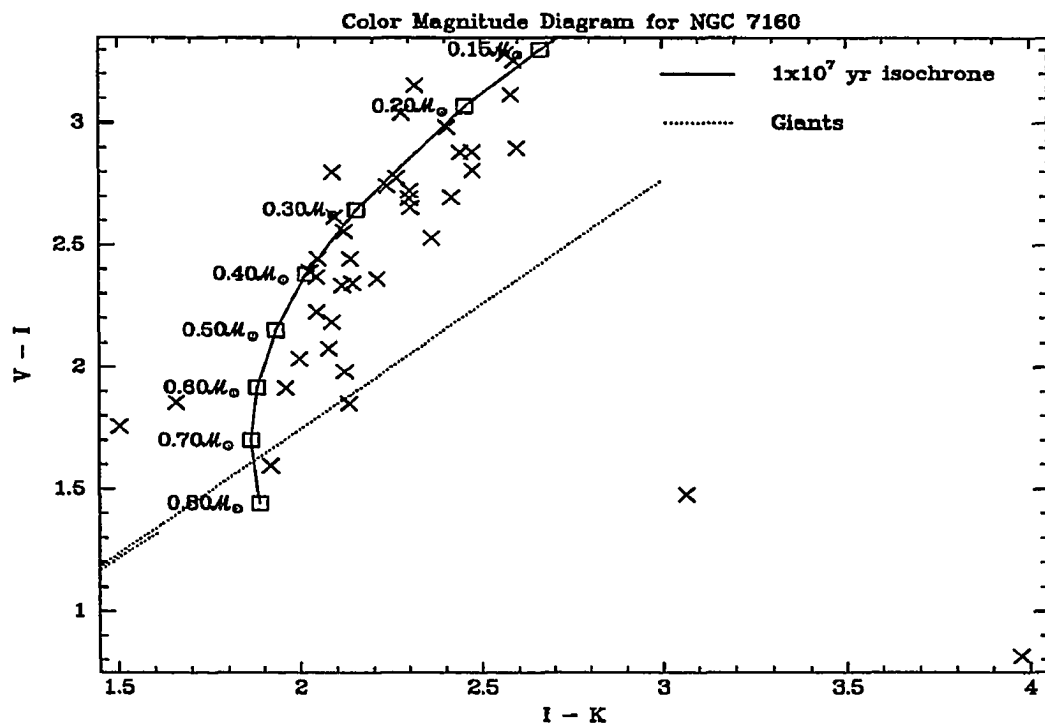


Fig. 6.2.— Color-Color Diagram $V-I$, $I-K$ for NGC 7160. Objects within 0.4 mag of isochrone in m_V , $V-K$ are shown, as is the adopted 10 Myr isochrone (solid line), and the location of Giants.

Table 6.1. Probable NGC 7160 M-Dwarfs

ID	RA ^a	DEC ^a	m_V	m_I	m_K
1	21:52:26.73	62:19:00.5	19.62	17.29	15.17
2	21:52:41.91	62:19:07.3	21.38	18.23	15.91
3	21:52:33.11	62:19:08.7	20.18	17.14	14.86
4	21:52:30.36	62:19:13.1	21.85	18.56	15.99
5	21:52:27.70	62:19:58.5	18.40	16.22	14.13
6	21:52:34.64	62:20:57.7	17.60	15.56	13.57
7	21:52:41.78	62:21:04.7	19.67	16.98	14.68
8	21:52:07.92	62:19:00.7	19.37	16.68	14.26
9	21:52:09.62	62:19:11.9	18.29	16.21	14.13
10	21:52:11.09	62:20:33.2	20.36	17.58	15.32
11	21:52:07.70	62:20:41.0	20.12	17.59	15.23
12	21:52:29.77	62:17:03.9	19.04	16.82	14.77
13	21:52:43.60	62:17:15.8	19.67	17.05	14.95
14	21:52:37.49	62:17:17.5	18.64	16.20	14.06
15	21:52:29.69	62:17:28.1	16.25	14.65	12.73
16	21:52:38.31	62:18:20.5	19.74	16.99	14.75
17	21:52:32.72	62:18:41.7	19.75	17.10	14.80
18	21:52:08.19	62:16:52.1	17.05	15.20	13.07
19	21:52:18.53	62:17:21.9	19.57	17.20	15.15
20	21:52:16.31	62:17:31.3	21.70	18.58	16.00
21	21:52:09.08	62:18:20.1	20.90	18.01	15.41
22	21:52:15.55	62:18:41.4	20.63	17.75	15.27
23	21:52:19.17	62:18:42.7	20.52	17.71	15.24
24	21:52:05.01	62:25:01.6	21.03	18.15	15.70
25	21:52:10.96	62:25:31.8	17.63	15.77	14.11
26	21:51:40.58	62:26:35.2	20.27	17.28	14.88
27	21:52:05.02	62:22:22.4	19.15	16.79	14.58
28	21:52:09.62	62:22:24.3	19.03	16.69	14.54
29	21:52:13.23	62:22:31.5	17.73	15.74	13.62
30	21:52:14.89	62:23:28.5	20.32	17.52	15.43
31	21:52:06.37	62:24:15.4	16.49	14.73	13.23
32	21:52:02.06	62:24:17.3	20.51	17.78	15.48
33	21:52:06.97	62:24:26.6	17.70	15.79	13.83
34	21:51:49.78	62:23:35.2	18.23	15.83	13.80
35	21:51:44.84	62:23:60.0	19.89	17.33	15.21
36	21:51:41.85	62:24:39.4	20.96	17.70	15.11
37	21:51:54.17	62:24:43.5	18.95	16.50	14.45

^aAll coordinates are for the 1950.0 equinox and accurate to $\sim 3''$

is truncated at $0.8\mathcal{M}_{\odot}$ due to the saturation limit of the CCD at $m_V = 16$. The luminosity function (LF) of these sources is shown in Figure 6.3, along with the luminosity function of other well studied clusters.

In this chapter we will use $N(m)dm$ for the mass function (sometimes referred to as the mass spectrum), which represents the number of stars per unit mass in the box described below whose masses are in the range $m - \frac{dm}{2} < m(\mathcal{M}_{\odot}) < m + \frac{dm}{2}$. Reference fields taken at the same galactic latitude, but offset by $\pm \sim 1^\circ$ in galactic longitude and analyzed using techniques identical to those for NGC 7160 were used to estimate the background contamination. The background-corrected counts and computed mass function are listed in Table 6.2. The final bin, $0.1 < m(\mathcal{M}_{\odot}) < 0.2$, is assumed to be incomplete, and will not be used in the following fits.

The IMF determined from our data are not changed significantly if the assumed age of NGC 7160 is changed by a factor of two in either direction. The different isochrones are displayed in Figure 6.1. The IMFs resulting from assuming that the age of NGC 7160 is 5, 10, and 20 Myr are displayed in Figure 6.4. The errors plotted represent the \sqrt{N} counting errors in each bin, including the contributions from the subtracted reference field counts.

Connecting the low mass IMF with the values at higher mass is somewhat problematical. If we create a box containing our survey area and centered on the apparent cluster center, i.e., with NW and SE corners corresponding to the extreme NW and SE corners of our survey, this box contains 85 arcmin². Hoag et al. (1961) have surveyed this region photoelectrically; the box contains 13 of the 16 probable cluster members they observed with $m_V < 12$. A correction factor is required to make these counts comparable with our data, and the size of this factor depends on the cluster geometry. For a spherical cluster, the factor would be the areal ratio,

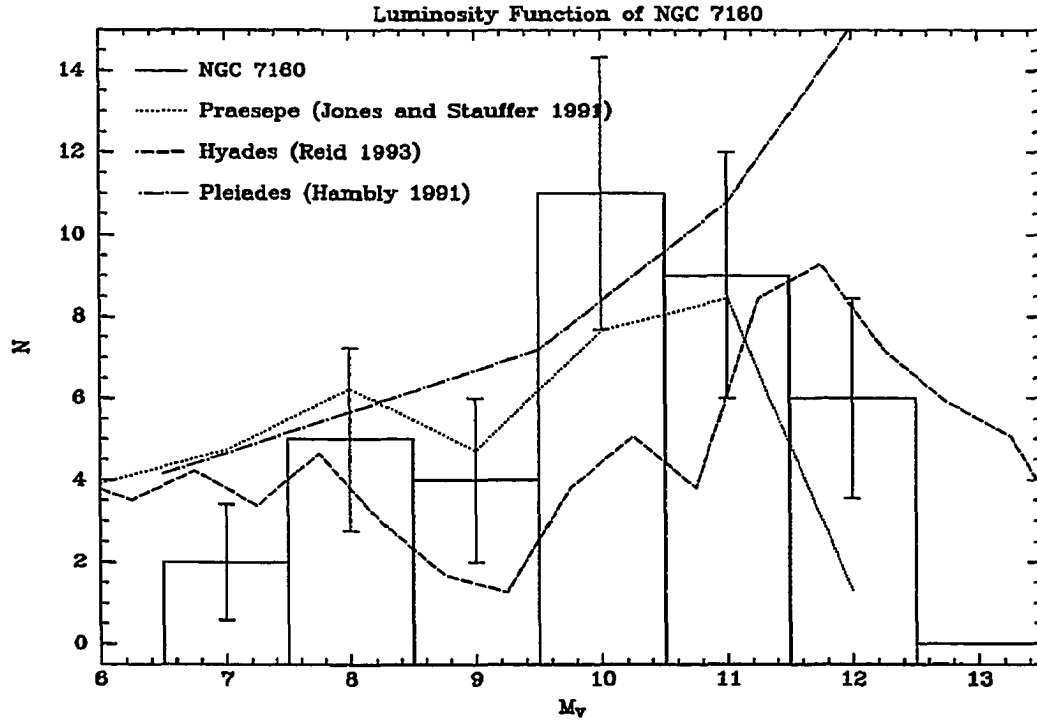


Fig. 6.3.— Luminosity Function of NGC 7160.

The luminosity function of the objects within 0.4 magnitudes of the 10Myr isochrone is shown as a bargraph, using the assumed distance modulus of the cluster of 9.38 mag. The vertical error bars reflect \sqrt{N} counting errors. For comparison, the luminosity functions of three other open clusters (the Pleiades, the Hyades, and Praesepe) are also plotted. These other LF's have been normalized to have the same counts in the displayed magnitude range.

Table 6.2. The Mass Function of NGC 7160

m_{max} \mathcal{M}_{\odot}	m_{min} \mathcal{M}_{\odot}	N	$N(m)$
17.5	2.0	13 ^a	0.84 ± 0.23^b
0.8	0.5	7	151 ± 57
0.5	0.3	6	195 ± 80
0.3	0.2	12	780 ± 225
0.2	0.1	5	325 ± 132^c

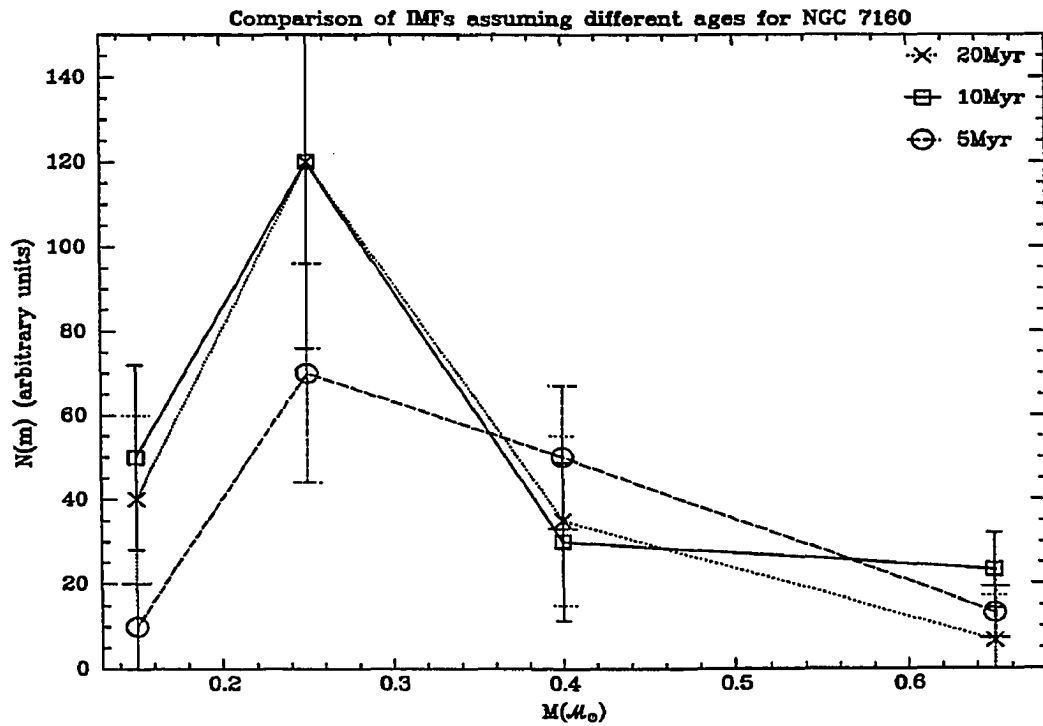
^aHoag et al. (1961)^bFinal value after performing an iterative fit, see text for details. Initial value: 1.66^cLower Limit

Fig. 6.4.— Low Mass Functions of NGC 7160 Assuming Different Ages.

The IMFs resulting from different assumed ages of NGC 7160 are plotted. The vertical error bars reflect \sqrt{N} counting errors. Our results are unchanged if the age of NGC 7160 is 10 Myr to within a factor of two.

$85/50 = 1.7$, between the whole box and the portion we surveyed. At the other extreme, if the approximately linear configuration of the bright stars indicates, for example, that the cluster is in a flat configuration seen edge-on, then the correction might be better taken to be $13/2 = 6.5$, the ration of bright stars in the box to the number on our frames.

To improve the averaging over the large mass range of the Hoag et al. (1961) point, an iterative fitting process was performed. The initial value for this point was determined by noting that at the adopted distance and reddening, the absolute V magnitudes under consideration are: $-2.7 < M_V < 1.96$, which according to the Tables in Lang (1991) imply MS spectral types ranging from B2 to A5, and masses in the range $2.0 < m(\mathcal{M}_\odot) < 9.8$. Thus the Hoag et al. (1961) higher mass data may be initially summarized as $N(m = 5.9\mathcal{M}_\odot) = 1.66 \pm 0.46$, where the error is from Poisson statistics. A power law of the form $N(m) \propto m^\alpha$, was fit, where α is the slope of the mass function on a log-log plot. The slope was assumed to be valid throughout the Hoag et al. (1961) data. A new value for $N(m = 5.9\mathcal{M}_\odot)$ was determined, based on the slope just fit and the total number of stars in the Hoag et al. (1961) mass range – 13. This procedure was iterated until the slope did not change from one step to the next. The final value for $N(m = 5.9\mathcal{M}_\odot)$ was determined to be 0.89 for the 6.5 (high) normalization, 1.13 for the 1.7 (low) normalization. The final fits to the whole mass range ($0.2 < m(\mathcal{M}_\odot) < 6$) were as follows; high: $N(m) = 40.46m^{-2.11 \pm 0.16}$; low: $N(m) = 18.0m^{-1.57 \pm 0.14}$. The MFs are shown graphically in Figure 6.5.

The difference in these two extreme normalizations for the high mass point enters in a minor way in our comparison of low mass IMFs in Section 7. We have determined this dependence by renormalizing the above fits to produce 100 stars

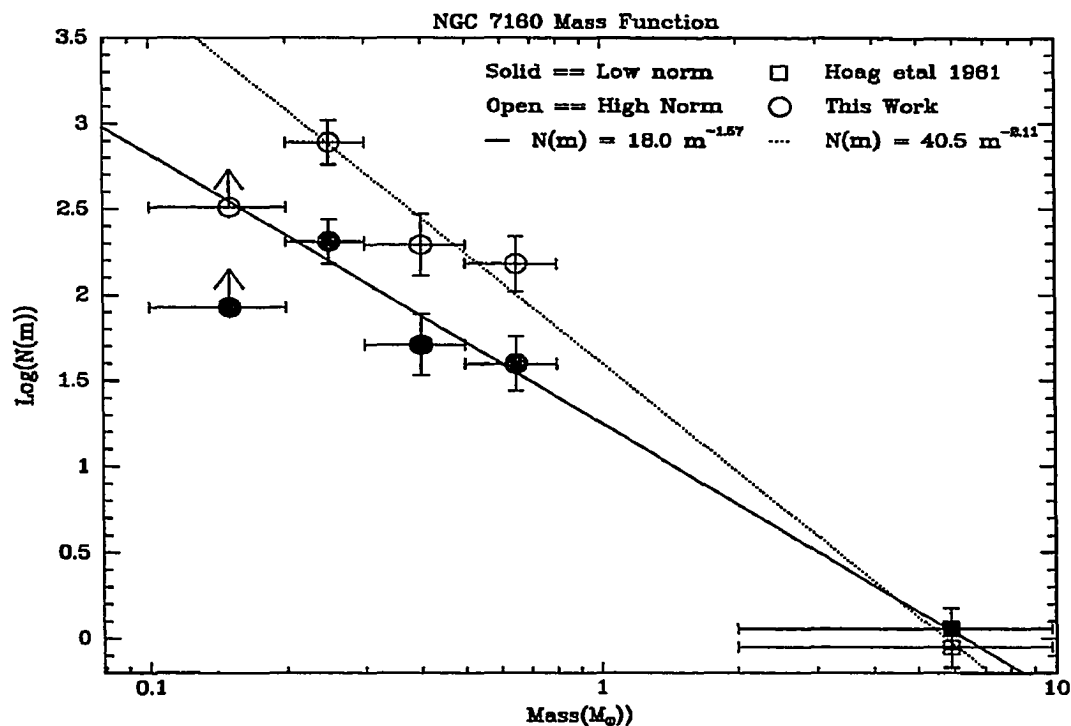


Fig. 6.5.— Mass Functions of NGC 7160.

The vertical error bars reflect \sqrt{N} counting errors. The horizontal error bars represent the sizes of the bins. The results of the normalization extremes are presented. The open points and dotted line represent the higher normalization; the solid points and solid line represent the lower normalization. The best fitting power law ($N(M)dM \propto M^n dM$) has a slope (n) of -2.11 ± 0.16 for the high normalization, and a slope of -1.57 ± 0.14 for the low normalization.

in the range $0.5 < m(\mathcal{M}_{\odot}) < 2$. All of the low mass points are within the Poisson errors with the two extreme normalizations; the higher mass point is more affected by the cluster normalization, the difference being about twice the Poisson noise between points. We have chosen the higher normalization which brings the high mass point closer to the Basu & Rana (1992) field star IMF, but we also note that this point is beyond the scope of this work.

Stecklum (1985) computed mass functions based on the catalogs of Hagen (1970) and Mermilliod (1976) (which are in turn both based on Hoag et al. (1961)) and the models of both Mengel et al. (1979) and Maeder (1981). The slopes determined from this analysis (from all four possible combinations of catalogs and models) range from -2.37 to -3.45 for the mass range of $\sim 1 < m(\mathcal{M}_{\odot}) < \sim 9$. Zakharova (1989) also has computed a mass function whose slope is -2.4 , for roughly the same mass range. Given that the slope of the mass function is known to get shallower with decreasing mass, these two previous studies are consistent with each other, and the slope determined in the last section, particularly the slope derived for the higher normalization.

6.3 Conclusions

We have extended the long-baseline photometric technique of Chapters 3 and 4 to a very young, fairly distant open cluster, NGC 7160. We have identified numerous M-dwarfs contracting towards the Main Sequence in this cluster. The mass function (MF) of this cluster was computed and fit to a power law, the index of which was found to be ~ -2 in linear units (~ -1 in logarithmic mass units) for the range $0.2 < m(\mathcal{M}_{\odot}) < 6$.

Chapter 7

RESULTS

7.1 Comparison of Open Clusters

We now compare the results for the studied open clusters to constrain the IMF in this environment. In Figure 7.1, the MFs of the three unembedded clusters studied with our long-baseline photometric technique (Praesepe (Chapter 3), the Pleiades (Chapter 4), and NGC 7160 (Chapter 6)), and two embedded clusters (ρ Ophiuchus (Chapter 5), and NGC 2024 (Comerón et al. (1995))) are presented. The different MFs have each been normalized to give 100 stars in the range $0.5 < \mathcal{M}_{\odot} < 2$ (summed for Praesepe and the Pleiades, integrating the original fits for NGC 7160, NGC 2024, and ρ Ophiuchus).

For ρ Ophiuchus, we have ignored the highest mass bin of Chapter 5 for two reasons. First, the authors themselves note a degeneracy in their method for stars between $1 < m(\mathcal{M}_{\odot}) < 3$ (Comerón et al. (1993)). Second, Greene & Meyer (1995) observed some of the sources classified as intermediate mass by Comerón et al. (1993) spectroscopically and classified them to be low mass sources. The

change in assigned mass is primarily the result of the younger age estimate used by Greene & Meyer (1995): ~ 1 Myr. Comerón et al. (1995) have shown that the low mass ρ Ophiuchus IMF is not strongly affected by this change of assumed age; however, the IMF above $\sim 0.6M_{\odot}$ will be affected because reclassifying massive sources to younger ages will move them across the inflection in the IMF that occurs near this mass (see Figure 7.1).

The data for NGC 2024 have been taken from Comerón et al. (1995). The authors obtained deep J , H , and K images of the central region of the NGC 2024 embedded cluster in Orion, allowing three-color measurements of 151 sources. This photometry is analyzed by fitting models of young stars and substellar objects, using a method which contains slight improvements to the methods described in Comerón et al. (1993). At the age of NGC 2024 (1 Myr), the substellar objects should be in a stage of deuterium burning that provides a brief interval of stability, so slight errors in the assumed age of the cluster will not substantially change the derived mass function.

There is excellent agreement among the low mass IMFs for the different clusters whose ages vary by a factor of ~ 1000 . The peak of the NGC 7160 MF could be the result of a potential systematic error based on the assumed age of the cluster, or on the assumption that there is no age spread in the NGC 7160 members. As shown in Figure 6.4, if the age of the cluster as a whole, or the objects in this bin are younger than 10 Myr, this point drops down closer to the other cluster MFs. Perhaps a more striking result is the agreement between the two methods used to determine the various MFs. There is also evidence from Figure 7.1 that the slope of the MF is a function of mass. A power-law fit to all the points in Figure 7.1 has a slope of -1.39 (linear mass units). However, if the regions above

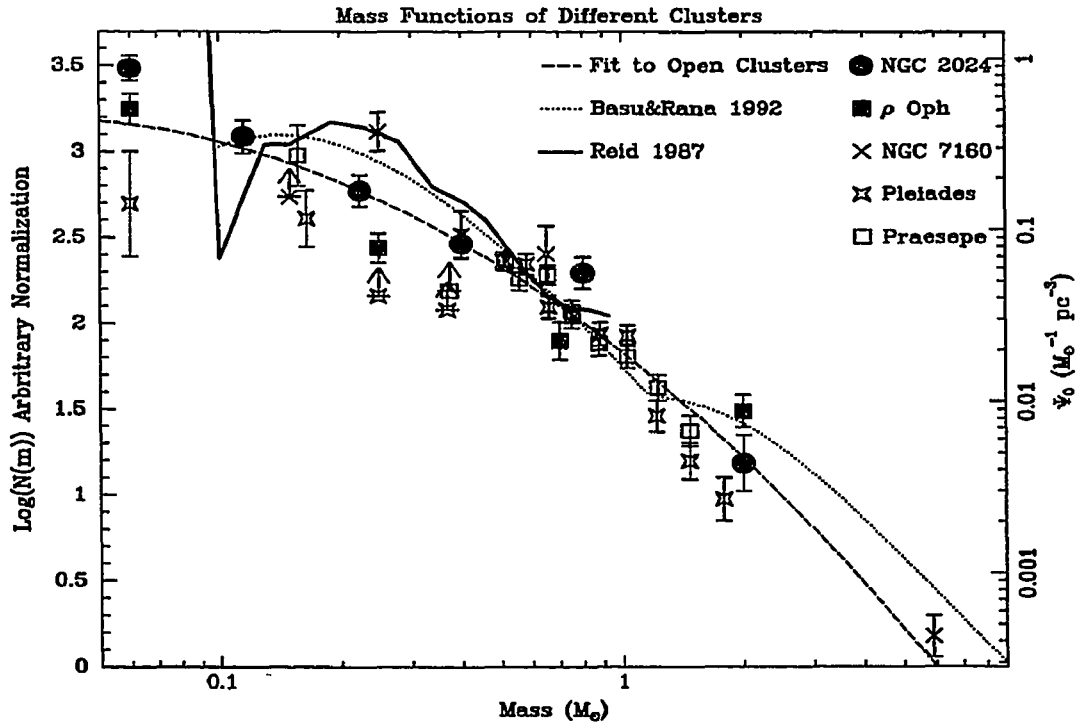


Fig. 7.1.— Comparison of Open Cluster IMFs to the Field Star MF. The error bars reflect \sqrt{N} counting errors. The solid line is the MF of Reid (1987) which also describes the more comprehensive study of Tinney (1993). The dotted line is the quartic fit to the local IMF from Basu & Rana (1992). The dashed line is a parabolic fit to the Open Cluster data. All of the MFs have been normalized to contain 100 stars in the range $0.5 < m(M_{\odot}) < 2$; this scale is reflected on the left-hand side of the Figure. The right-hand scale reflects the original data of Reid (1987) and Basu & Rana (1992) in units of $M_{\odot}^{-1} pc^{-3}$.

and below $0.5\mathcal{M}_\odot$ are fit separately, the slopes of power-law fits to the different regions are: -0.75 ± 0.3 for $m(\mathcal{M}_\odot) < 0.5$ and -2.12 for $m(\mathcal{M}_\odot) > 0.5$. A parabolic fit has been performed on all the open cluster data as well to produce a single representative open cluster mass function. The results of this fit are given in Equation 7.1.

$$\log N(m) = (1.838 \pm 0.016) + (-1.86 \pm 0.06) \log m + (-0.52 \pm 0.06) \log m^2 \quad (7.1)$$

Phelps & Janes (1993) have examined the IMFs of 8 young clusters, in the range of $1.4 < m(\mathcal{M}_\odot) < 7.9$. They determined that a power law IMF with a slope of -2.40 ± 0.13 is a good approximation, although deviations do occur. This slope is nearly identical to the Salpeter (1955) slope of -2.35 . The next obvious step is to attempt a comparison of the field star and open cluster IMFs at subsolar and substellar masses.

7.2 Comparison to the Field

There are three recent determinations of the field star IMF. Tinney (1993) obtained some deep photographic images of 270 degree² with followup K observations for complete samples of very low mass candidate objects, and claims the MF of Reid (1987) is a good fit to his data. Basu & Rana (1992) were able to approximate their MF as a quartic function in the logarithm of mass. Kirkpatrick et al. (1994) obtained deep CCD strip scans, and reported that their MF could be fit by a power law with a slope of -0.40 ± 0.16 for $m < 0.5\mathcal{M}_\odot$. They also possibly saw a slight break in the IMF, as the slope for the mass region $0.15 < m(\mathcal{M}_\odot) < 0.5$ was slightly steeper at -0.88 ± 0.12 than for the whole very

low mass region. The MFs of Reid (1987) and Basu & Rana (1992) are shown in Figure 7.1, each also normalized to have 100 stars in the range $0.5 < m(\mathcal{M}_\odot) < 2$. The scale on the right-hand side of Figure 7.1 is calibrated for the field star IMFs in units of $\mathcal{M}_\odot^{-1}pc^{-3}$, and is shifted by a factor of $10^{3.5456}$ due to the normalization discussed earlier. The IMF of Basu & Rana (1992) was converted from surface to volume density by using their estimate of the scale heights for different masses (see their Figure 3).

Except for the two lowest mass points of Reid (1987) (which are based on one star each, and thus have overall little weight, as pointed out by Reid (1987)), the agreement amongst all the studies is very good. The most problematic aspect of the field star IMFs below $m < 0.1\mathcal{M}_\odot$ is that the luminosities of these objects evolve by as much as a magnitude over the age of the disk. Thus the ages of these objects are needed to accurately assign masses to them; however, the IMFs determined from open clusters do not have this handicap. Because the open cluster IMFs extend smoothly into the substellar range, it is plausible that the field star IMF behaves the same way.

Low mass members account for a significant portion of the integrated mass of a stellar population only if the IMF in linear units is at least as steep as $N(M)dM \propto M^{-2}dM$. There is now a significant body of evidence that the IMF in open clusters for single stars and the primary members of doubles is roughly one power of mass less steep than this critical dependence. If the properties of binary systems in these clusters resembles the properties of binaries in the solar neighborhood (Duquennoy & Mayor (1991)), then it can be shown that unresolved secondary stars in binaries do not contribute significantly to the integrated mass. Therefore, it appears that low mass stars and massive brown dwarfs appear to

contribute only a small portion of the integrated mass of an open cluster. The differential mass density, Υ , and total mass density, ρ , are related to the IMF, $N(M)$, by the following equations:

$$\Upsilon dm = mN(m)dm \quad (7.2)$$

$$\rho = \int \Upsilon dm \quad (7.3)$$

The total mass density, ρ , can be computed by integrating Equation 7.3 with the appropriate mass limits. Tinney (1993) has computed the mass density due to stars more massive than $0.4\mathcal{M}_{\odot}$ by integrating the data in Scalo (1986). His result was $\rho(m > 0.4\mathcal{M}_{\odot}) = 0.025\mathcal{M}_{\odot}pc^{-3}$. We have integrated our open cluster MF (Equation 7.1) (after taking into account the factor of $10^{3.546}$ normalization discussed above) to determine the contribution to the mass density both down to the edge of the Main Sequence, and beyond. Our results for the very low mass stars are in very good agreement with the values derived by Tinney (1993). The open cluster value applied to the field mass density is: $\rho(0.08 < m(\mathcal{M}_{\odot}) < 0.4) = 0.013\mathcal{M}_{\odot}pc^{-3}$, while Tinney's value was approximately $0.017\mathcal{M}_{\odot}pc^{-3}$. Thus, the total contribution to the mass density from main sequence stars is $\rho(ms) = 0.038\mathcal{M}_{\odot}pc^{-3}$. The only other major source of mass density in the Galaxy is the material tied up in the interstellar medium. Bahcall (1984) and Hill et al. (1979) estimate the contribution to the mass density from the ISM to be $\sim 0.04\mathcal{M}_{\odot}pc^{-3}$. An upper limit to the contribution of substellar objects to the total mass density can be computed by integrating Equation 7.1 from 0 to $0.08\mathcal{M}_{\odot}$. This limit is $\rho(m < 0.08\mathcal{M}_{\odot}) = 0.0021\mathcal{M}_{\odot}pc^{-3}$. We have also calculated the total mass density below $0.08\mathcal{M}_{\odot}$ assuming a power law behavior below $0.08\mathcal{M}_{\odot}$, whose slope is the same as the slope of our fit at $0.08\mathcal{M}_{\odot}$,

$\alpha = -0.75$. The total mass density from 0 to $0.08\mathcal{M}_{\odot}$ assuming this power law is $0.0026\mathcal{M}_{\odot}pc^{-3}$. Either way, brown dwarfs and substellar objects contribute at most 3% of the total mass density. If the field star IMF behaves similarly, as our data suggests, then such objects cannot be an important constituent of dark matter.

Chapter 8

CONCLUSIONS

The MFs of five young open clusters of various ages and environments were compared; the agreement was found to be excellent, lending credibility to the methods of Comerón et al. (1993) and Comerón et al. (1995) for the lower mass sources. The composite open cluster MF was found to be consistent with many recent determinations of the local field star IMF. The field and open cluster IMFs extend smoothly into the substellar range.

Our results are inconsistent with steeply falling (increasing number of objects for decreasing mass) low-mass IMFs, for example with $n = -2$, as have been found in other studies. If the IMF in open clusters is representative of star formation generally, then massive brown dwarfs and very low mass stars do not account for a very large fraction of the mass in a volume of space, *i.e.*, such objects do not provide significant dark matter.

No generally agreed brown dwarfs have been found in clusters but numerous candidates have been proposed, many of which are still not ruled out. Further observations are needed in many cases and we need to be more confident of the

theoretical predictions.

REFERENCES

- Adams, F. C., Lada, C. J., & Shu, F. H. 1987, *ApJ*, 312, 788
- Ambartsumian, V. A. 1938, *Scientific Trans. Leningrad State Univ.*, 20, 19
- Ambartsumian, V. A. 1985, in, *Dynamics of Star Clusters*, ed. J. Goodman & P. Hut, (Dordrecht: Reidel), 521
- André, P. & Montmerle, T. 1994, *ApJ*, 420, 837
- Bahcall, J. N. 1984, *ApJ*, 287, 926
- Basri, G. & Marcy, G. M. 1995, *AJ*, 109, 762
- Basri, G., Marcy, G. W., & Graham, J. R. 1995, preprint,
- Basu, S. & Rana, N. C. 1992, *ApJ*, 393, 373
- Becker, W. & Fenkart, P. R. 1971, *A&AS*, 4, 241
- Berriman, G. & Reid, N. 1987, *MNRAS*, 227, 315
- Berriman, G., Ried, N., & Leggett, S. K. 1992, *ApJ*, 392, L31
- Bessel, M. S. 1991, *AJ*, 101, 662
- Binney, J. & Tremaine, S. 1987, *Galactic Dynamics*, (Princeton: Princeton University Press)
- Brand, P. W. J. L. 1993, in, *Dust and Chemistry in Astronomy*, ed. T. J. Millar & D. A. Williams, (London: Institute of Physics Publishing)
- Burrows, A., Hubbard, W. B., Saumon, D., & Lunine, J. I. 1993, *ApJ*, 406, 158
- Burrows, A. & Liebert, J. 1993, *Rev. Mod. Phys.*, 65, 301
- Comerón, F., Rieke, G. H., Burrow, A., & Rieke, M. J. 1993, *ApJ*, 416, 185
- Comerón, F., Rieke, G. H., & Rieke, M. R. 1995, preprint,
- Conti, P. S. & van de Heun, E. P. J. 1970, *A&A*, 9, 466
- D'Antona, F. & Mazzitelli, I. 1985, *ApJ*, 296, 502
- D'Antona, F. & Mazzitelli, I. 1994, *ApJS*, 90, 467
- Davidge, T. J. & Boeshaar, P. C. 1993, *ApJ*, 403, L47

- Duquennoy, A. & Mayor, M. 1991, *A&A*, 248, 485
- Elias, J. H., Frogel, J. A., Matthews, K., & Neugebauer, G. 1982, *AJ*, 87, 1029
- Giovanardi, C., Gennari, S., Natta, A., & Stange, R. 1991, *ApJ*, 367, 173
- Gray, D. F. 1965, *ApJ*, 70, 362
- Greene, T. P. & Meyer, M. R. 1995, *ApJ*, 450, 233
- Grigsby, J. A. & Morrison, N. D. 1995, *ApJ*, 442, 794
- Hagen, G. L. 1970, *Pub. David Dunlop Obs.*, 4, 1
- Hambly, N., Hawkins, M. R. S., & Jameson, R. F. 1993, *A&AS*, 100, 607
- Hambly, N. C., Hawkins, M. R. S., & Jameson, R. F. 1991, *MNRAS*, 253, 1
- Hambly, N. C., Steele, I. A., Hawkins, M. R. S., & Jameson, R. F. 1995, *A&A*, in press
- Hayashi, C. & Nakano, T. 1965, *Prog. Theor. Phys.*, 34, 754
- Henry, T. J. & McCarthy, D. W. 1992, in, *IAU Colloq. 135, Complementary Approaches to Double and Multiple Star Research*, ed. H. A. McCalister & W. I. Hartkopf, (San Francisco: ASP), 10
- Henry, T. J. & McCarthy, D. W. 1993, *AJ*, 106, 773
- Hill, G., Hilditch, R. W., & Barnes, J. V. 1979, *MNRAS*, 186, 813
- Hoag, A. A. & Applequist, N. L. 1968, *ApJS*, 12, 215
- Hoag, A. A., Johnson, H. L., Iriarte, B., Mitchell, R. I., Hallam, K. L., & Sharpless, S. 1961, *Publications of the USNO*, 17, 347
- Hoyle, F. 1953, *ApJ*, 118, 513
- Hron, J. 1987, *A&A*, 176, 34
- Iben, I. 1966, *ApJ*, 143, 516
- Janes, K. A. & Adler, D. 1982, *ApJS*, 49, 425
- Johnson, H. L., Hoag, A. A., Iriarte, B., Mitchel, R. I., & Hallam, K. L. 1961, *Lowell Obs. Bull.*, 5, No. 8, 133
- Johnstone, D. 1993, *AJ*, 105, 155

- Jones, B. F. & Stauffer, J. R. 1991, *AJ*, 102, 1080
- Jones, H. R. A., Longmore, A. J., Jameson, R. F., & Mountain, C. M. 1994, *MNRAS*, 267, 413
- Kirkpatrick, J. D., Kelley, D. M., Rieke, G. H., Liebert, J., Allard, F., & Wehrse, R. 1993, *ApJ*, 402, 643
- Kirkpatrick, J. D., McGraw, J. T., Hess, T. R., Liebert, J., & McCarthy Jr, D. W. 1994, *ApJS*, 94, 749
- Kleinmann, S. G. & Hall, D. N. B. 1986, *ApJS*, 62, 501
- Kroupa, P., Tout, C. A., & Gilmore, G. 1993, *MNRAS*, 262, 545
- Lada, C. J. 1990, in, *The Physics of Star Formation and Early Stellar Evolution*, ed. C. J. Lada & N. D. Kylafis, (Dordrecht: Kluwer), 329
- Landolt, A. U. 1992, *ApJ*, 104, 340
- Lang, K. R. 1991, *Astrophysical Data: Planets and Stars*, (New York: Springer-Verlag)
- Lee, H. M., Fahlman, G. G., & Richer, H. B. 1991, *ApJ*, 366, 455
- Leggett, S. 1992, *ApJS*, 82, 351
- Lindoff, U. 1968, *Ark. Astr.*, 5, 1
- Lunine, J. I., Hubbard, W. B., Burrows, A., Wang, Y.-P., & Garlow, K. 1989, *ApJ*, 338, 314
- Lyngå, G. 1987, *Catalogue of Open Cluster Data*, (Observatoire de Strasbourg: Stellar Data Center), 5th edition
- Maeder, A. 1981, *A&A*, 102, 401
- Magazzu, A., Martin, E. L., & Rebolo, R. 1993, *ApJ*, 404, L17
- Marcy, G. W., Basri, G., & Graham, J. R. 1994, *ApJ*, 428, L57
- Mengel, J. G., Sweigart, A. V., Demarque, P., & Gross, P. G. 1979, *ApJS*, 40, 733
- Mermilliod, J. C. 1976, *A&AS*, 24, 159
- Mermilliod, J. C. 1981a, *A&AS*, 44, 467
- Mermilliod, J. C. 1981b, *A&A*, 97, 235

- Mermilliod, J. C. 1981c, *A&A*, 97, 235
- Mermilliod, J. C. & Maeder, A. 1986, *A&A*, 158, 45
- Mould, J. R. 1978, *ApJ*, 226, 923
- Odewahn, S. C., Bryja, C., & Humphreys, R. M. 1992, *PASP*, 104, 553
- Oliva, E. & Origlia, L. 1992, *A&A*, 254, 466
- Phelps, R. L. & Janes, K. A. 1993, *AJ*, 106, 1870
- Rebolo, R., Martin, E. L., & Magazzu, A. 1992, *ApJ*, 389, L83
- Reid, N. 1987, *MNRAS*, 225, 873
- Reid, N. 1993, *MNRAS*, 265, 785
- Reid, N. & Majewski, S. 1993, *ApJ*, 409, 635
- Rieke, G. H. & Lebofsky, M. J. 1985, *ApJ*, 288, 618
- Rieke, G. H. & Rieke, M. J. 1990, *ApJ*, 362, L21
- Salpeter, E. E. 1955, *ApJ*, 121, 161
- Sandage, A. R. 1963, *ApJ*, 138, 863
- Sauval, A. J. & Tatum, J. B. 1984, *ApJS*, 56, 193
- Scalo, J. 1986, *Fund. Cos. Phys.*, 11, 1
- Silk, J. 1987, in, *Star Forming Regions*, IAU Symposium 115, ed. M. Peimbert & J. Jagaku, (Dordrecht: Reidel)
- Simons, D. A. & Becklin, E. E. 1992, *ApJ*, 390, 431
- Simonson III, S. C. 1968, *AJ*, 154, 923
- Spitzer, L. 1940, *MNRAS*, 100, 396
- Spitzer, L. 1987, in, *Dynamical Evolution of Globular Clusters*, , (Princeton: Princeton University Press), 40
- Stauffer, J. R. 1984, *ApJ*, 280, 189
- Stauffer, J. R., Hamilton, D., Probst, R., Rieke, G. H., & Mateo, M. 1989, *ApJ*, 344, L21

- Stauffer, J. R., Hamilton, D., & Probst, R. G. 1994a, *AJ*, 108, 155
- Stauffer, J. R., Klemola, A., Prosser, C., & Probst, R. 1991, *AJ*, 101, 980
- Stauffer, J. R., Liebert, J., & Giampapa, M. 1995, *AJ*, 109, 298
- Stauffer, J. R., Liebert, J., Giampapa, M., MacIntosh, B., Reid, I. N., & Hamilton, D. 1994b, *AJ*, 108, 160
- Stecklum, B. 1985, *Astronomische Nachrichten*, 306, 45
- Steele, I. A. & Jameson, R. F. 1995, *MNRAS*, 272, 630
- Steele, I. A., Jameson, R. F., & Hambly, N. C. 1993, *MNRAS*, 263, 647
- Stevenson, D. J. 1991, *ARA&A*, 29, 163
- Strom, K. M., Kepner, J., & Strom, S. E. 1995, *ApJ*, 438, 813
- Strom, K. M. & Strom, S. E. 1994, *ApJ*, 424, 237
- Terlevich, E. 1987, *MNRAS*, 224, 193
- Tinney, C. G. 1993, *ApJ*, 414, 279
- Turner, J., Kirbey-Docken, K., & Dalgarno, A. 1977, *ApJS*, 35, 281
- Wiling, B. A., Lada, C. J., & Young, E. T. 1989, *ApJ*, 340, 823
- Zakharova, P. E. 1989, *Astronomische Nachrichten*, 310, 127